Distribution of this document is unlimited. Release to CFSTI is authorized.

AD 658684

TECHNICAL REPORT
67-71-GP

BIAXIAL TENSILE TESTER FOR FABRICS

by

R.E. Sebring
and
W.D. Freeston, Jr.

Fabric Research Laboratories
Dedham, Massachusetts

Contract No. DA19-129-AMC-1042(N)

May 1967

General Equipment & Packaging Laboratory
U. S. ARMY NATICK LABORATORIES
Natick, Massachusetts 01760

Best
Available
Copy

FOREWORD

This report was prepared by Fabric Research Laboratories, Inc., under U. S. Army Contract No. DA 19-129-AMC-1042(N). The work was administered under the direction of the U. S. Army Natick Laboratories with Mr. C. J. Monego acting as project engineer.

Dr. M. M. Platt was the FRL officer responsible for the contract. The biaxial tensile tester was designed by Mr. R. E. Sebring, the FRL project engineer. The theoretical analysis of the stress-strain response of fabrics under two-dimensional loading and the evaluation of the Government furnished coated fabrics were carried out under the direction of Dr. W. Denney Freeston, Jr.

The authors wish to express their appreciation to Mr. J. H. Ross of the Fibrous Materials Branch of the Air Force Materials Laboratory for his encouragement throughout this program and particularly for making the Air Force fabric biaxial tensile tester available for the testing and the Air Force computer facility available for the numerical computations. The authors would also like to take this opportunity to thank Mr. James P. Hudson and Mrs. Joyce A. Freeman, of the Digital Computation Division, Systems Engineering Group, U. S. Air Force, Wright-Patterson Air Force Base, Ohio, for their assistance in obtaining solutions of the various sets of non-linear equations involved in the theoretical analyses. The labors of Mr. Rolf A. Frantz, Jr. and Mrs. Meredith M. Schoppee of our Laboratory in performing the numerous tests and reducing the data are also gratefully acknowledged.

TABLE OF CONTENTS

Section		Page
	List of Illustrations	vi
	List of Tables	ix
	Abstract	x
I	INTRODUCTION	1
II	TEST-INSTRUMENT DESIGN CRITERIA	1
	A. General Requirements	1
	B. Detailed Requirements	2
III	LITERATURE SURVEY	4
	A. References	8
IV	MECHANICAL DESIGN FEATURES	9
	A. Specimen	9
	B. Jaws	9
	C. Load Application System	10
	D. Load Sensors	10
	E. Strain Sensors	12
	F. Data Presentation	12

Page

APPENDIX 1 – Stress-Strain Response of Fabrics Under Two-Dimensional Loading

LIST OF SYMBOLS 1

INTRODUCTION 4

Fabric Model 6

Fabric Deformation 9

Limiting Fabric Geometries 11

ANALYTICAL RESULTS 15

Square Fabric, Inextensible Yarn-Crimp Interchange 15

Filling Yarn Initially Straight, Inextensible Yarn-Crimp Interchange 28

Square Fabric, Extensible Yarn (Linearly Elastic, $\nu = 0$), $\sigma_w/\sigma_f = 1$ 37

Square Fabric, Extensible Yarn (Linearly Elastic, $\nu = 1/2$), $\sigma_w/\sigma_f = 1$ 42

Filling Yarn Initially Straight, Extensible Yarn (Linearly Elastic, $\nu = 0$), $\sigma_w/\sigma_f = 1$ 45

Square Fabric, Extensible Yarn (Linearly Elastic, $\nu = 0$), $\sigma_w/\sigma_f > 1$ 50

Square Fabric, Extensible Yarn (Elasto-Plastic, $\nu = 0$), $\sigma_w/\sigma_f = 1$ 59

EXPERIMENTAL PROCEDURE 63

EXPERIMENTAL RESULTS ON MODEL FABRICS 67

CONCLUSION 79

LITERATURE CITED 81

APPENDIX 2 – Evaluation of Government-Furnished Coated Fabrics 82

LIST OF ILLUSTRATIONS

Figure		Page
1	Biaxial Tensile Tester Schematic	5
2	Test Instrument Layout	11
3	Control Panel Layout	14
4	Test Instrument	15
5	Control Panel	16
Appendix 1		
1	Fabric Model	8
2	Limiting Fabric Geometry; Maximum Filling Contraction	13
3	Limiting Fabric Geometry; Contact Between Adjacent Warp Yarns	14
4	N_1 R vs θ_1 for a Square Fabric with Inextensible Yarn	17
5	L/R vs θ_1 for a Square Fabric with Inextensible Yarn	18
6	L/R vs N_1 R for a Square Fabric with Inextensible Yarn	19
7(a)	Fabric Extension in the Warp Direction: Inextensible Yarn, Initially Square Fabric	21
7(b)	Fabric Extension in the Warp Direction: Inextensible Yarn, Initially Square Fabric	22
8(a)	Fabric Contraction in the Filling Direction: Inextensible Yarn, Initially Square Fabric	23
8(b)	Fabric Contraction in the Filling Direction: Inextensible Yarn, Initially Square Fabric	24
9(a)	Poisson's Ratio for an Initially-Square Fabric with Inextensible Yarn	26
9(b)	Poisson's Ratio for an Initially-Square Fabric with Inextensible Yarn	27
10	N_1 R vs θ_{1w} for a Fabric with Inextensible Yarn and Initially Straight Filling	29
11	L/R vs θ_{1w} for a Fabric with Inextensible Yarn and Initially Straight Filling	30
12	L/R vs N_1 R for a Fabric with Inextensible Yarn and Initially Straight Filling	31

LIST OF ILLUSTRATIONS (Cont.)

Figure		Page
13(a)	Fabric Extension in the Warp Direction: Inextensible Yarn, Initially Straight Filling	33
13(b)	Fabric Extension in the Warp Direction: Inextensible Yarn, Initially Straight Filling	34
14(a)	Fabric Contraction in the Filling Direction: Inextensible Yarn, Initially Straight Filling	35
14(b)	Fabric Contraction in the Filling Direction: Inextensible Yarn, Initially Straight Filling	36
15(a)	Poisson's Ratio for Fabric with Inextensible Yarn and Initially Straight Filling	38
15(b)	Poisson's Ratio for Fabric with Inextensible Yarn and Initially Straight Filling	39
16	Fabric Extension: Linearly Elastic Yarn ($\nu = 0$), Square Fabric, $\sigma_w/\sigma_f = 1$	41
17	Fabric Extension: Linearly Elastic Yarn ($\nu = 1/2$), Square Fabric, $\sigma_w/\sigma_f = 1$	44
18	Fabric Extension in the Warp Direction: Linearly Elastic Yarn ($\nu = 0$), Initially Straight Filling, $\sigma_w/\sigma_f = 1$	47
19	Fabric Extension in the Filling Direction: Linearly Elastic Yarn ($\nu = 0$), Initially Straight Filling, $\sigma_w/\sigma_f = 1$	48
20	Fabric Poisson's Ratio: Linearly Elastic Yarn ($\nu = 0$), Initially Straight Filling, $\sigma_w/\sigma_f = 1$	49
21	Fabric Extension: Linearly Elastic Yarn ($\nu = 0$), Initially Square Fabric, $\sigma_w/\sigma_f = 2$	51
22	Fabric Extension: Linearly Elastic Yarn ($\nu = 0$), Initially Square Fabric, $\sigma_w/\sigma_f = 5$	52
23	Fabric Extension: Linearly Elastic Yarn ($\nu = 0$), Initially Square Fabric, $\sigma_w/\sigma_f = 10$	53
24	Fabric Extension: Linearly Elastic Yarn ($\nu = 0$), Initially Square Fabric, $N_1R = 0.050$	54
25	Fabric Extension: Linearly Elastic Yarn ($\nu = 0$), Initially Square Fabric, $N_1R = 0.240$	55
26	Fabric Poisson's Ratio: Linearly Elastic Yarn ($\nu = 0$), Initially Square Fabric, $N_1R = 0.050$	56

LIST OF ILLUSTRATIONS (Cont.)

Figure		Page
27	Fabric Poisson's Ratio: Linearly Elastic Yarn ($\nu = 0$), Initially Square Fabric, $N_1R = 0.240$	57
28	Fabric Extension: Elasto-Plastic Yarn ($E_f = 1 \times 10^6$ psi, $\epsilon_f^* = 0.015$, $\alpha = 8 \times 10^4$ psi, $\nu = 0$), Square Fabric, $\sigma_w/\sigma_f = 1$	61
29	Fabric Extension: Elasto-Plastic Yarn ($E_f = 2.0 \times 10^6$ psi, $\epsilon_f^* = 0.005$, $\alpha = 3 \times 10^5$ psi, $\nu = 0$), Square Fabric, $\sigma_w/\sigma_f = 1$	62
30	Biaxial Tensile Tester	64
31	Cruciform Test Specimen	65
32	Biaxially Stressed Fabric	66
33	Biaxial Load-Extension Response of Gray Saran Fabric at $\sigma_w/\sigma_f = 1$	68
34	Biaxial Load-Extension Response of Gray Saran Fabric at $\sigma_w/\sigma_f = 2$	69
35	Biaxial Load-Extension Response of Gray Saran Fabric at $\sigma_w/\sigma_f = 5:1$ and 1:5	70
36	Biaxial Load-Extension Response of Undyed Saran Fabric at $\sigma_w/\sigma_f = 1$	71
37	Biaxial Load-Extension Response of Undyed Saran Fabric at $\sigma_w/\sigma_f = 2$	72
38	Biaxial Load-Extension Response of Undyed Saran Fabric at $\sigma_w/\sigma_f = 5:1$ and 1:5	73
Appendix 2		
1	Biaxial Load-Extension Response of 2.9-oz/sq yd Vinyl-Coated Nylon Fabric at $\sigma_w/\sigma_f = 1$	84
2	Biaxial Load-Extension Response of 2.9-oz/sq yd Vinyl-Coated Nylon Fabric at $\sigma_w/\sigma_f = 2$	85
3	Biaxial Load-Extension Response of 2.9-oz/sq yd Vinyl-Coated Nylon Fabric at $\sigma_w/\sigma_f = 5:1$ and 1:5	86
4	Uniaxial Load-Extension Diagrams for 2.9-oz/sq yd Vinyl-Coated Nylon Fabric	87

LIST OF TABLES

Table		Page
Appendix 1		
1	Fabric Construction	74
2	Fabric Uniaxial Tensile Properties	74
Appendix 2		
1	Coated Fabric Uniaxial Tensile Properties	83

ABSTRACT

The overall goal of the program is the development of an instrument for determining the stress-strain response of coated fabrics used in the construction of air-supported tents.

During Phase I of the program a survey of the scientific literature on biaxial tensile testers was carried out. The purpose of the survey was to examine the design features and operating techniques of previously constructed testers and to note design innovations and shortcomings.

A theoretical analysis of the load-extension behavior of idealized plain-weave fabrics subjected to biaxial stresses is presented. Fabric strains resulting from both crimp interchange and yarn extension are considered. The analytical expressions derived have been solved with the aid of a digital computer for both linearly elastic and elasto-plastic materials. Time effects, although not explicitly included, are discussed.

Generalized plots of the results are given for the two extremes of initial fabric structure: (1) equal crimp distribution in both sets of yarns, (2) one set of yarns straight (noncrimped). The predicted and measured response of two model fabrics are compared.

Two typical coated fabrics representing approximately the extremes in fabric weight and strength currently of interest for air-supported tent applications were evaluated.

The design of an improved biaxial tensile tester is outlined. The proposed design concept utilizes the results of the literature survey, model fabric study and coated fabric evaluation.

BIAXIAL TENSILE TESTER FOR FABRICS

I. INTRODUCTION

A survey of the scientific literature which describes previous work with biaxial tensile testers has been completed. The purpose of the survey was to examine the design features and operating techniques of previously constructed biaxial tensile testers and to note desirable design innovations and obvious shortcomings. This information has contributed to the development of an improved testing-machine design concept which is ideally suited for the proposed work of examining the biaxial stress-strain behavior of fabrics used in construction of air-supported tent structures.

II. TEST-INSTRUMENT DESIGN CRITERIA

Performance requirements of the machine are listed in the schedule of the contract, and are reviewed here for reference:

A. General Requirements

1. Prime consideration shall be given to providing a reliable, rugged tester of minimum weight and size that can be quickly and simply installed, operated, and maintained under indoor textile and/or film laboratory conditions.

2. The following human engineering factors shall be integrated into the device.

   a. Safety in operation and maintenance

   b. Simplicity of maintenance

3. Environmental operating conditions

   Range 68° - 78°F db (dry bulb)
   56° - 68°F wb (wet bulb)

   Prime consideration is to be given for operation at

   70°F - db
   62°F - wb

4. The instrument shall be constructed to minimize maintenance and simplify necessary maintenance by the application of the following principles.

   a. Provide ready access to controls, lubrication fittings, adjustment controls, major components, and high-mortality parts. Use permanently lubricated bearings wherever feasible.

b. Use materials, finishes and fabrication techniques that minimize deterioration, lubrication, adjustments and painting

5. Electrical components shall be shielded and bonded to prevent radio interference, and comply with test provisions of Specification MIL-I-11748.

6. The contractor shall promptly inform the Contracting Officer of any modifications which may expedite fabrication, effect economies or improve capabilities.

B. Detailed Requirements

1. The machine shall be capable of applying loads on a fabric in two orthogonal directions simultaneously.

2. The test specimen size shall be appropriate for an accurate evaluation of the biaxial load-elongation characteristics of woven fabrics or films at low loads as well as at rupture.

3. The instrument shall have a load range of 10 lbs/inch to 800 lbs/inch.

4. Loading may be accomplished by the use of multiple loading devices.

5. The instrument shall be capable of measuring extensions up to 50%.

6. The ratio of the loads applied to the test specimen in the orthogonal directions shall be adjustable. Load ratios of 1:1 and 1:2 are essential. However, an effort should be made to obtain load ratios greater than 1:2.

7. The instrument should be capable of attaining the following accuracy for load and extension measurements:

Load application	± 2.5% of full scale
Extension	± 0.25% of gauge length

8. The instrument shall be equipped with automatic recording devices which will record load-elongation data in two directions

Detailed Requirements 1, 5 and 6 demand a flat test specimen, strained by the relative motions of two sets of jaws. They also rule out biaxial testing schemes based on inflated cylinder or inflated diaphragm-shaped specimens.

Flat, orthogonally loaded, biaxial tensile specimens can provide uniform force fields only at the specimen center, with nearly uniaxial forces acting in the areas adjacent to the jaws, and with stress concentrations localized in the corners generated by the two orthogonal jaw motions. Although this latter effect cannot be entirely overcome, it can be minimized by using cruciform test specimens, with the gripping jaws clamped to fabric tails extending away from the square biaxial stress field at the center of the specimen.

Klein[1] has proposed three conditions for biaxial tensile testing of fabric specimens. These are:

1. Straining must be such that a controlled biaxially strained region exists at the specimen center.

2. Strains must be measured in this region.

3. The ratio of the loads in the X and Y directions must be held constant at some predetermined value during a test.

   This is the characterizing parameter of the test

The relationships between stress and strain are, of course, properties of the particular specimen undergoing test. In a uniaxial tester either load or extension can be varied, usually at a constant rate, and the resulting change in the other variable measured. A biaxial tester must be capable of doing this in two directions simultaneously, with the added condition that the loads in the two directions must bear a fixed ratio to one another.

This latter consideration complicates any design using a motor and gear train jaw-drive system, because even with a constant rate of jaw motion in one direction, the complimentary jaw motion can be very complex, depending on the test specimen properties. It is much simpler to use a force-balance principal, and directly maintain the X and Y load ratio by a loading scheme which programs load level rather than jaw displacements. This suggests pneumatic cylinder load applicators with which output forces are always proportional to cylinder pressure and system displacements are dependent variables whose magnitudes are functions of load level and specimen properties.

Detailed Requirement 6 can be met with a ratio pressure control relay. This will allow the selection and pre-setting of a fixed ratio between the X-direction and Y-direction pressure levels. The test procedure will entail manually controlling excursion in the X direction from zero to full load; the pressure level in the Y direction will follow at the constant pre-set fraction of the instantaneous value in the X direction.

Each pair of opposing jaws must move equally and oppositely, to prevent inadvertent skewing of the specimen. These motions can be conveniently obtained in a symmetrical machine design which employs four pneumatic cylinders, one at each end of the specimen tails. Opposite pairs of cylinders are linked hydraulically to insure equal jaw motions. (See Figure 1.)

Detailed Requirement 3 requires load ranges from 10 to 800 lbs/inch of specimen width. Since the low end of this range requires only moderate operating forces, a test specimen with 4-inch wide tails is suggested to provide a generous central area for strain measurements in a uniform biaxial field. However, if the upper load limit of 800 lbs/inch is applied to a 4-inch wide specimen, the total force necessary is 3200 lbs. This would require either high operating pressures, or oversized pneumatic components which, in turn, would result in a loss of sensitivity at the lower force ranges. We suggest instead, the design compromise of using a smaller specimen at high force levels on the infrequent occasions when a very high strength specimen must be extended to rupture. A two-inch wide specimen at 800 lbs/inch requires only a 1600-lb operating force, which can be comfortably achieved with efficiently sized pneumatic components. If the machine force-application and force-measurement systems are designed for a maximum pull of 1600 lbs, loads up to 400 lbs/inch could be applied to four-inch wide specimens.

III. LITERATURE SURVEY

The scientific literature pertaining to experimental biaxial stress-strain measurement has been reviewed. The following citations refer to machines applicable to the testing of fabrics or other flat-sheet specimens. Apparatus for measuring combined stresses and strains in rods and tubes due to tension, torsion, or internal inflation pressure do not readily apply to the general flat-sheet material biaxial-loading problem and are not included in the following evaluation.

In 1953, Reichart, Woo and Montgomery[2] reported on a biaxial tester for fabrics. This apparatus was an adaptation of a standard, uniaxial, vertical tensile-testing machine which was fitted with supplementary horizontal jaws. These jaws were linked to the lower traveling jaw with tension rods and inclined wedges. Movement of the crosshead would result in a secondary transverse motion of the supplementary jaws at a fraction of the crosshead speed determined by the selection of the angle of the inclined plane. Loads were sensed with resistance load cells.

Checkland, Bull and Bacher[3], reported on a biaxial fabric tester which utilized a large four-jaw chuck as the mechanism for producing related biaxial jaw motions. This machine could provide only a 1:1 ratio of X and Y extensions. Forces were sensed with strain gauge load cells linked to the jaws, and strain information was obtained from successive photographs taken during the loading cycle.

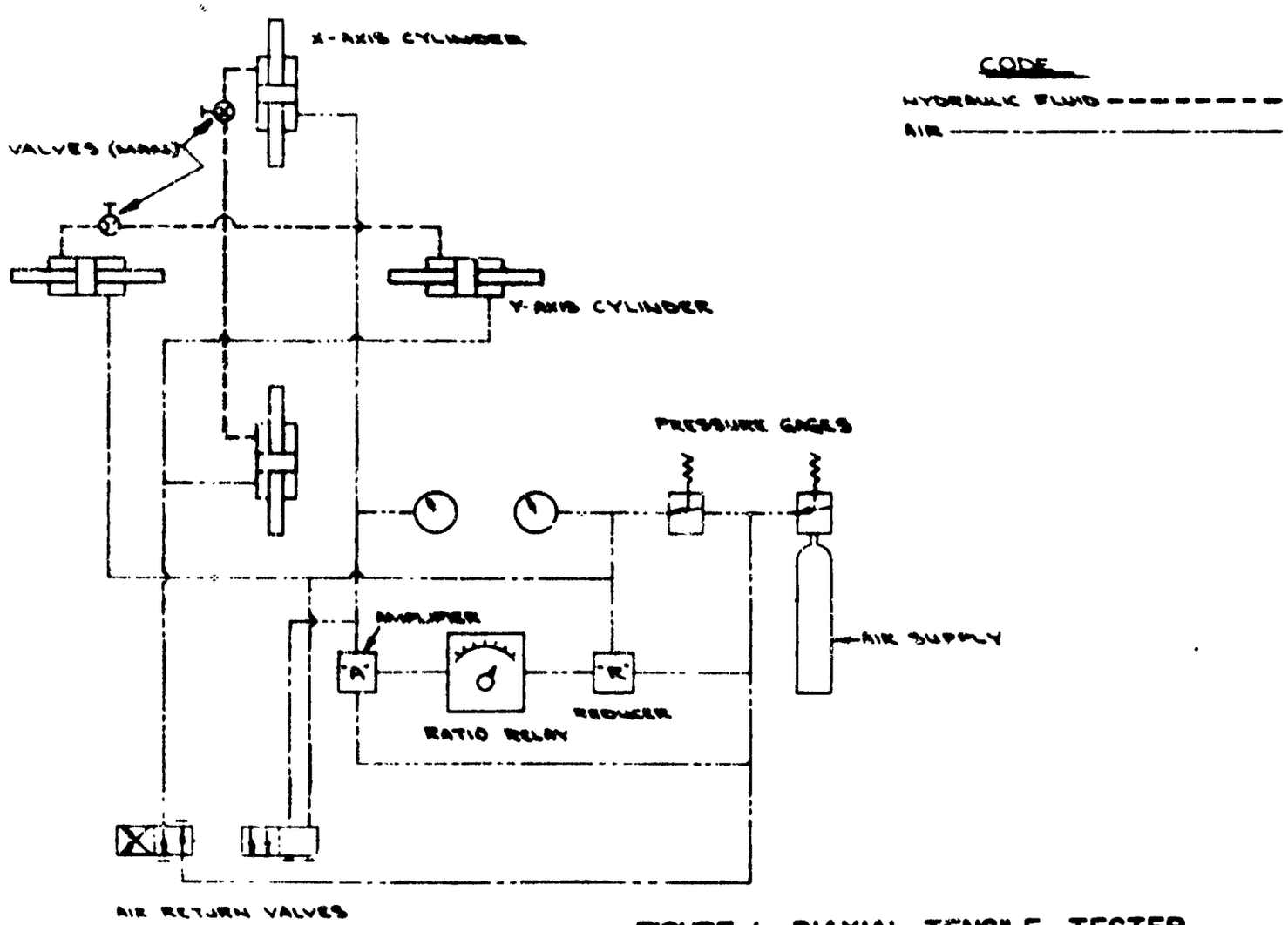

FIGURE 1. BIAXIAL TENSILE TESTER SCHEMATIC.

NOTES:
1) AIR LINES ¼" FITTINGS, ¼ OD TUBING
2) HYDRAULIC LINES ½ FITTINGS, ½ OD TUBING

In 1959, Klein[1] reported on a machine which met all the theoretical requirements for biaxial tensile testing. These included:

a. Controlled biaxial straining at the center region of the specimen.

b. Measurement of strains in this region.

c. Constant, pre-set ratio of X- and Y-direction load levels.

d. Cruciform specimen.

e. Capability for other than a 1:1 ratio of X and Y loads.

f. Autographic read-out of load and strain signals.

Operation of this device allowed jaw motion in one direction, ϵ_x, to proceed at a predetermined constant rate while the jaw motion in the other direction was controlled so that the load levels were maintained at a constant ratio. This can be described as a closed-loop automatic control system, with combined cascade and ratio control features.

Operating difficulties with this system stemmed from the fact that the fabric extensions and applied loads were measured and transduced as low-voltage electrical signals. After amplification and comparison of the signals, the overall system signal-to-noise ratio was not high enough to permit constant stable operation, and the charted machine output data was often erratic and unreliable.

Mönch and Galster[4] show that a cruciform, flat specimen shape with longitudinal slits in the tail sections can improve the uniformity of the biaxial force field at the specimen center.

San Miguel[5] built a biaxial machine for testing flat sheets of solid propellant rocket fuel. This was a controlled-extension system with a built-in capacity for transverse stretching of the pin-type grips to compensate for specimen deformation at high strains.

Davidson[6], describes a biaxial tensile tester for fabrics which employs a cruciform specimen. Loading is accomplished with a single hydraulic cylinder, a series of variable length lever arms and whiffle-trees serving to distribute force outputs to the four specimen jaws in a pre-selected fixed ratio. A noteworthy feature of this machine is the capability for programming shear loads to the specimen jaws, as well as direct tension loads. Force is measured with a spring-scale dynamometer linked to the main hydraulic cylinder, and strain measurements are obtained from successive photographs of this test specimen at specified load intervals.

This instrument is now installed at FRL® and was used in obtaining the experimental data presented in the Appendices.

Seshadri, Brown, Backer, Krizik and Mellen[7] utilized a biaxial fabric tensile tester at MIT to further their work on parachute fabrics. This machine is an accessory added to a standard floor-model Instron tensile tester. It consists of a frame which is driven up and down by two vertical lead screws linked with drive chains to the Instron crosshead drive and geared to produce a motion equal to one half of the crosshead motion. This frame carries clamp-type flat jaws which are separated manually by means of horizontal lead screws driven by a handwheel and gear train. Any desired load level can be applied in the horizontal direction while the specimen is strained by the Instron crosshead in the vertical direction. The chain linkage to the auxiliary loading frame keeps the cruciform specimen centered and prevents unwanted shear deformations. Loads are sensed by resistance strain-gauge load cells and recorded by means of strip chart recorders.

The principal operating difficulty with this device has been the inability to co-ordinate X- and Y-direction load programs. In one operating mode, the Instron jaws are operated at a constant rate to provide a uniform rate of jaw separation in one direction while an operator manipulates the horizontal loading screw in an effort to maintain a continuously balanced ratio of the changing X- and Y-load levels. Other loading modes are possible at specified load increments. The jaws along one axis can be separated to provide an incremental load increase and this jaw position maintained while the load along the other axis is increased by an appropriate increment. Specimen behavior observed with this kind of incremental loading is not the same as that observed during continuous loading. This substantiates the contention that a valid biaxial test procedure must provide for co-ordinated load programming along both axes.

McClaren and Best[8] describe a biaxial tensile-test machine used in their work on fatigue of metallic materials in a multi-axial stress field. This machine applied loads to the tails of a cross-shaped metallic sheet specimen The machine was another example of an adaptation of a standard vertical testing machine with a supplementary transverse loading frame. The interesting feature here is that the transverse loading frame is suspended from cables with counterweights and is free to move vertically as required to maintain symmetry of loading without unwanted shear loads applied to the specimen.

Becker[9] has demonstrated another system for adapting a standard uniaxial testing machine for biaxial deformations. This device employs two right-angle guide beams which are interlocked with sliding joints so that they form an expandable rectilinear frame. A sheet specimen is linked to the inside edge of this frame with a series of pins and clamping jaws. The entire frame is mounted in the tensile tester and oriented with the test machine axis at a pre-determined angle to the specimen and guide beams. Varying this angle provides an operating parameter for proportioning strains in the X and Y directions of the specimen. Horizontal and vertical load components are sensed with commercial strain-gauge load cells providing data for calculation of principal specimen loads. Specimen strains are measured with a cathetometer aimed at target figures imprinted on the specimen

Seshadri, Brown, Backer, Krizik and Mellen[7] utilized a biaxial fabric tensile tester at MIT to further their work on parachute fabrics. This machine is an accessory added to a standard floor-model Instron tensile tester. It consists of a frame which is driven up and down by two vertical lead screws linked with drive chains to the Instron crosshead drive and geared to produce a motion equal to one half of the crosshead motion. This frame carries clamp-type flat jaws which are separated manually by means of horizontal lead screws driven by a handwheel and gear train. Any desired load level can be applied in the horizontal direction while the specimen is strained by the Instron crosshead in the vertical direction. The chain linkage to the auxiliary loading frame keeps the cruciform specimen centered and prevents unwanted shear deformations. Loads are sensed by resistance strain-gauge load cells and recorded by means of strip chart recorders.

The principal operating difficulty with this device has been the inability to co-ordinate X- and Y-direction load programs. In one operating mode, the Instron jaws are operated at a constant rate to provide a uniform rate of jaw separation in one direction while an operator manipulates the horizontal loading screw in an effort to maintain a continuously balanced ratio of the changing X- and Y-load levels. Other loading modes are possible at specified load increments. The jaws along one axis can be separated to provide an incremental load increase and this jaw position maintained while the load along the other axis is increased by an appropriate increment. Specimen behavior observed with this kind of incremental loading is not the same as that observed during continuous loading. This substantiates the contention that a valid biaxial test procedure must provide for co-ordinated load programming along both axes.

McClaren and Best[8] describe a biaxial tensile-test machine used in their work on fatigue of metallic materials in a multi-axial stress field. This machine applied loads to the tails of a cross-shaped metallic sheet specimen. The machine was another example of an adaptation of a standard vertical testing machine with a supplementary transverse loading frame. The interesting feature here is that the transverse loading frame is suspended from cables with counterweights and is free to move vertically as required to maintain symmetry of loading without unwanted shear loads applied to the specimen.

Becker[9] has demonstrated another system for adapting a standard uniaxial testing machine for biaxial deformations. This device employs two right-angle guide beams which are interlocked with sliding joints so that they form an expandable rectilinear frame. A sheet specimen is linked to the inside edge of this frame with a series of pins and clamping jaws. The entire frame is mounted in the tensile tester and oriented with the test machine axis at a pre-determined angle to the specimen and guide beams. Varying this angle provides an operating parameter for proportioning strains in the X and Y directions of the specimen. Horizontal and vertical load components are sensed with commercial strain-gauge load cells providing data for calculation of principal specimen loads. Specimen strains are measured with a cathetometer aimed at target figures imprinted on the specimen

A. REFERENCES

1. Klein, Stress-Strain Response of Fabrics under Two Dimensional Loading, Textile Research Journal, Vol. XXIX, #10, October 1959

2. Reichert, Woo and Montgomery, Textile Research Journal, 23, 424 (1953).

3. Checkland, Bull and Bacher, Textile Research Journal, 28, 431 (1958).

4. Mönch and Galster, A Method of Producing a Defined Uniform Biaxial Tensile Stress Field, British Journal of Applied Physics, 1963, Vol. 14.

5. San Miguel, A Biaxial Tester, Bulletin, Third Meeting, Working Group on Mechanical Behavior, Chemical Propulsion Information Agency, APL, Johns Hopkins University.

6. Davidson, The Mechanical Behavior of Fabrics Subjected to Biaxial Stress, ML-TDR-64-239.

7. Seshadri, Brown, Backer, Krizik and Mellen, WADC Technical Report, 59-374.

8. McClaren and Best, Low Cycle Fatigue Performance of Materials in a Uniaxial and Multiaxial Stress Field, paper presented at Joint Meeting ASME, SAE, April 27-30, 1964 - Paper #843-B.

9. Becker, NASA Tech. Brief, 65-10189.

IV. MECHANICAL DESIGN FEATURES

A. Specimen

The machine is designed to accommodate flat specimens of fabric, sheet, or film. Specimens are cross-shaped to provide a biaxial force field at the center. The extended tails are connected to the four orthogonally aligned jaws. The instrument is capable of accommodating specimen widths up to four inches.

B. Jaws

Flat jaws are used with most specimens since no difficulty will be experienced with specimens failing at the jaw, a condition prevalent when this kind of jaw is used in uniaxial tensile testing. This confidence stems from the fact that the biaxial loading mode will produce higher localized stresses in the biaxial stress zone than the generally uniaxial stress levels which will occur near the jaws.

A specimen loading fixture is provided to aid in centering the specimen in the four jaws. This fixture accurately locates and positions the four jaws relative to each other so that the specimen can be lined up and clamped in each jaw successively without disturbing the alignment of the other jaws. When all four jaws are securely clamped, the entire assembly of jaws and specimens is secured into the machine loading frame without distorting the specimen. The alignment fixture is removed before the tensile test loads are applied.

Linkage between the jaws and the load application system are of two separate types. One of these is a pivoted link which permits the specimen tails to skew as required to balance any variations in yarn tensions across the fabric. The alternate linkage system is a rigid connection of the jaws to the force cylinders such that opposing jaw edges are always parallel and perpendicular to their complementary jaws on the other axis.

When a cruciform specimen is strained biaxially, the throughgoing yarns at the outer edges of the specimen tails are elongated more than than the throughgoing yarns at the centers of the specimen tails. This effect increases with increasing elongation and, of course, tends to distort the otherwise uniform biaxial stress field at the center of the specimen producing high localized stresses in the specimen corners. The effect is minimized by extending the length of the specimen tails to lessen the divergence angle of the throughgoing yarns from the jaw to the specimen center. The effect is further diminished by removing cross yarns from the specimen tail area or by carefully cutting slits parallel to the direction of pull in these tails.

The flat jaws are fabricated from high strength materials and can accommodate any of several different high-friction jaw facing materials including serrated, hardened metal and leather jaw faces. The clamping arrangement for the jaws features adjustable clamping screws to aid initially in positioning the specimen and a wedge action linkage which will increase the clamping force as the load increases.

C. Load Application System

Tension loads are generated by four identical pneumatic cylinders located along the X and Y jaw axes. They are double-rod-end cylinders with equal volumetric displacements and equal effective piston areas on both sides of the piston for motion in both directions. This permits a simple scheme for synchronizing the motion of opposing pairs of cylinders by displacing hydraulic fluid from behind the piston of one to the front end of the piston in the other as shown in Figure 1. This transfer of fluid is accomplished through a line with a variable restriction, or throttling, valve so that the rate of flow can be controlled. This control of fluid flow prevents any surging or stick-slip motion which might otherwise be manifested in the pneumatically driven system; it also provides a means for limiting the rate of travel of the testing-machine jaws. Compressed gas for system operation is furnished either from a compressed air system or from bottled nitrogen gas supplied through a suitable pressure reducing regulator valve. The standard pneumatic cylinders are shown in Figure 2.

A force-balancing type of ratio relay is the instrument which regulates the relative air pressure in the two separate loading axes of the machine. This relay is the heart of the system design providing the means for setting and maintaining constant ratios between the X-axis load and the Y-axis load levels.

D. Load Sensors

Measurement of the pulling load at the specimen jaws is accomplished with electronic load cells. These are standard commercial force transducers with electronic resistance strain gauges arranged in a four-arm Wheatstone Bridge circuit. Exictation voltage is supplied from batteries. Two load cells will also be provided for installation at opposite ends of the specimen to maintain the mechanical symmetry of the machine design.

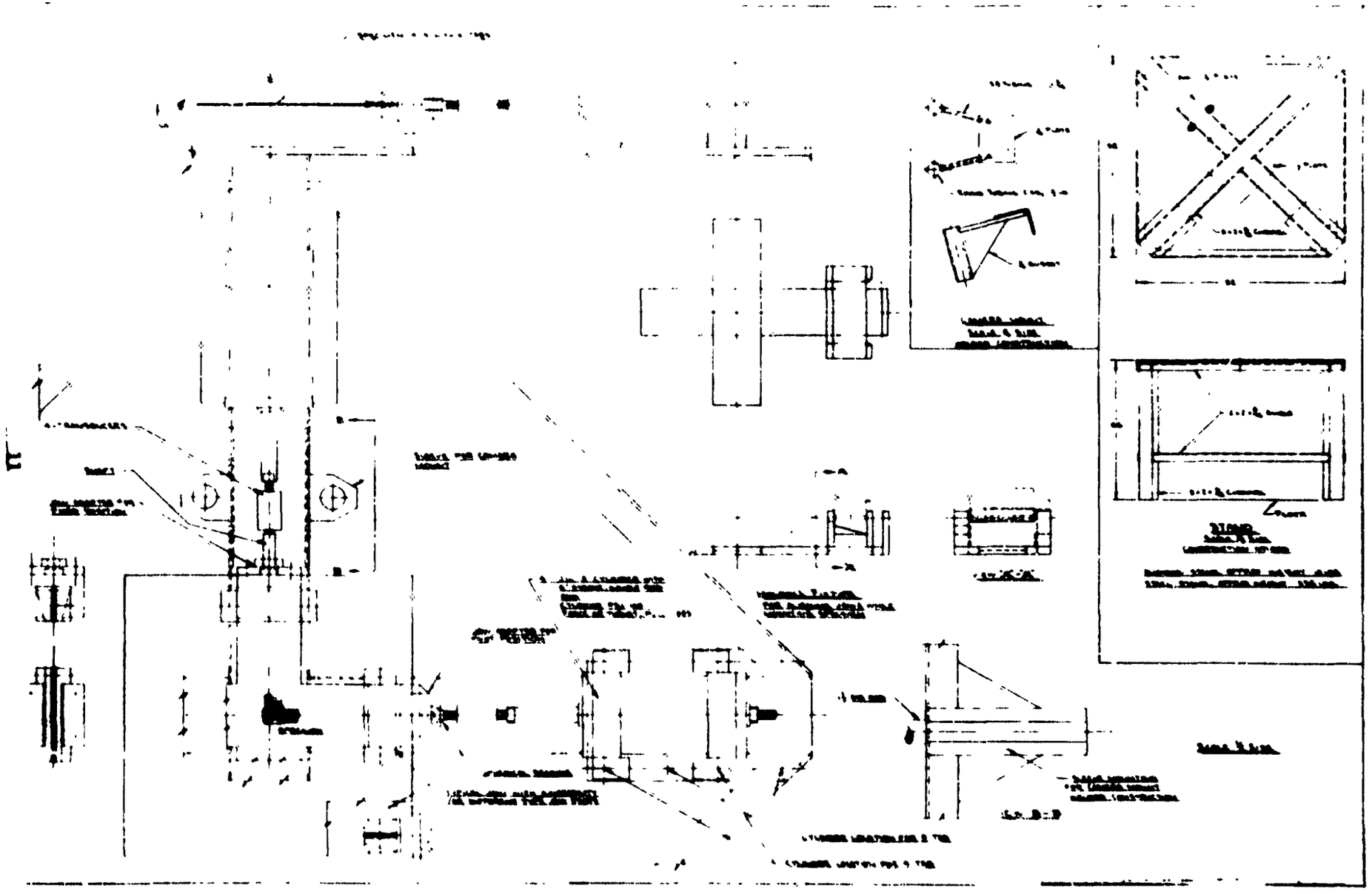

FIGURE 2. TEST INSTRUMENT LAYOUT.

E. Strain Sensors

Accurate measurement of strain in textile tensile specimens, which is always difficult, is doubly so for the case of biaxial testing. In uniaxial testing strain measurements are often derived from jaw separation measurements with corrections wherever necessary for slippage in capstan jaws, etc. With a cruciform test specimen jaw separation measurements are not accurate indications of dimensional changes in the biaxially stressed zone, therefore, strain measurements must be made directly on finite gauge lengths located entirely within the biaxially stressed zone. Our literature survey revealed that the most popular scheme for obtaining such measurements has been a system for photographing a two-dimensional gauge length target on the specimen at a number of load increments and later measuring the changes in specimen geometry recorded in the photographs. This provides accurate data with all kinds of specimens without the need for mechanical connections to the specimen or the involvement of any mechanisms which would possibly affect the specimen response. It is handicapped by a more involved data reduction procedure without the convenience of autographic recording of load and elongation relationships. The machine includes a camera and mounting equipment necessary for photographic elongation measurement.

The second scheme used is the direct attachment of mechanical links so the specimen gauge marks; dimensional changes are measured with suitable position-sensitive transducers. Position transducers having built-in electronic carrier wave and demodulating circuits and providing a d.c. voltage output for connecting directly to a recorder read-out instrument without other signal conditioning circuitry are used. Mechanical connection of the transducer probes to the specimen is made with needle points perforating the fabric at the gauge marks. (Obviously, this scheme will not be satisfactory with film specimens, or some kinds of coated fabrics, where the needle perforations would initiate stress concentrations. For these specimens the photographic strain-measurement technique would be utilized.)

F. Data Presentation

Electrical signals from the two strain-gauge load cells and from the two strain transducers are fed to the input stages of a four-channel, electronic, strip-chart recording system (Varian potentiometer type recorder.)

Instruments and controls are mounted on heavy-gauge aluminum panels supported in a standard relay rack enclosure as shown in Figure 3. This control station connects to the machine frame with ten-foot long air hoses and electrical cables with suitable connectors so that the control stand is conveniently oriented to the machine frame.

All other components of the test apparatus are mounted on the machine frame (see Figure 2). This is a welded steel structure, of table-top height, designed to support and align the force cylinders, specimen jaws, and associated parts. All hydraulic elements and piping are self-contained on the machine stand to eliminate liquid-line connections to the control stand and thereby minimize problems of leakage, air bleeding, etc. Pneumatic hoses which are connected to the control stand can readily be removed or reconnected with no interference with the machine operation.

General arrangement provides easy access for adjustments. Materials and finishes were selected for durability and compliance with the general requirements of the specifications.

The test instrument is shown in Figure 4, while Figure 5 is a photograph of the control panel

Scale:
1/2 size

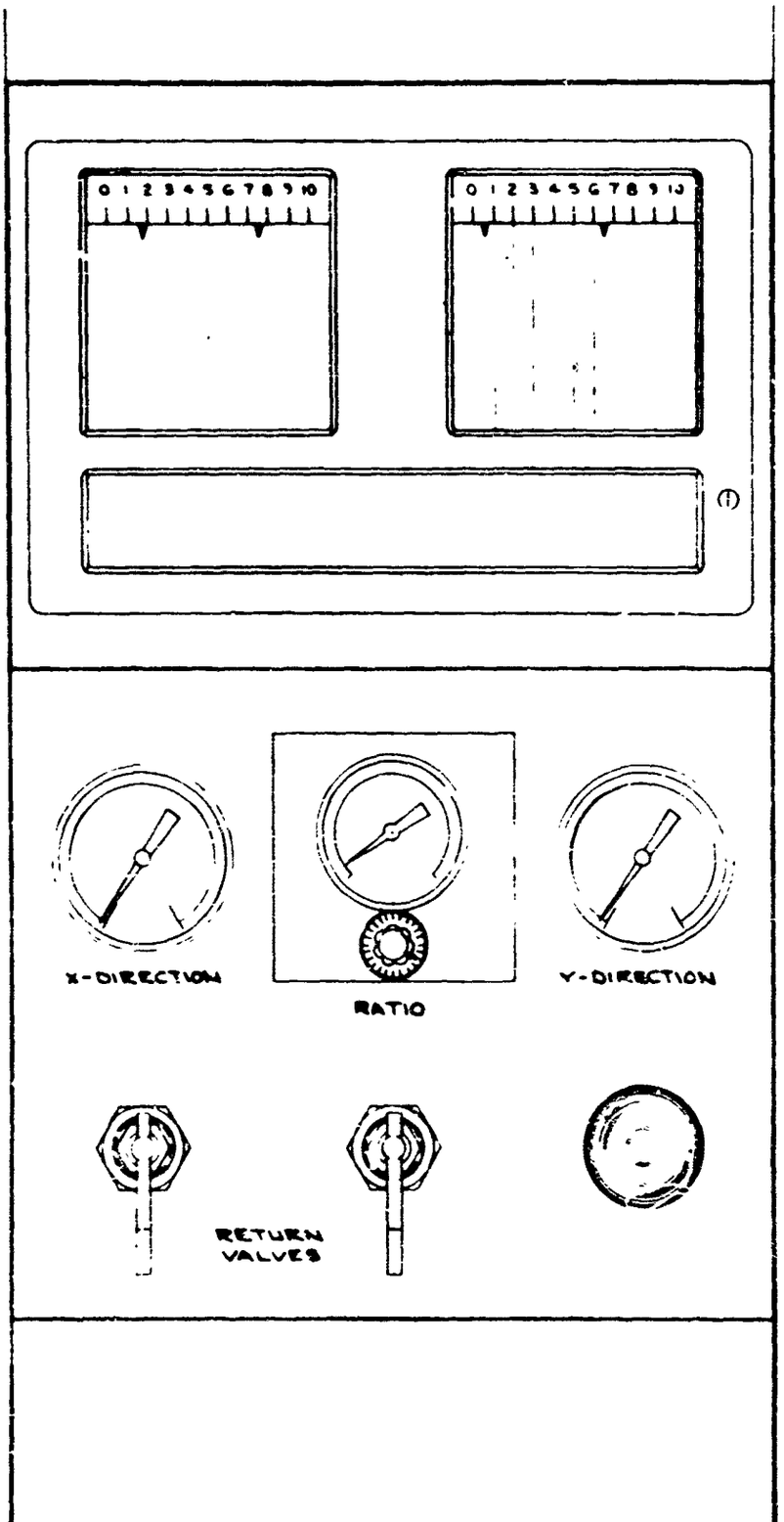

FIGURE 3. CONTROL PANEL LAYOUT.

Figure 4. Test Instrument

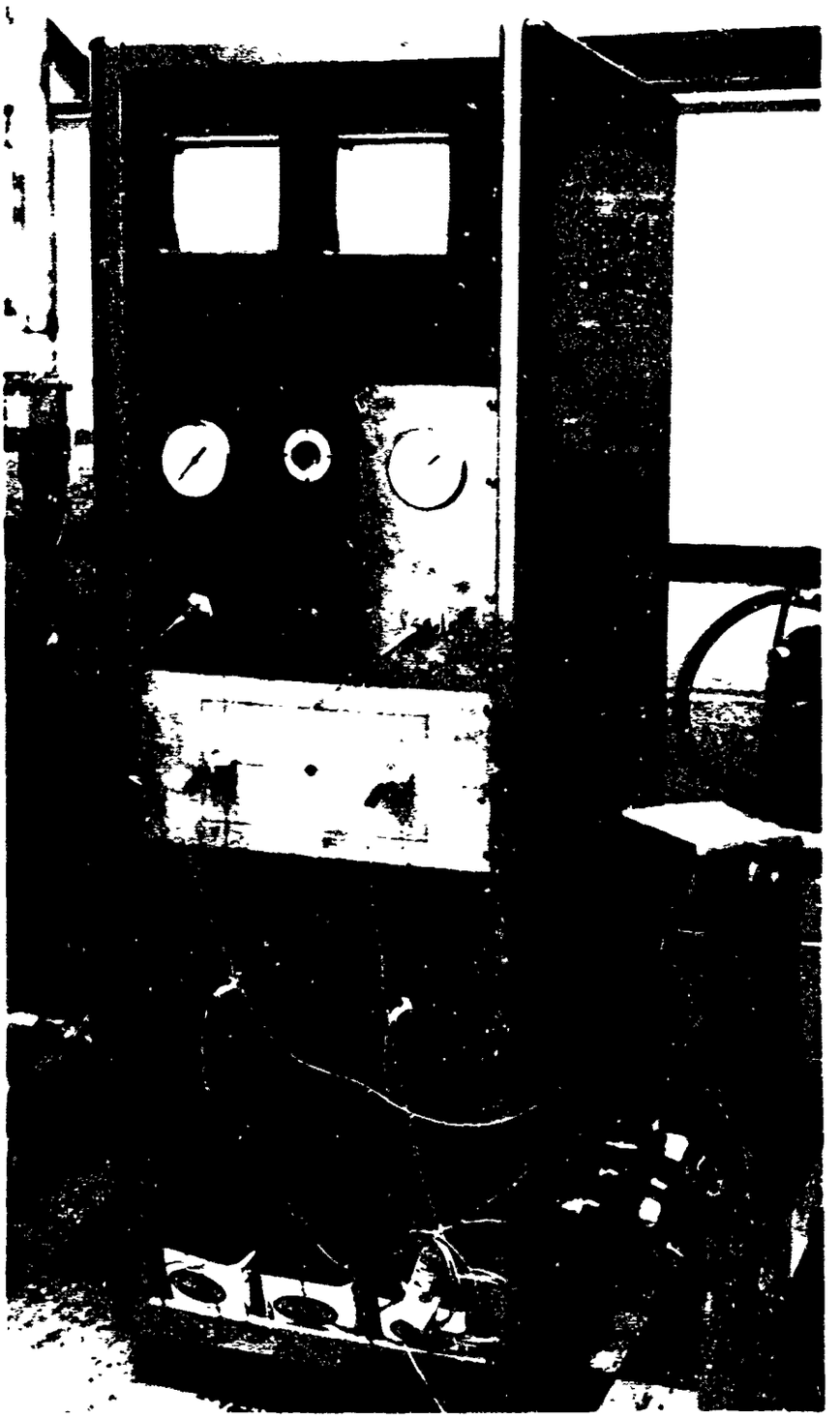

Figure 5. Control Panel

APPENDIX I

STRESS-STRAIN RESPONSE OF FABRICS UNDER TWO-DIMENSIONAL LOADING

LIST OF SYMBOLS

The symbols used in the analysis are:

A_y = yarn cross-sectional area

E_f = fiber modulus of elasticity

h_{1w} = maximum distance perpendicular to the fabric plane between cross-section centers of warp yarns before application of loads, i.e., the distance perpendicular to the fabric plane between warp yarn cross-section centers at two successive yarn crossovers

h_{2w} = same distance as h_{1w} but measured after application of loads

h_{1f} = maximum distance perpendicular to the fabric plane between cross-section centers of filling yarns before application of loads

h_{2f} = same distance as h_{1f} but measured after application of loads

L_w, L_{1w} = length of warp yarn between adjacent filling yarn centers before application of loads

L_{2w} = length of warp yarn between adjacent filling yarn centers after application of loads

L_f, L_{1f} = length of filling yarn between adjacent warp yarn centers before application of loads

L_{2f} = length of filling yarn between adjacent warp yarn centers after application of loads

L, L_1 = length of yarn between adjacent yarn centers before application of loads

L_2 = length of yarn between adjacent yarn centers after application of loads

N_{1w} = number of warp yarns per unit width of fabric before application of loads

N_{2w} = number of warp yarns per unit width of fabric after application of loads

N_{1f} = number of filling yarns per unit length of fabric before application of loads

N_{2f} = number of filling yarns per unit length of fabric after application of loads

N_1 = number of yarns per unit width of fabric before application of loads

N_2 = number of yarns per unit width of fabric after application of loads

n_f = number of fibers in yarn

p = yarn packing factor; ratio of the solid material contained in the yarn cross section to the area of the circumscribed circle enclosing the cross section $= \dfrac{n_f \pi r_f^2}{\pi R_y^2}$

P_y = total axial tensile load on a yarn

P_w = total axial tensile load on a warp yarn

P_f = total axial tensile load on a filling yarn

r = radial polar coordinate

r_f = fiber radius

R, R_y = yarn radius

R_{1w} = warp yarn radius before application of loads

R_{2w} = warp yarn radius after application of loads

R_{1f} = filling yarn radius before application of loads

R_{2f} = filling yarn radius after application of loads

T = yarn twist in turns per unit length

α = slope of post-yield region of the fiber tensile stress-strain diagram

$\beta = \left[\dfrac{3 \sin^2 \theta_s - \ln \sec^2 \theta_s}{2 \tan^2 \theta_a}\right]$

ϵ = tensile strain in a fiber; fractional fabric extension

ϵ_y = fractional yarn axial extension

ϵ^* = tensile yield strain in a fiber

ε_w = fractional fabric extension in the warp direction, $\varepsilon_w = \frac{N_{1f} - N_{2f}}{N_{2f}}$

ε_f = fractional fabric extension in the filling direction, $\varepsilon_f = \frac{N_{1w} - N_{2w}}{N_{2w}}$

θ = helix angle of a filament located at the radial position r in the yarn cross section

θ_{1w} = angle between the warp yarns and the fabric plane at the midpoint between yarn crossovers before application of loads; one-half the angle over which the warp yarn is in contact with the filling yarn at yarn crossovers, before application of loads to the fabric

θ_{2w} = angle between the warp yarns and the fabric plane at the midpoint between yarn crossovers after application of loads, one-half the angle over which the warp yarn is in contact with the filling yarn at yarn crossovers, after application of loads

θ_{1f} = angle between the filling yarns and the fabric plane at the midpoint between yarn crossovers before application of loads; one-half the angle over which the filling yarn is in contact with the warp yarn at yarn crossovers before application of loads to the fabric

θ_{2f} = angle between the filling yarns and the fabric plane at the midpoint between yarn crossovers after application of loads, one-half the angle over which the filling yarn is in contact with the warp yarn at yarn crossovers, after application of loads

θ_1 = angle between the yarns and the fabric plane at the midpoint between yarn crossovers before application of loads

θ_2 = angle between the yarns and the fabric plane at the midpoint between yarn crossovers after application of loads

θ_s = surface helix angle of a twisted yarn

σ = external load on the fabric per unit width of fabric, tensile stress acting on a fiber

σ^* = fiber tensile yield stress

σ_w = external load on the fabric warp yarns per unit width in the filling direction

σ_f = external load on the fabric filling yarns per unit width in the warp direction

μ = effective fabric Poisson's ratio

ν = yarn Poisson's ratio

INTRODUCTION

The tensile properties of fabrics are usually given in terms of loads and deformations applied and measured along only one axis. For many applications this data is adequate, it gives an index of relative strength. However, rarely are truly uniaxial loads imposed upon fabrics in the numerous applications in which they find use. In most instances loads are imposed simultaneously in more than one direction; e.g., the deformations at the knee or elbow of a garment, the canopy of a parachute, the walls of inflated structures, etc.

The efficient use of fabrics in these structures requires the development of precise design formulas. Additionally, as fabrics find more widespread use in complex military, aerospace, and industrial systems, stringent specifications on the biaxial stress-strain response of fabrics will have to be established. However, before design formulas and specifications can be written, a more thorough knowledge and understanding of the two-dimensional load-extension characteristics of fabrics than is presently available is required.

Although the stress-strain response of fabrics under two-dimensional loading has received the attention of previous researchers,[2, 4, 7, 9, 10, 16, 17, 18] analytical expressions that engineers can readily use have yet to be developed. The results reported herein are an initial attempt to fulfill this need. It is anticipated that further analysis, some of the basic work for which has been completed, will extend the practical and theoretical utility of the results.

In most fabric applications deformations out of the plane of the fabric are encountered and are the cause of the stresses in the fabric. However, these stresses can be considered membrane-type stresses, i.e., stresses acting in the plane of the fabric. It is therefore not necessary to consider explicitly out of plane deformations of the fabric center layer. Only loads and deformations applied and measured in the fabric plane have to be considered in determining the stress-strain response appropriate for most fabric applications. Since fabrics, in general, possess only two principal directions and the stresses in most fabric structures can be resolved into two orthogonal components, only loads and deformations simultaneously applied to and measured along two orthogonal axes are considered in this initial work. Loads or strains applied simultaneously along two axes are usually referred to as 'biaxial.'

The stress-strain response of fabrics under biaxial loading is strongly dependent on the ratio of the loads in the two directions. The appropriate ratio depends on the fabric application. In inflated spherically-shaped structures, the nominal loading ratio is 1:1; in inflated cylindrically-shaped structures, 2:1. Other structural shapes may impose higher ratios of loads.

Although it is possible to reduce the load-deformation analysis of a knitted fabric to a two-dimensional problem,[10, 15] this is not possible in the case of a woven fabric. The woven fabric model comparable to the two-dimensional

knitted fabric model is a planar array of crossed rods, each rod under uniaxial tension. Such a model would neglect crimp interchange, the major mechanism of fabric extension at low-to-moderate loads.

The complete deformation analysis of a biaxially-stressed woven fabric involves the use of a large number of parameters and the consideration of many deformation mechanisms. For example, eleven parameters are required to define the geometry of a plain-weave fabric and four to express the orthogonal components of stress and strain.[9, 10] The consideration of yarn structure and filament properties necessitates the introduction of more parameters.

The mechanisms involved in the deformation of a biaxially-stressed fabric include:

1. crimp interchange
2. change in angle between yarns (thread shear)
3. yarn bending
4. yarn flattening
5. yarn extension
6. friction between filaments; friction between yarns at crossovers
7. yarn nesting at yarn crossovers
8. yarn swelling
9. yarn and fabric rupture.

The loading sequence, loading rate, and load distribution (uniformity of stress distribution) also influence the deformation of a fabric.

An analysis of a biaxially-stressed woven fabric that includes all of the parameters, deformation mechanisms and their interrelationships, if it were possible to obtain, would no doubt be so unwieldy that it would be of no practical use to a design engineer. Rather than consider all of the interrelationships, an attempt has been made to understand separately some of the various mechanisms affecting fabric performance. It is assumed that an understanding of the separate phenomena will ultimately lead to a complete understanding of the stress-strain response of fabrics under two-dimensional loading.

A theoretical analysis of the load-elongation behavior of idealized plain-weave fabrics subjected to biaxial stresses is presented. Fabric strains resulting from both crimp interchange and yarn extension are considered. The analytical expressions derived have been solved with the aid of a digital computer for inextensible, linearly elastic and elasto-plastic materials. Results are obtained for yarn extension at constant radius and at constant volume. Generalized plots of the results are presented for the two extremes of initially square fabric structure: (1) equal crimp distribution in both sets of yarns, (2) one set of yarns straight (noncrimped). These plots give the fabric extension in both the warp and filling directions as a function of the loads applied along the warp and filling axes, the product of the yarn radius and number of yarns per unit width in the unloaded fabric, the yarn construction and the filament tensile properties.

Fabric Model

The initial geometric fabric model used duplicates that described by Peirce,[9] it assumes a structure composed of circular yarns which do not flatten or slip at yarn crossovers during fabric extension. This reduces the required number of geometric parameters to six: warp and filling yarn diameters, number of warp and filling yarns per unit width of fabric; angle between warp and filling yarns and the fabric plane at the mid-point between yarn crossovers. The complete list of assumptions and limitations imposed in the analyses are:

1. The fabric is a plain weave.
2. The yarns are uniform along their length, circular and do not flatten during application of loads to the fabric.
3. The fibers in the yarn are circular in cross section and their radii are negligibly small compared to the yarn radius.
4. The fibers fall into a rotationally symmetric array in cross-sectional view about the center of the yarn. Each fiber forms a perfect cylindrical helix about the yarn center line.
5. The fibers are homogeneous and linearly elastic for tensile stresses below the yield stress.
6. The elastic limit of the fibers in tension is sharply defined and the material exhibits linear work-hardening beyond the yield.
7. The influences of strain-rate, creep and stress relaxation on the response of the fibers is negligible.
8. The warp yarns are initially perpendicular to the filling yarns and remain so during loading.
9. Orthogonal yarns remain in contact during the loading cycle; there is no yarn slippage at yarn crossovers.
10. The radius of curvature of the yarn is equal to the sum of the yarn radii in the regions of yarn contact and equal to infinity between yarn crossovers.
11. The yarns are infinitely flexible (i.e., the yarns do not support any bending moments, $EI = 0$) and therefore support only tensile loads.
12. The intrinsic tensile response of the bent yarn is the same as that of the yarn when straight.
13. The fabric is loaded in its plane. The loads are uniformly distributed along the fabric edges. The load on the edges parallel to the filling yarns is parallel to the warp yarns, and the load on the edges parallel to the warp yarns is parallel to the filling yarns.

The geometry of the fabric model corresponding to the above assumptions is illustrated in Figure 1. Using the symbols shown in Figure 1 and further defined in the List of Symbols, it can be shown that for this fabric geometry, before loading:

$$\frac{1}{N_{1w}} = [L_{1f} - 2(R_{1f} + R_{1w})\,\theta_{1f}]\cos\theta_{1f} + 2(R_{1f} + R_{1w})\sin\theta_{1f} \tag{1}$$

$$\frac{1}{N_{1f}} = [L_{1w} - 2(R_{1f} + R_{1w})\,\theta_{1w}]\cos\theta_{1w} + 2(R_{1f} + R_{1w})\sin\theta_{1w} \tag{2}$$

$$h_{1f} = [L_{1f} - 2(R_{1f} + R_{1w})\,\theta_{1f}]\sin\theta_{1f} + 2(R_{1f} + R_{1w})(1 - \cos\theta_{1f}) \tag{3}$$

$$h_{1w} = [L_{1w} - 2(R_{1f} + R_{1w})\,\theta_{1w}]\sin\theta_{1w} + 2(R_{1f} + R_{1w})(1 - \cos\theta_{1w}) \tag{4}$$

$$h_{1w} + h_{1f} = 2(R_{1f} + R_{1w}) \tag{5}$$

(The validity of the relationship given in Equation (5) is seen more easily when the expression is written in the following form:

$$h_{1w} = R_w + R_f - h_{1f} + R_f + R_w; \quad \text{see Figure 1)}$$

and after loading:

$$\frac{1}{N_{2w}} = [L_{2f} - 2(R_{2f} + R_{2w})\,\theta_{2f}]\cos\theta_{2f} + 2(R_{2f} + R_{2w})\sin\theta_{2f} \tag{6}$$

$$\frac{1}{N_{2f}} = [L_{2w} - 2(R_{2f} + R_{2w})\,\theta_{2w}]\cos\theta_{2w} + 2(R_{2f} + R_{2w})\sin\theta_{2w} \tag{7}$$

$$h_{2f} = [L_{2f} - 2(R_{2f} + R_{2w})\,\theta_{2f}]\sin\theta_{2f} + 2(R_{2f} + R_{2w})(1 - \cos\theta_{2f}) \tag{8}$$

$$h_{2w} = [L_{2w} - 2(R_{2f} + R_{2w})\,\theta_{2w}]\sin\theta_{2w} + 2(R_{2f} + R_{2w})(1 - \cos\theta_{2w}) \tag{9}$$

$$h_{2w} + h_{2f} = 2(R_{2f} + R_{2w}) \tag{10}$$

In general, the geometric quantities describing the fabric structure in its initial configuration that are most easily measured are probably warp and filling yarn radii, R_{1w} and R_{1f}, and number of warp and filling yarns per unit width of fabric, N_{1w} and N_{1f}. Using these measured quantities and Equations (1) through (5), the lengths of warp and filling yarns between yarn crossovers, L_{1w} and L_{1f}, and the warp and filling yarn angles, θ_{1w} and θ_{1f}, can be determined for the two extremes of initial fabric geometry: (1) equal crimp distribution in both sets of yarns; (2) one set of yarns straight (noncrimped). For initial fabric geometries

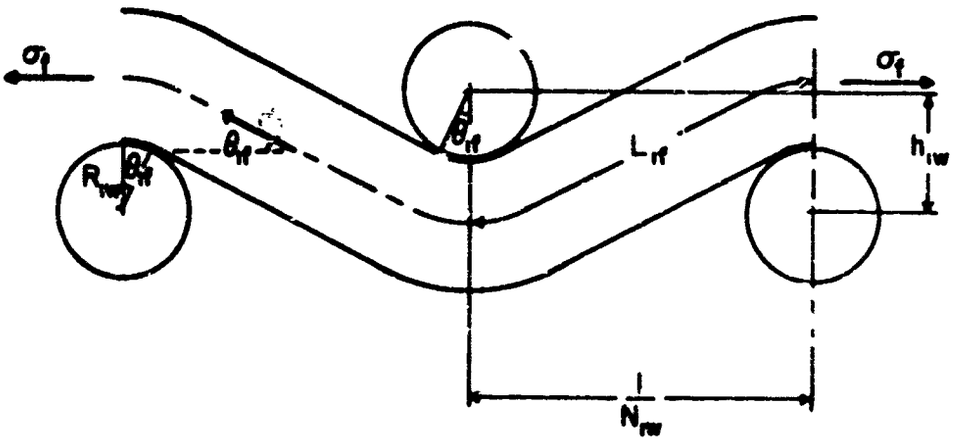

FIGURE 1. FABRIC MODEL.

between these two extremes, either the maximum distance between filling yarn cross-section centers, h_{1f}, the maximum distance between warp yarn cross-section centers, h_{1w}, the filling yarn crimp, or the warp yarn crimp as the yarn lays in the fabric is also required. However, these parameters are not easily determined, the fabric must be imbedded, sectioned and examined under a microscope.

Fabric Deformation

Referring to Figure 1 and using the equations of static equilibrium, i.e., summing the forces in the filling direction

$$\sigma_f = P_f \cos \theta_{2f} N_{2f}, \tag{11}$$

summing the forces in the warp direction

$$\sigma_w = P_w \cos \theta_{2w} N_{2w}, \tag{12}$$

and summing the components of the forces perpendicular to the fabric plane

$$P_w \sin \theta_{2w} - P_f \sin \theta_{2f} = 0. \tag{13}$$

In the case of uniaxial loading, Equation (13) shows that the yarns under stress are pulled out straight. However, in an actual fabric the yarns may become jammed before the crimp is completely pulled out. Jamming may also occur in a biaxially stressed fabric with certain combinations of initial fabric geometries and loading ratios. Therefore, the above analysis is only applicable when jamming does not occur. The jammed geometry of plain weave, round-yarn fabrics is discussed further in the next section.

If it is assumed that there is no axial yarn extension ($E = \infty$, $L_{2w} = L_{1w}$, $L_{2f} = L_{1f}$, $R_{2w} = R_{1w}$ and $R_{2f} = R_{1f}$) during fabric loading, the analysis of the fabric load-extension behavior can be reduced to four simultaneous algebraic equations [Eqs. (6), (7), (10), and (13), where Eqs. (8) and (9) are substituted in Eq. (10) and Eqs. (11) and (12) into (13)] in the four unknowns θ_{2f}, θ_{2w}, N_{2f}, and N_{2w}. These four equations are independent of the filament and yarn properties. They are a function only of the original fabric geometry and the loading ratio, and not of the magnitudes of the individual loads. To solve the equations the fabric loading ratio, σ_w/σ_f; initial yarn spacing, $1/N_{1w}$ and $1/N_{1f}$; yarn radii, R_{1f} and R_{1w}; and yarn lengths between crossovers, L_{1f} and L_{1w}, must be known. The latter two parameters are determined from Equations (1) through (5), as discussed previously.

If yarn extension during fabric loading is considered, ($L_{2w} \neq L_{1w}$ and $L_{2f} \neq L_{1f}$), Equations (11) and (12) become coupled with Equations (6) through (10). The functional relationship between the tensile loads, P_f and P_w, on the yarns in the fabric and the yarn construction, filament properties and change in yarn length between crossovers is developed below.

It is assumed that the load-elongation diagram of the fabric yarns in the zero-twist state can be represented by

$$P_y = \sigma p A_y = a + b\epsilon \tag{14}$$

where the yarn cross-sectional area, $A_y = \pi R_y^2$, p = yarn packing factor $= n\pi r_f^2/\pi R_y^2$, n_f = number of fibers in the yarn, r_f = fiber radius, R_y = yarn radius, ϵ = yarn or fiber tensile strain, σ = tensile stress (force per unit area) acting on a fiber, and a and b are constants. The case of the yarn radius remaining constant during yarn extension ($\nu = 0$) is considered first.

If the fibers are linearly elastic, $\sigma = E_f\epsilon$, where E_f is the fiber modulus of elasticity, and $a = 0$, $b = pA_yE_f$ in Equation (14). Similarly, if the fibers are elasto-plastic and exhibit linear work-hardening beyond the yield, $\sigma = \sigma^* + \alpha(\epsilon - \epsilon^*) = E_f\epsilon^* + \alpha(\epsilon - \epsilon^*)$[3], where σ^* is the fiber yield stress, ϵ^* the fiber yield strain in tension, and α the slope of the post-yield region of the fiber tensile stress-strain diagram. Therefore, for the elasto-plastic material $a = (\sigma^* - \alpha\epsilon^*)pA_y = \epsilon^*(E_f - \alpha)pA_y$ and $b = \alpha pA_y$.

Neglecting pressures transverse to the fiber axis,[6] friction between fibers and yarn radial growth with increasing yarn twist, the total axial load on an idealized, close-packed, twisted yarn is given by[11, 12, 14]

$$P_y = 2\pi p\int_{r=0}^{R_y}\sigma r\cos^2\theta dr = \frac{2\pi}{A_y}\int_0^{R_y}(a + b\epsilon_y\cos^2\theta)\, r\cos^2\theta dr, \tag{15}$$

where ϵ_y is the fractional yarn extension, $\epsilon = \epsilon_y\cos^2\theta$.[13] Carrying out the indicated integration it can be shown that

$$P_y = \frac{\pi}{A_y}\left[\frac{a}{(4\pi^2T^2)}\ln(1 + 4\pi^2T^2R_y^2) + b\epsilon_y\frac{R_y^2}{1 + 4\pi^2T^2R_y^2}\right] \tag{16}$$

where T is the yarn twist in turns per unit length. This expression can be rewritten in the following form

$$P_y = \frac{1}{\tan^2\theta_s}\left[a\ln\sec^2\theta_s + b\epsilon_y\sin^2\theta_s\right] \tag{17}$$

where θ_s is the surface helix of the twisted yarn. If the first term is expanded in a power series and the higher order terms are neglected, Equation (17) can be reduced to the following simplified form

$$P_y = \left[a(1 - \frac{1}{2}\tan^2\theta_s) + b\epsilon_y\cos^2\theta_s\right] \tag{18}$$

or $P_y = A + B\epsilon_y$, (19)

where $A = 0$, $B = pE_fA_y\cos^2\theta_s$ for linearly elastic materials

and $A = p\epsilon^*(E_f - \alpha)A_y(1 - \frac{1}{2}\tan^2\theta_s)$

$B = p\alpha A_y\cos^2\theta_s$ for elasto-plastic materials [i.e., if $\sigma = \sigma^* + \alpha(\epsilon - \epsilon^*)$]

In light of the above relations and noting that the extension of the filling yarns in the fabric is given by $\epsilon_y = (L_{2f} - L_{1f})/L_{1f}$, and similarly for the warp yarns by $\epsilon_y = (L_{2w} - L_{1w})/L_{1w}$, Equations (11) and (12) can be rewritten in the following form

$$\sigma_f = N_{2f}\left[A + B\left(\frac{L_{2f}}{L_{1f}} - 1\right)\right]\cos\theta_{2f} \tag{20}$$

$$\sigma_w = N_{2w}\left[A + B\left(\frac{L_{2w}}{L_{1w}} - 1\right)\right]\cos\theta_{2w} \tag{21}$$

If constant volume yarn extension ($\nu = 1/2$) is assumed instead of constant yarn radius as above, Equation (15) takes the following form[13]

$$P_y = \frac{2\pi}{A_y}\int_{r=0}^{R_y}\left[a + b\frac{\epsilon_y}{2}(3\cos^2\theta - 1)\right] r\cos^2\theta dr. \tag{22}$$

After carrying out the indicated integration, an expression identical to Equation (19) is obtained with $A = 0$ and $B = pE_fA_y[3\sin^2\theta_s - \ln\sec^2\theta_s]/2\tan^2\theta_s$ when $\sigma = E_f\epsilon$. Additionally, σ_f and σ_w are given by Equations (20) and (21), as for the previous case. It can also be shown that for constant-volume yarn extension

$$R_{2f} = R_{1f}\sqrt{L_{1f}/L_{2f}}, \tag{23}$$

$$R_{2w} = R_{1w}\sqrt{L_{1w}/L_{2w}}. \tag{24}$$

Limiting Fabric Geometries

As previously noted, the derivation of the foregoing expressions for predicting the response of fabrics under biaxial tensile loading does not take into account the possibility of geometric limitations at large fabric extensions. Careful analysis of the idealized fabric model being used shows that there are three possible limiting geometries.[8, 9, 16] The descriptions of these given below assume that the load applied in the warp direction is equal to or greater than the load applied in the filling direction ($\sigma_w \geq \sigma_f$).

1. Warp yarns pulled straight - If $L_{2f}/(R_{2f} + R_{2w}) \geq 2\pi$ as $\sigma_w/\sigma_f \to \infty$ the warp yarns can be pulled straight. When this occurs

$$\frac{1}{N_{2f}} = L_{2w}. \tag{25}$$

This limiting geometry, if attained, defines the maximum fabric extension possible from crimp interchange. Any further fabric extension requires yarn elongation.

2. Maximum filling contraction - The fabric extension in the warp direction can be limited by the inability of the fabric to contract further in the filling direction. This occurs when the maximum possible crimp has been developed in the filling yarn. If the loads applied to the fabric are greater than the level which just results in the development of this maximum filling yarn crimp, solutions to Equations (6) through (13) can be obtained which result in physically impossible fabric deformations.

The filling yarn crimp is at its maximum when there are no straight sections along the filling yarn length, i.e., when $L_{2f}/(R_{2f} + R_{2w}) < 2\pi$ (see Figure 2). Under these conditions

$$L_{2f} = 2(R_{2f} + R_{2w})\,\xi_{2f}, \tag{26}$$

and from Equation (6)

$$\frac{1}{N_{2w}} = 2(R_{2f} + R_{2w}) \sin\left(\frac{L_{2f}}{2(R_{2f} + R_{2w})}\right) \tag{27}$$

The corresponding filling yarn spacing is determined from Equations (7) through (13).

Assuming a fabric woven from inextensible yarns, the above limiting geometry can be readily determined. It is given simply by

$$\left(\frac{1}{N_{2w}}\right)_{\text{minimum}} = 2(R_{1f} + R_{1w}) \sin\left(\frac{L_{1f}}{2(R_{1f} + R_{1w})}\right) \tag{28}$$

3. Contact between adjacent warp yarns - The fabric extension in the warp direction can also be limited by adjacent warp yarns coming into contact with each other.[16] When this occurs and, simultaneously, maximum crimp is developed in the filling yarns, it can be shown from Figure 3 that

$$\theta_{2f} = \frac{L_{2f}}{2(R_{2f} + R_{2w})}, \tag{29}$$

$$\sin \theta_{2f} = \frac{2R_{2w}}{2(R_{2f} + R_{2w})}, \tag{30}$$

and

$$\frac{1}{N_{2w}} = 2R_{2w}. \tag{31}$$

If $R_{2f} = R_{2w}$, $\sin \theta_{2f} = 1/2$, $\xi_{2f} = \pi/6 = 30°$, and $L_{2f}/2(R_{2f} + R_{2w}) = \pi/6 \cong 0.5236$.

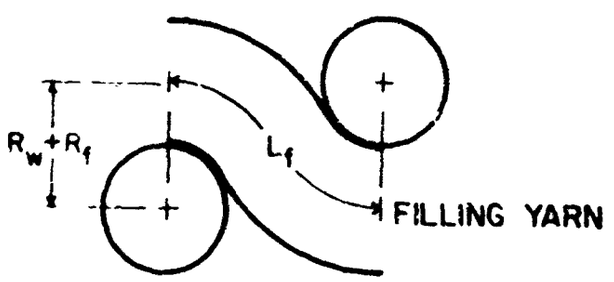

FIGURE 2. LIMITING FABRIC GEOMETRY; MAXIMUM FILLING CONTRACTION.

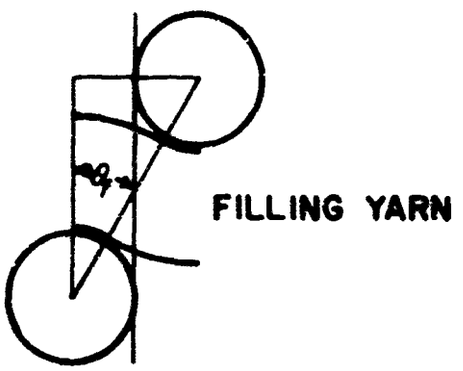

FIGURE 3. LIMITING FABRIC GEOMETRY; CONTACT BETWEEN ADJACENT WARP YARNS.

The minimum value of filling yarn length possible when warp yarns are touching occurs when the filling yarn is straight. For this case

$$L_{2f} = 2R_{2w} = \frac{1}{N_{2w}} . \tag{32}$$

Therefore, contact between adjacent warp yarns can only occur when $0.500 \leq L_{2f}/2(R_{2f} + R_{2w}) \leq 0.5236$, assuming $R_{2f} = R_{2w}$. The corresponding filling yarn spacing for this limiting geometry is calculated from Equations (7) through (13). (As pointed out in a later section, this type of limiting geometry has not been encountered for any of the fabric geometries and loading conditions examined to date.)

Although the limiting geometries are readily determined when it is assumed that the fabrics are woven from inextensible yarns, there does not appear to be a direct method for determining the second or third type of limiting geometry when the effects of yarn extension are included. However, an indirect approach is given in a later section.

ANALYTICAL RESULTS

The analytical expressions derived above for the load-extension behavior of idealized plain-weave fabrics subjected to biaxial stresses have been solved for various combinations of initial fabric geometries and filament properties. The Newton-Raphson iterative method for the solution of simultaneous nonlinear algebraic equations and an IBM 7094 digital computer were used to obtain the solutions. Descriptions of the cases solved and the results obtained are given below.

Solutions are given first for the case of no axial yarn extension ($E = \infty$), during fabric loading. Only the contribution of crimp interchange to the load-extension response of the biaxially stressed fabrics is considered. Results are given for the two extremes of initial fabric structure: (1) equal crimp distribution in both sets of yarns; (2) one set of yarns straight (noncrimped). As noted previously, the results are a function only of the loading ratio σ_w/σ_f and not of the magnitudes of the imposed loads.

Square Fabric, Inextensible Yarn - Crimp Interchange

For initially square, plain-weave fabric with the same infinitely flexible and inextensible yarn in both the warp and filling

$$N_{1w} = N_{1f} = N_1$$

$$R_{1f} = R_{1w} = R_{2f} = R_{2w} = R$$

$$\theta_{1f} = \theta_{1w} = \theta_1$$

$$L_{1f} = L_{1w} = L_{2f} = L_{2w} = L$$

With these assumptions, Equations (1) through (5) describing the geometry of the fabric in the unloaded state reduce to the following two simplified expressions

$$N_1 R = \frac{\sin \theta_1}{2(2 - \cos \theta_1)} \tag{33}$$

$$\frac{L}{R} = \frac{1}{N_1 R \cos \theta_1} + 4\theta_1 - 4 \tan \theta_1 \tag{34}$$

The dimensionless parameter, $N_1 R$, the product of the yarn radius and number of warp (or filling) yarns per unit length of fabric before application of the loads, is plotted in Figure 4 as a function of θ_1, the angle between the warp (or filling) yarns and the fabric plane at the mid-point between yarn crossovers before loading. As shown, $N_1 R = 0$ at $\theta_1 = 0$, increases with increasing θ_1 up to an angle of 60° and decreases beyond this angle.

Similarly, the dimensionless parameter, L/R, the ratio of the length of warp (or filling) yarn between yarn crossovers before, during, and after loading, to the yarn radius, is plotted in Figure 5 as a function of θ_1. As shown, L/R approaches infinity as θ_1 approaches 0°, decreases with increasing θ_1 up to an angle of 60°, and increases slightly above this angle.

L/R is plotted as a function of $N_1 R$ in Figure 6. As shown, as $N_1 R$ approaches zero, L/R approaches infinity, and at $N_1 R$ values ≥ 0.25, L/R is not a single-valued function. Therefore, to simplify the computer programming, in all the computations presented below which assume an initially square fabric, only $N_1 R$ values ≤ 0.24 are used. Since the maximum value of $N_1 R$ possible in an initially square, plain-weave fabric is 0.289, $\theta_1 = 60°$ (see Limiting Fabric Geometries, #2), not much is lost in using only values of $N_1 R \leq 0.24$. $N_1 R = 0.05$ corresponds to an angle θ_1 of 5.4°; $N_1 R = 0.24$, to 34.3°.

For the initially square, plain-weave fabric woven from infinitely flexible, inextensible yarns, substitution of Equations (8) and (9) into Equation (10) and Equations (6), (7), (11), and (12) into Equation (13), gives the following two simultaneous equations in the two unknowns θ_{2w} and θ_{2f}

$$\left(\frac{L}{4R} - \theta_{2w}\right) \sin \theta_{2w} - \cos \theta_{2w} = \left(\cos \theta_{2f} - 1\right) - \left(\frac{L}{4R} - \theta_{2f}\right) \sin \theta_{2f} \tag{35}$$

$$\cos \theta_{2w} \left[\left(\frac{L}{4R} - \theta_{2w}\right) \cot \theta_{2w} + 1\right] = \left(\frac{\sigma_w}{\sigma_f}\right) \cos \theta_{2f} \left[\left(\frac{L}{4R} - \theta_{2f}\right) \cot \theta_{2f} - 1\right] \tag{36}$$

Once θ_{2w} and θ_{2f} are determined, $N_{2f}R$ and $N_{2w}R$ can be obtained from Equations (6) and (7) which reduce to the following two expressions for this case.

$$\frac{1}{N_{2f}R} = \left(\frac{L}{R} - 4\theta_{2w}\right) \cos \theta_{2w} + 4 \sin \theta_{2w} \tag{37}$$

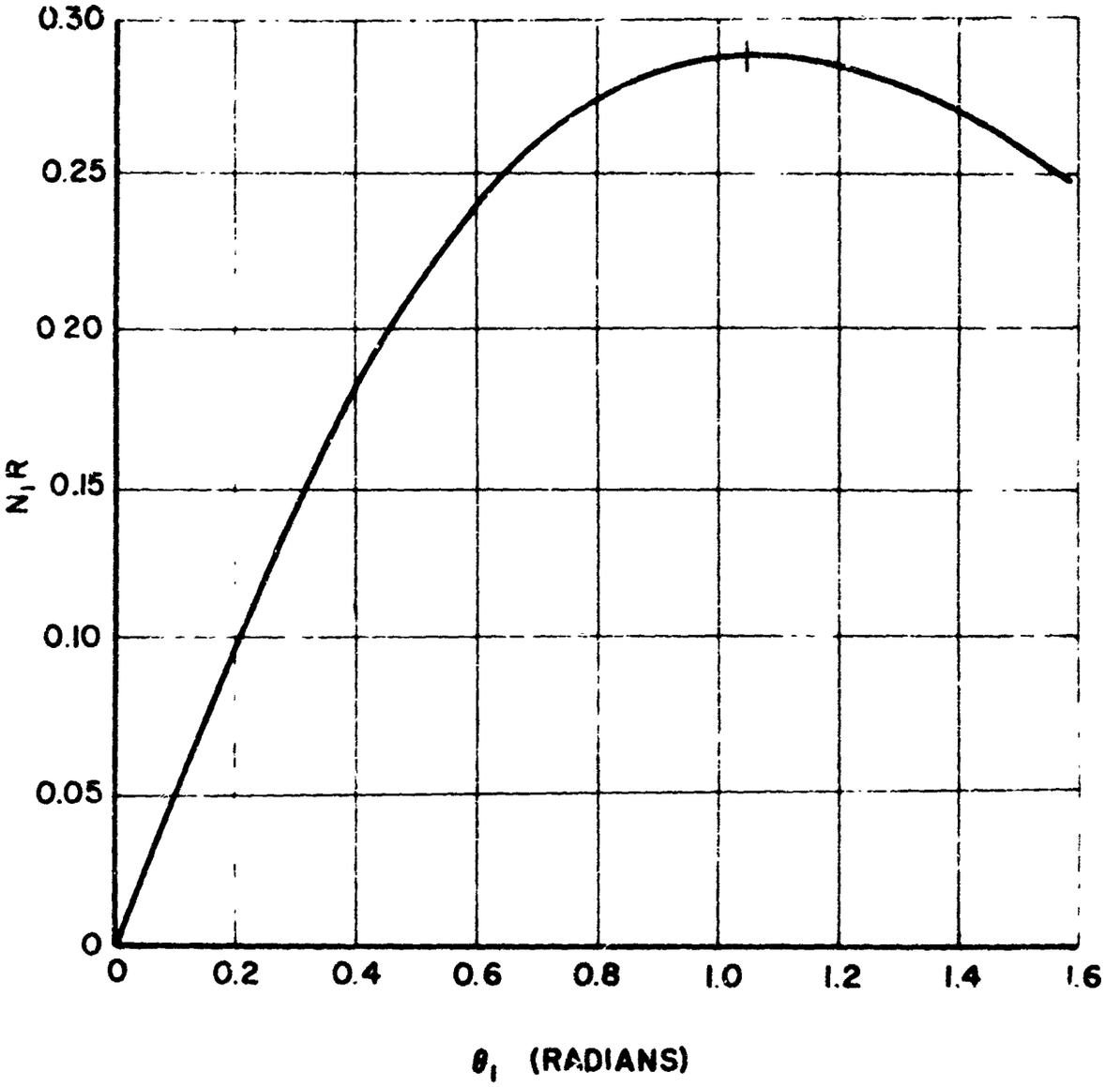

FIGURE 4. N_1R VS θ_1 FOR A SQUARE FABRIC WITH INEXTENSIBLE YARN.

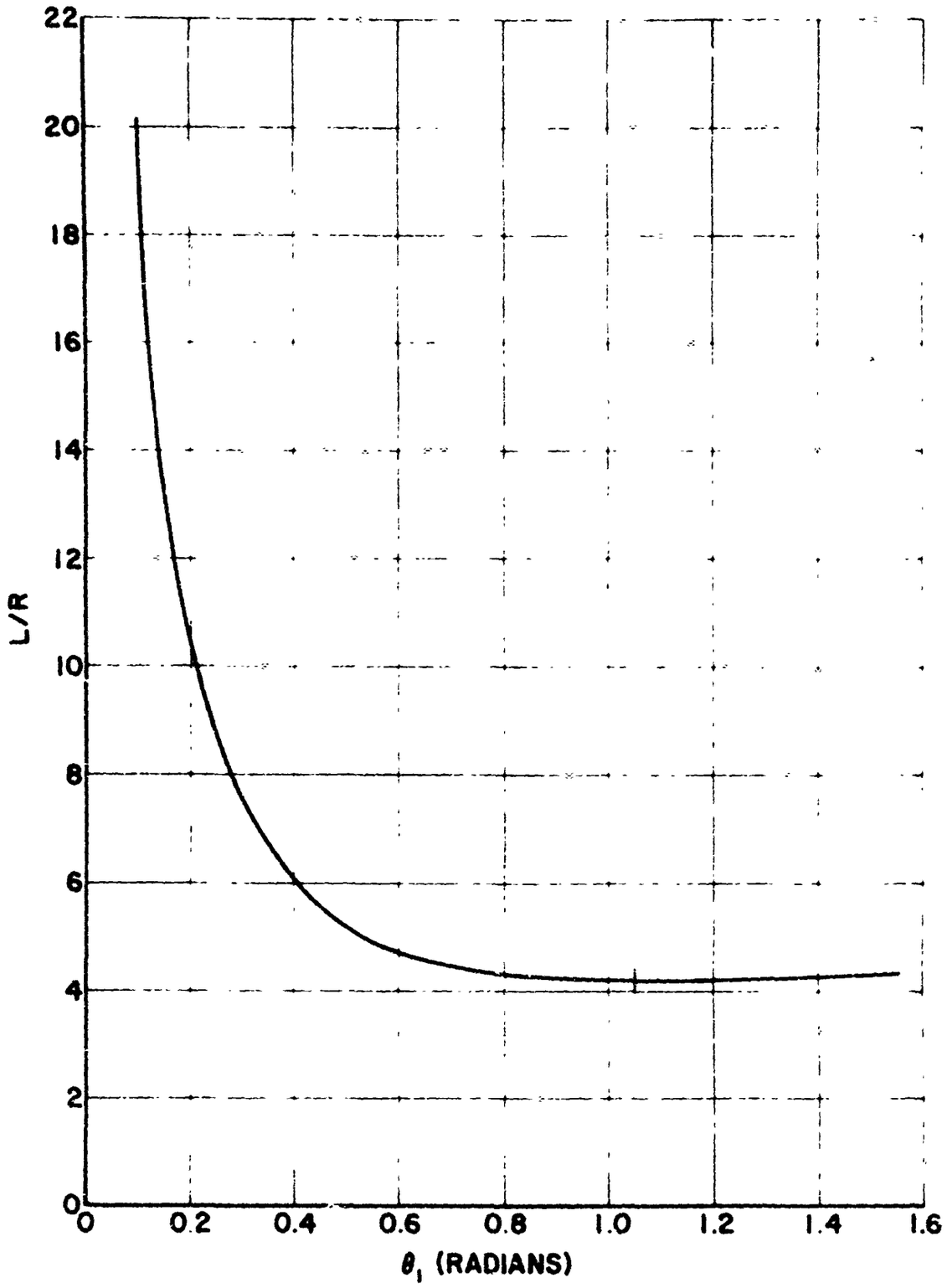

FIGURE 5. L/R VS θ_1 FOR A SQUARE FABRIC WITH INEXTENSIBLE YARN.

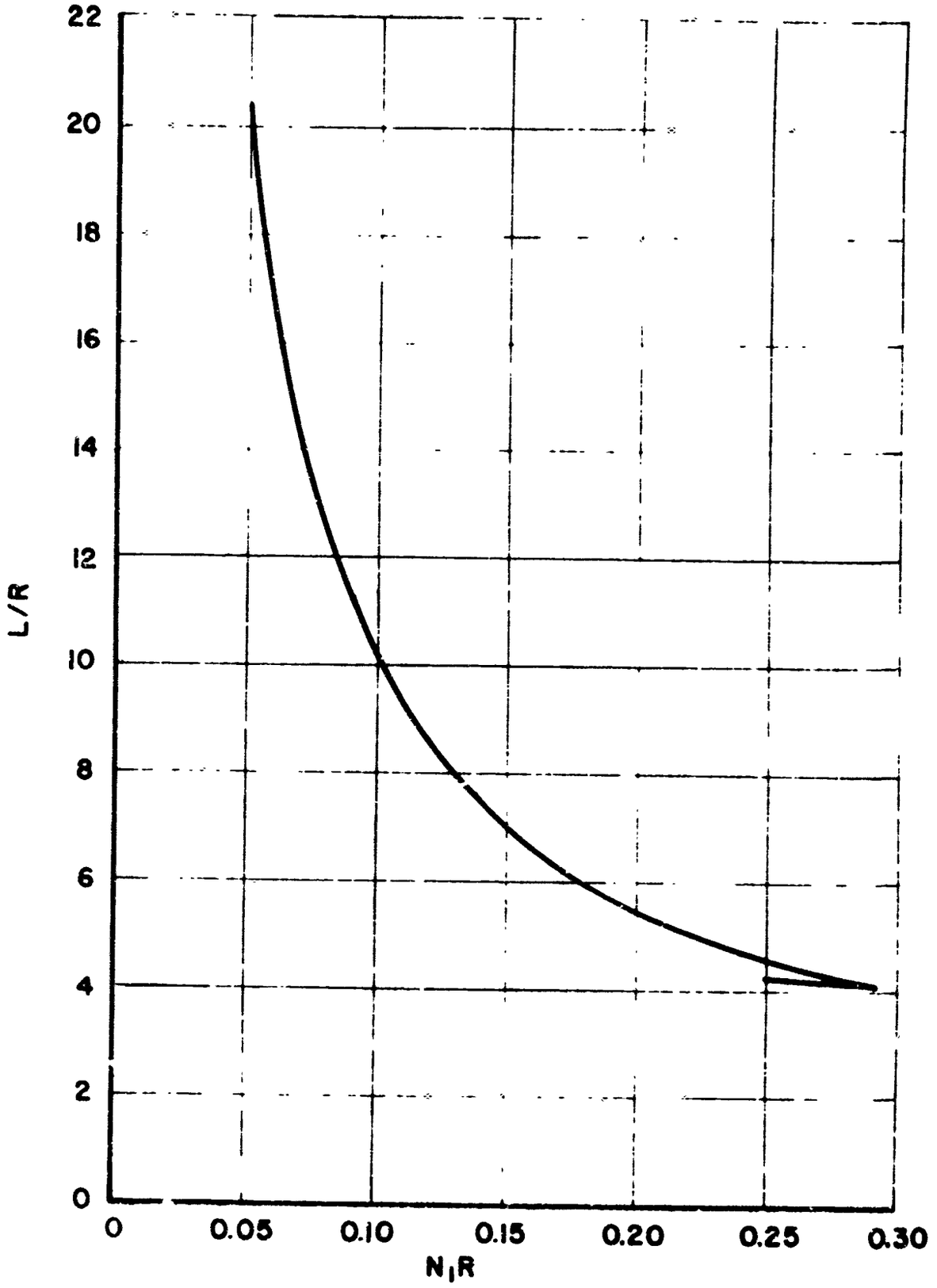

FIGURE 6. L/R VS N_1R FOR A SQUARE FABRIC WITH INEXTENSIBLE YARN.

$$\frac{1}{N_{2w}R} = \left(\frac{L}{R} - 4\theta_{2f}\right)\cos\theta_{2f} + 4\sin\theta_{2f} \tag{38}$$

The fractional fabric extensions in the warp an filling directions, ϵ_w and ϵ_f, are then given by the following two expressions

$$\epsilon_w = \left(\frac{N_1 R}{N_{2f} R} - 1\right) \tag{39}$$

$$\epsilon_f = \left(\frac{N_1 R}{N_{2w} R} - 1\right) \tag{40}$$

where a positive value for ϵ_w signifies an increase in the fabric length and similarly a positive value for ϵ_f, an increase in the fabric width.

Equations (33) through (40) were solved for $N_1 R$ = 0.240, 0.220, 0.200, 0.150, 0.125, 0.100, 0.050 and σ_w/σ_f = 1, 2, 3, 4, 5, 10. The results of these computations are plotted in Figures 7(a), 7(b), 8(a), and 8(b). The fabric extension in both the warp and filling directions is given as a function of the loading ratio, σ_w/σ_f, and the product of yarn radius and number of yarns per unit width in the unloaded fabric, $N_1 R$. Fabric extensions are also given for $\sigma_w/\sigma_f = \infty$, i.e., for uniaxial loading. These extension values represent the maximum fabric extensions possible from crimp interchange. For $N_1 R \leq 0.169$ the warp yarns are pulled straight as $\sigma_w/\sigma_f \to \infty$, and Equation (25) is used in determining the limiting fabric extensions. For $N_1 R \geq 0.169$ the fabric extension in the warp direction is limited by the inability of the fabric to contract further in the filling direction as $\sigma_w/\sigma_f \to \infty$ because of the development of the maximum possible crimp in the filling yarn. Equation (28) is used in determining the maximum fabric extensions for this case. For $N_1 R$ = 0.169 the warp yarns are pulled straight and the maximum crimp is developed in the filling yarn. The value $N_1 R$ = 0.169 for which this occurs is determined by substituting $\theta_{2w} = 0$ and $L_f = 4R\,\theta_{2f}$ into Equation (35), solving for $\theta_{2f}(\theta_{2f} = \pi/2)$ and obtaining the value of $N_1 R$ corresponding to $L_f/R = 2\pi$ from Figure 6.

When $\sigma_w/\sigma_f \to \infty$ and $N_1 R > 0.169$, the equilibrium equations, Equations (11) through (13), are not satisfied. The limiting fabric extensions are determined from purely geometric considerations. In a real fabric the filling yarns would be compressed and the projection of these compressive forces along an axis perpendicular to the plane of the fabric would balance the components of the tensile forces acting on the warp yarns and projected along the same axis.

As indicated in Figures 7 and 8, no fabric extension occurs for a loading ratio of one. This is because the fabric is assumed initially square, woven from inextensible yarns and subjected to equal loads in both directions. Under these conditions no crimp interchange can take place.

For loading ratios greater than one, the fabric elongates in the warp direction and contracts in the filling direction. The magnitudes of these extensions increase with increasing values of the loading ratio, approaching the $\sigma_w/\sigma_f = \infty$ extensions asymptotically.

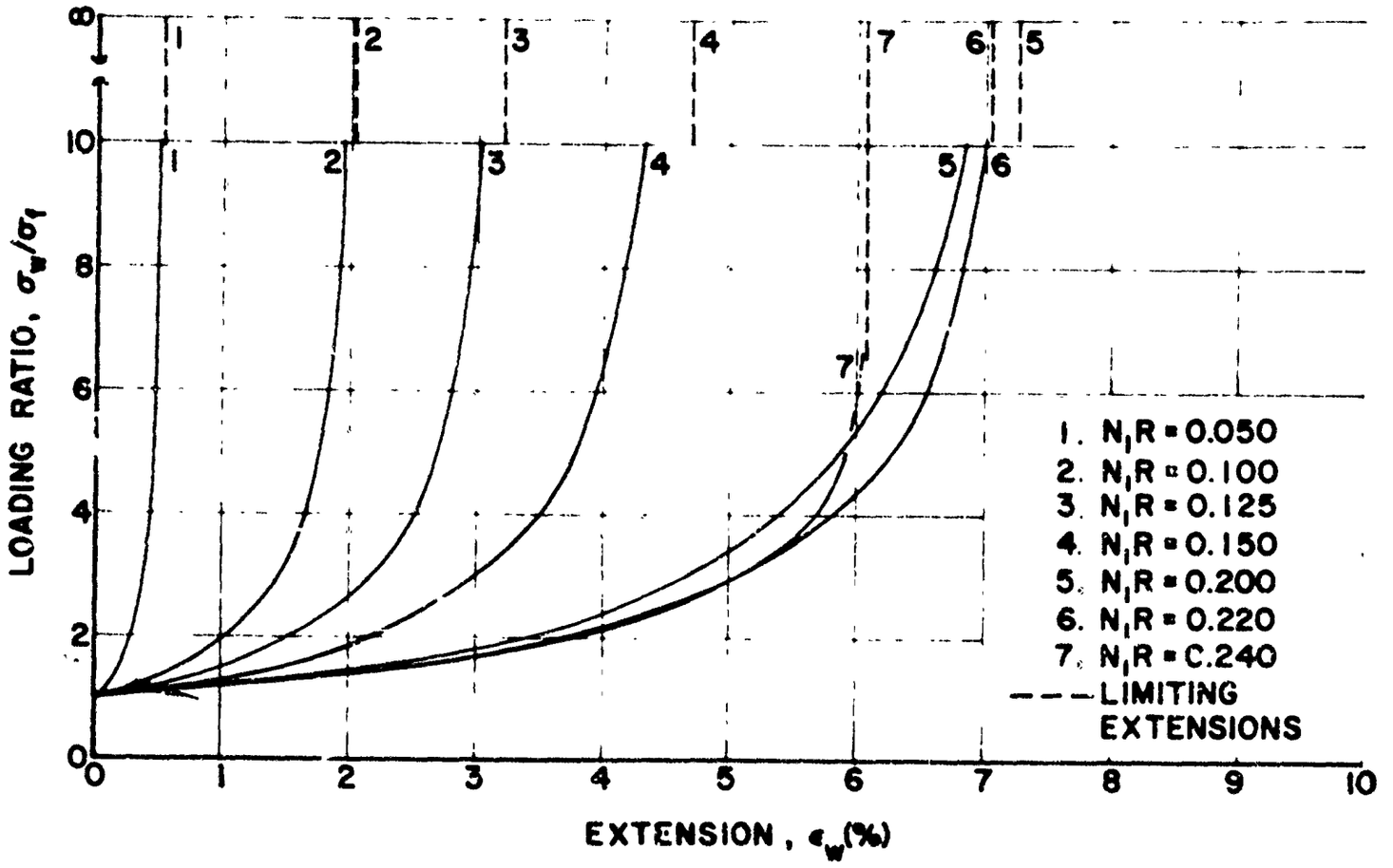

FIGURE 7(a). FABRIC EXTENSION IN THE WARP DIRECTION: INEXTENSIBLE YARN, INITIALLY SQUARE FABRIC.

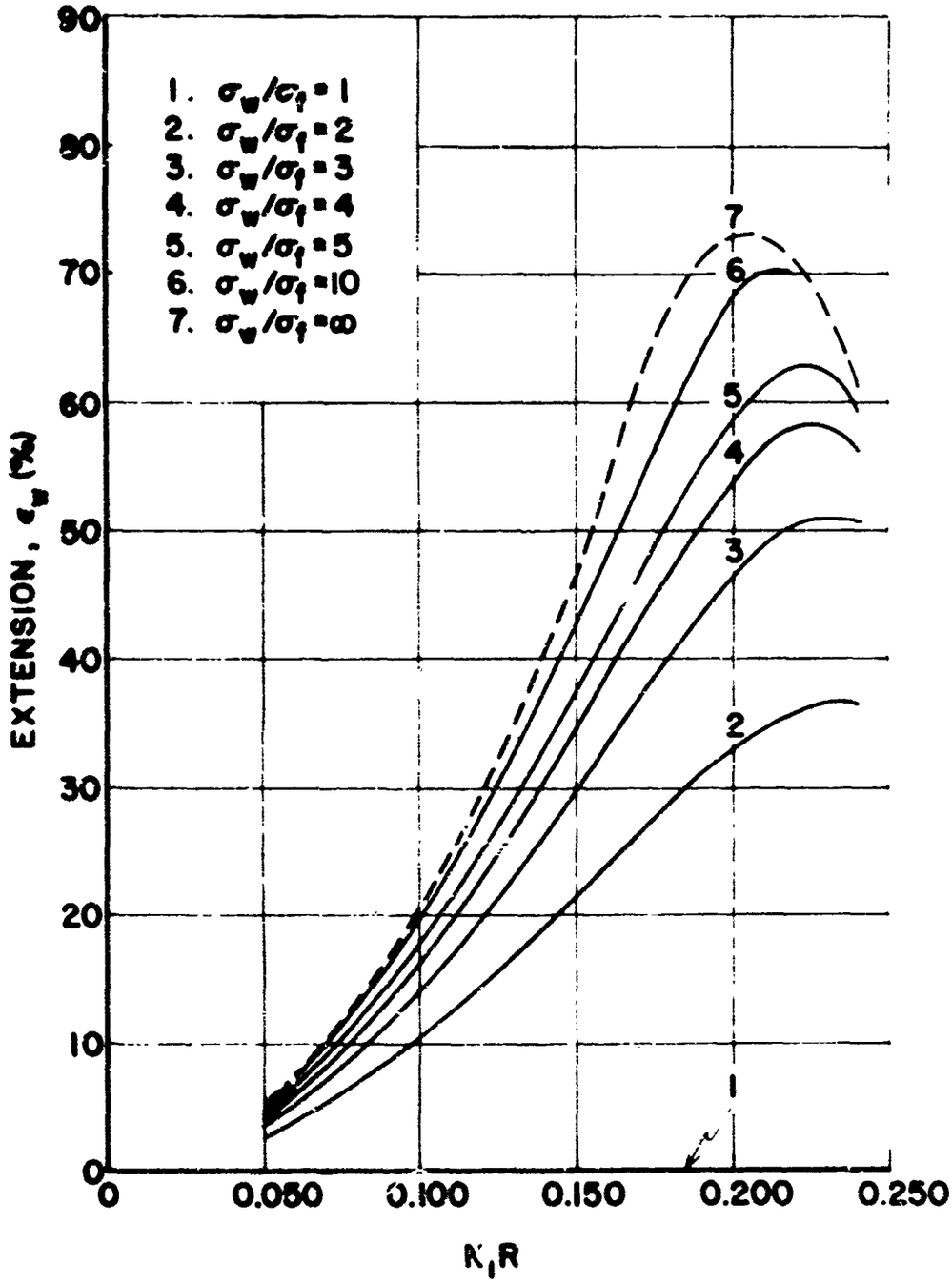

FIGURE 7(b). FABRIC EXTENSION IN THE WARP DIRECTION: INEXTENSIBLE YARN, INITIALLY SQUARE FABRIC.

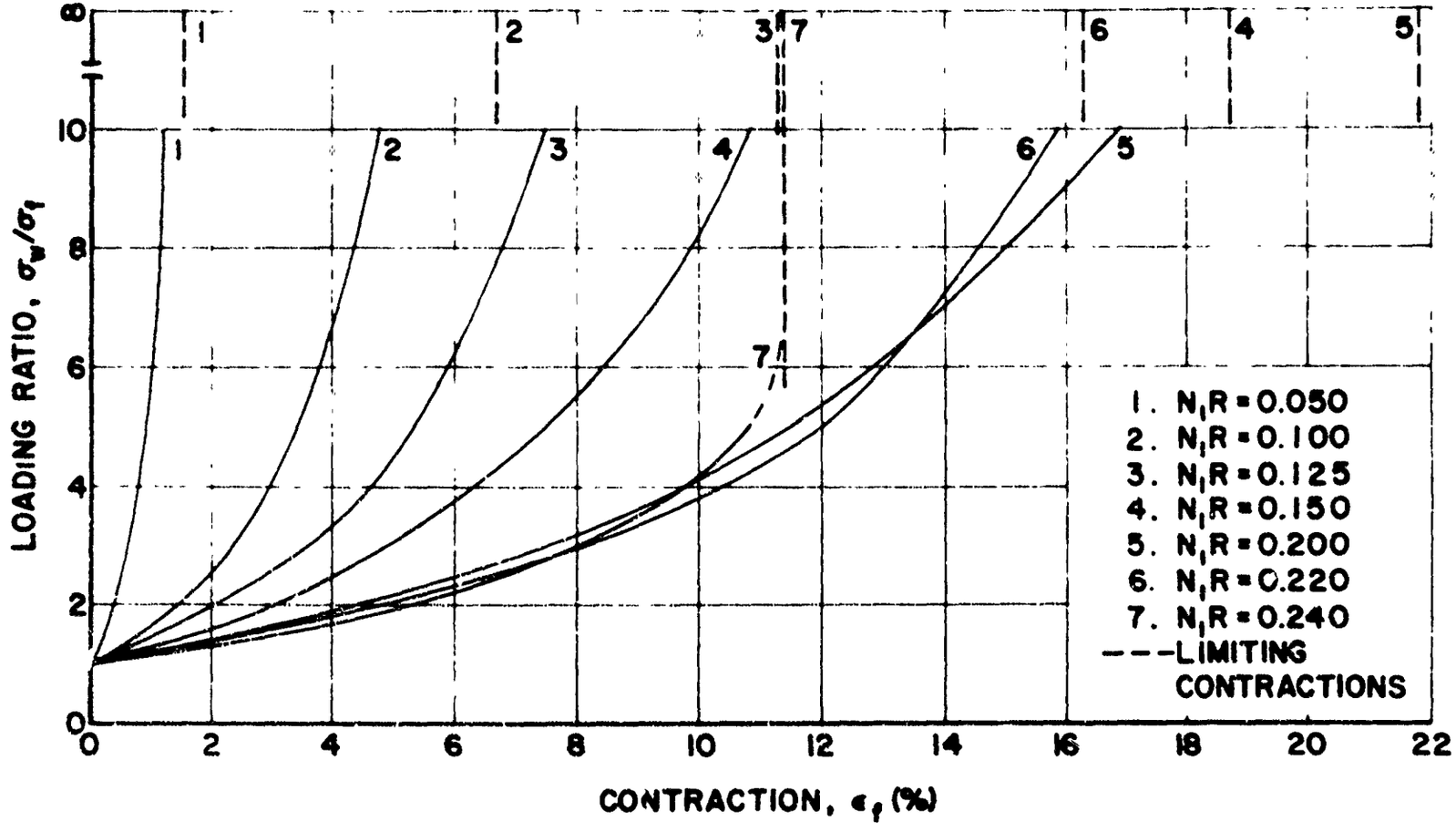

FIGURE 8(a). FABRIC CONTRACTION IN THE FILLING DIRECTION: INEXTENSIBLE YARN, INITIALLY SQUARE FABRIC.

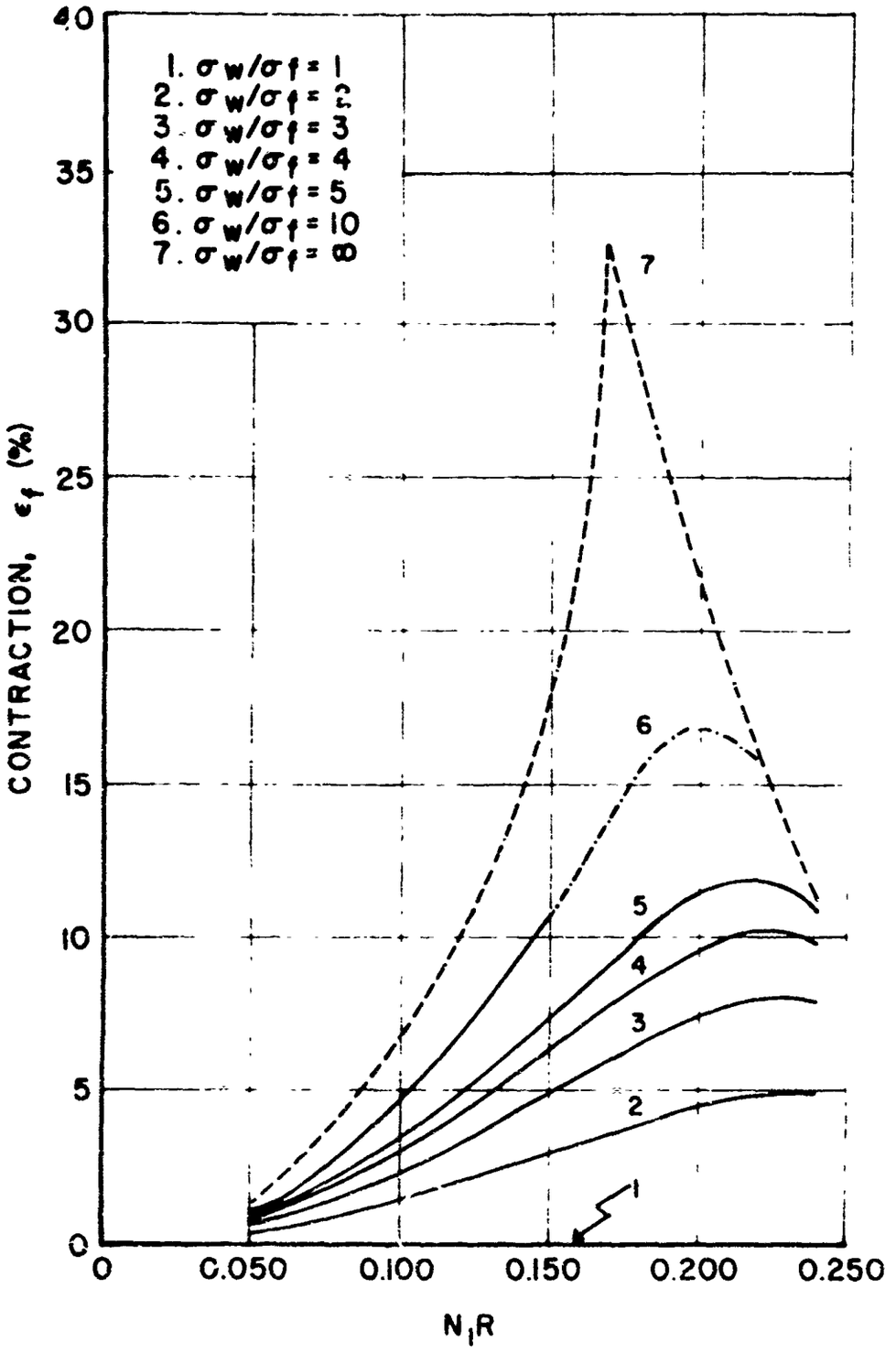

FIGURE 8(b). FABRIC CONTRACTION IN THE FILLING DIRECTION: INEXTENSIBLE YARN, INITIALLY SQUARE FABRIC.

The differences between the fabric extensions in the warp direction for $\sigma_w/\sigma_f = 10$ and $\sigma_w/\sigma_f = \infty$ are small. However, this is not the case in the filling direction, particularly for $0.100 \leq N_1R \leq 0.200$. A small load in the filling direction significantly restricts the fabric from contracting to the same extent as would occur under uniaxial loading.

As also shown in Figures 7 and 8, the fabric extension in the warp direction and contraction in the filling direction increase with increasing N_1R up to an N_1R between 0.200 - 0.240 and 0.169 - 0.240, respectively, depending on the loading ratio. For greater N_1R values, the fabric exhibits decreasing extension in the warp direction and decreasing contraction in the filling direction with increasing N_1R. The N_1R for which the greatest fabric extensions are obtained decreases with increasing loading ratio (see Figures 7(b) and 8(b)). However, in the limit as $\sigma_w/\sigma_f \to \infty$, a fabric with an N_1R of about 0.200 exhibits the greatest warp extension, and a fabric with $N_1R = 0.169$ the greatest filling contraction. The latter fabric construction is the one in which the maximum filling crimp is first developed. Fabrics with greater N_1R's are closer to the jammed state initially and therefore reach this limiting geometry sooner upon loading. Consequently, their filling contraction is less. (As mentioned earlier, it can be shown that an initially square fabric with $N_1R = 0.289$ and woven from inextensible yarns cannot exhibit any warp extension or filling contraction because its initial geometry is a jammed configuration.)

The ratio of the fabric contraction in the filling direction to the corresponding extension in the warp direction, i.e., the effective Poisson's ratio, μ, of the fabric ($\mu = -\epsilon_f/\epsilon_w$), is plotted in Figures 9(a) and 9(b). It is recognized that this is a non-standard definition of Poisson's ratio. Classically, it is the ratio of the lateral contraction to longitudinal extension of a homogeneous bar under axial tension. However, it is used herein to define the ratio of the lateral contraction to logitudinal extension of a structure, not a homogeneous material, under biaxial, as well as, uniaxial loading. Therefore, it is referred to throughout as the effective Poisson's ratio in an effort to distinguish it from the classical Poisson's ratio.

The effective fabric Poisson's ratios are given in Figures 9(a) and 9(b) as a function of loading ratio and N_1R. The values at an infinite loading ratio are noted. As shown, $\mu \approx 1.4$ at a loading ratio of two for all values of N_1R and increases with increasing loading ratio to 1.8 - 2.7 at a loading ratio of ten, and 1.8 - 5.4 at an infinite loading ratio. This is in contrast to conventional homogeneous engineering materials which rarely exhibit Poisson's ratios greater than 1/2. Furthermore, it can be shown that even when homogeneous materials are under biaxial stress the effective Poisson's ratio never exceeds the true Poisson's ratio for all positive values of the loading ratio.

At the lower values of loading ratio the Poisson's ratio does not exhibit a strong dependence on N_1R, it decreases slightly with increasing N_1R. However, as shown in Figure 9(b), at a loading ratio of ten μ increases with increasing N_1R up to an N_1R of about 0.175; at larger N_1R values μ decreases with increasing N_1R. As also shown in Figure 9(b), in the limit as $\sigma_w/\sigma_f \to \infty$, a fabric with an $N_1R = 0.169$ exhibits the largest effective Poisson's ratio 5.4.

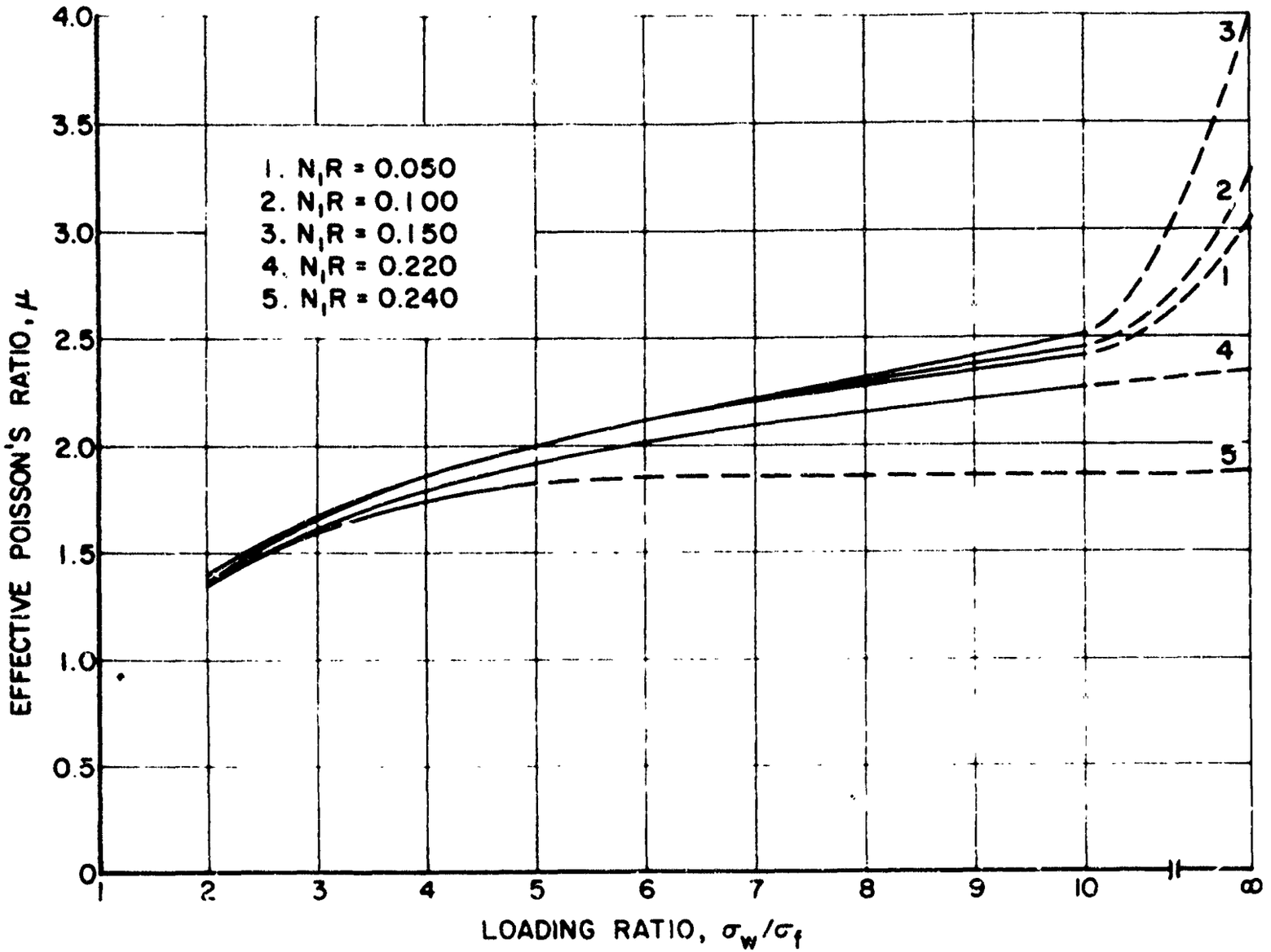

FIGURE 9(a). POISSON'S RATIO FOR AN INITIALLY SQUARE FABRIC WITH INEXTENSIBLE YARN.

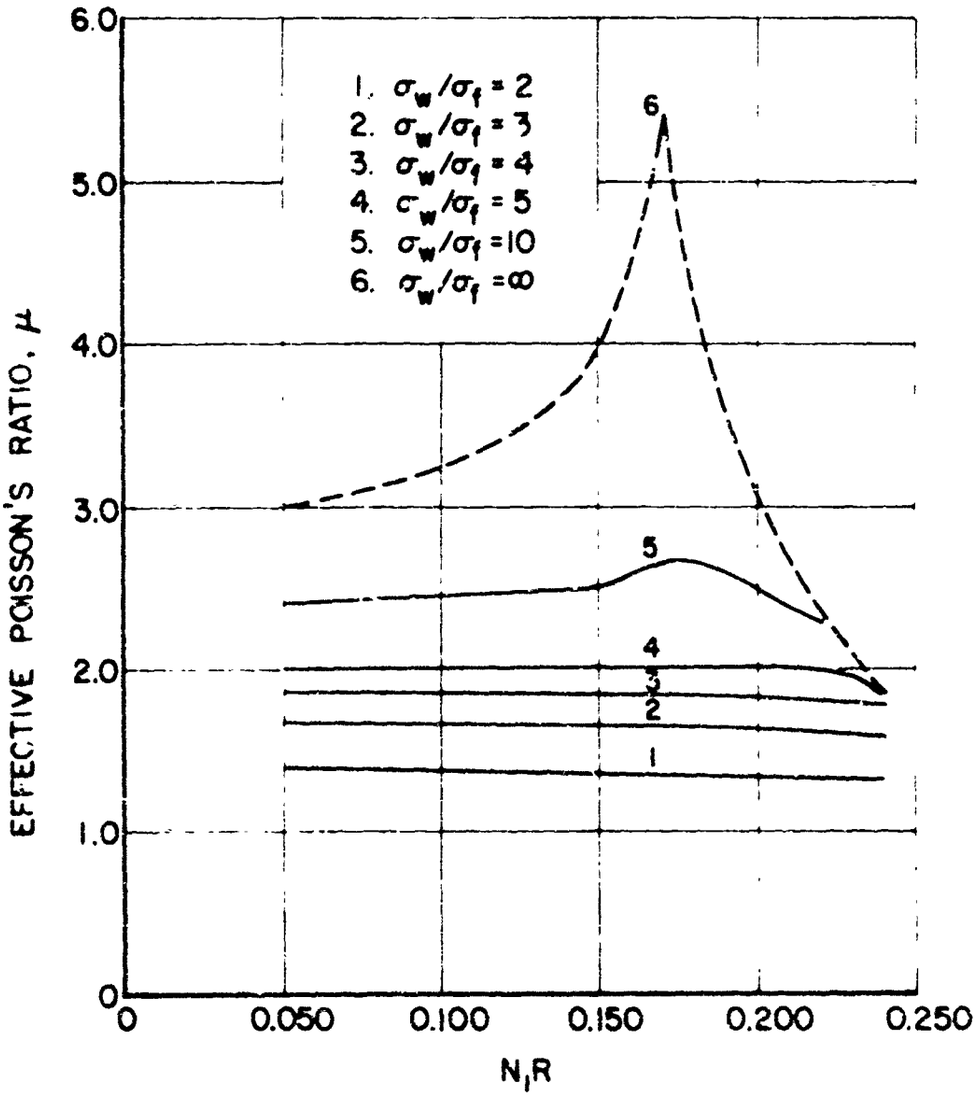

FIGURE 9(b). POISSON'S RATIO FOR AN INITIALLY SQUARE FABRIC WITH INEXTENSIBLE YARN.

Filling Yarn Initially Straight, Inextensible Yarn, Crimp Interchange

For a plain-weave fabric with the same number of identical, infinitely flexible, inextensible yarns in both the warp and filling and one set of yarns (filling yarns) initially straight (noncrimped)

$$N_{1w} = N_{1f} = N_1$$

$$R_{1f} = R_{1w} = R_{2f} = R_{2w} = R$$

$$\theta_{1f} = 0$$

$$L_{1f} = L_{2f} = L_f$$

$$L_{1w} = L_{2w} = L_w$$

With these assumptions Equations (1) through (5) reduce to the following three simplified expressions

$$\frac{L_f}{R} = \frac{1}{N_1 R} \tag{41}$$

$$\sin \theta_{1w} = 4N_1 R \tag{42}$$

$$\frac{L_w}{R} = \frac{4}{\sin \theta_{1w} \cos \theta_{1w}} - 4\theta_{1w} - 4 \tan \theta_{1w} \tag{43}$$

In contrast to the previous case where an initially square fabric was analyzed, L_w/R and L_f/R in this case are better-behaved functions. They approach infinity as θ_{1w} approaches zero, but are single-valued as θ_{1w} approaches 90°. N_1R vs. θ_{1w}, L_w/R and L_f/R vs. θ_{1w}, and L_w/R and L_f/R vs. N_1R are plotted in Figures 10, 11 and 12, respectively. In the computations presented below for a fabric with one set of yarns initially straight, again only N_1R values ≥ 0.05 and ≤ 0.24 are used. The $N_1R = 0.05$ corresponds to an angle θ_{1w} of 11.5°; $N_1R = 0.24$ to 73.7°.

As for the previous case, substitution of Equations (8) and (9) into Equation (10) and Equations (6), (7), (11) and (12) into Equation (13) gives the following two simultaneous equations in the two unknowns θ_{2w} and θ_{2f}.

$$\left(\frac{L_w}{4R} - \theta_{2w}\right) \sin \theta_{2w} - \cos \theta_{2w} = (\cos \theta_{2f} - 1) - \left(\frac{L_f}{4R} - \theta_{2f}\right) \sin \theta_{2f} \tag{44}$$

$$\cos \theta_{2w} \left[\left(\frac{L_w}{4R} - \theta_{2w}\right) \cot \theta_{2w} + 1\right] = \left(\frac{\sigma_w}{\sigma_f}\right) \cos \theta_{2f} \left[\left(\frac{L_f}{4R} - \theta_{2f}\right) \cot \theta_{2f} - 1\right] \tag{45}$$

These equations are identical to Equations (35) and (36) except that the distinction between the length of warp yarn and the length of filling yarn between yarn crossovers has been maintained.

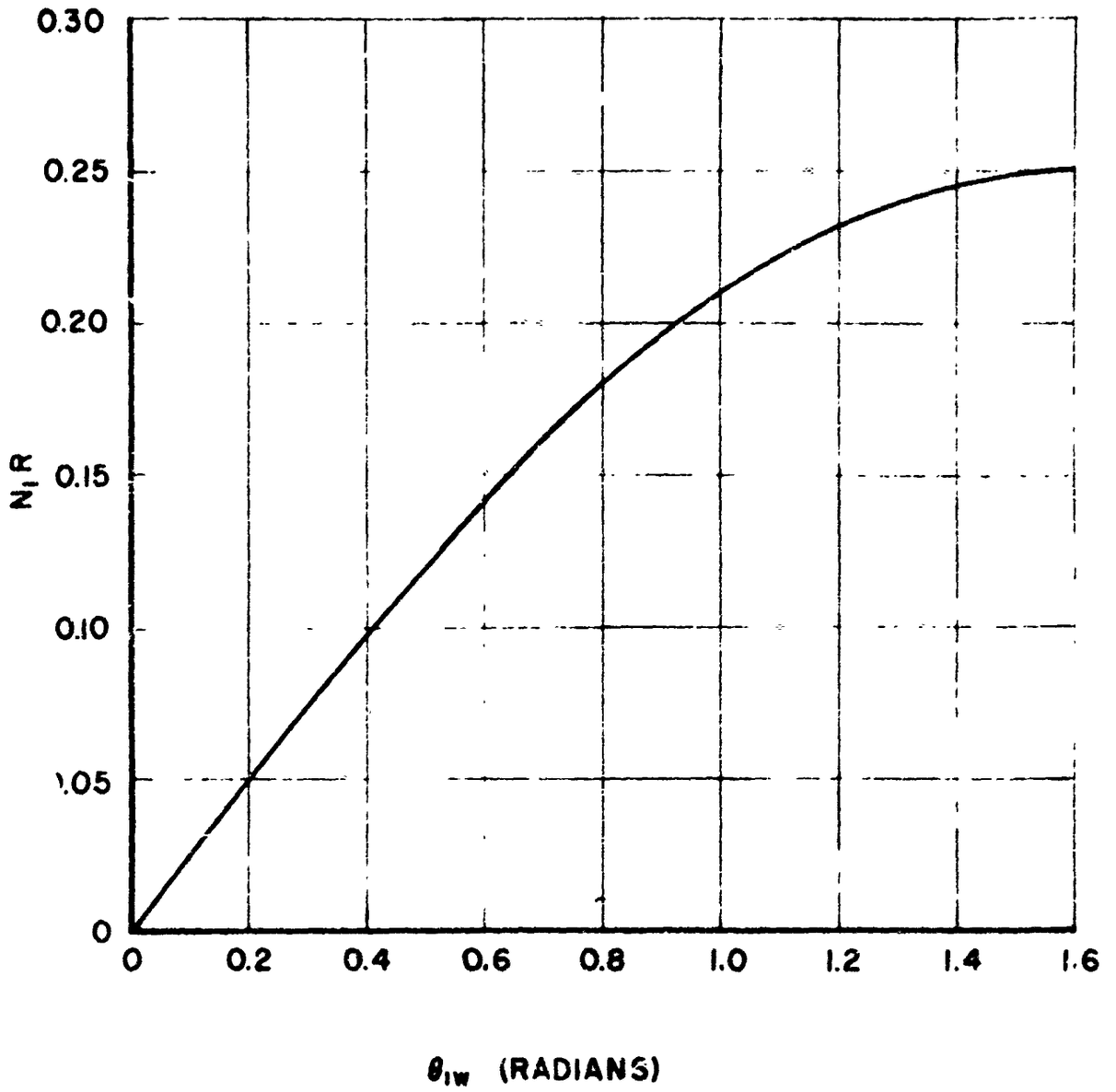

FIGURE 10. N_1R VS θ_{1W} FOR A FABRIC WITH INEXTENSIBLE YARN AND INITIALLY STRAIGHT FILLING.

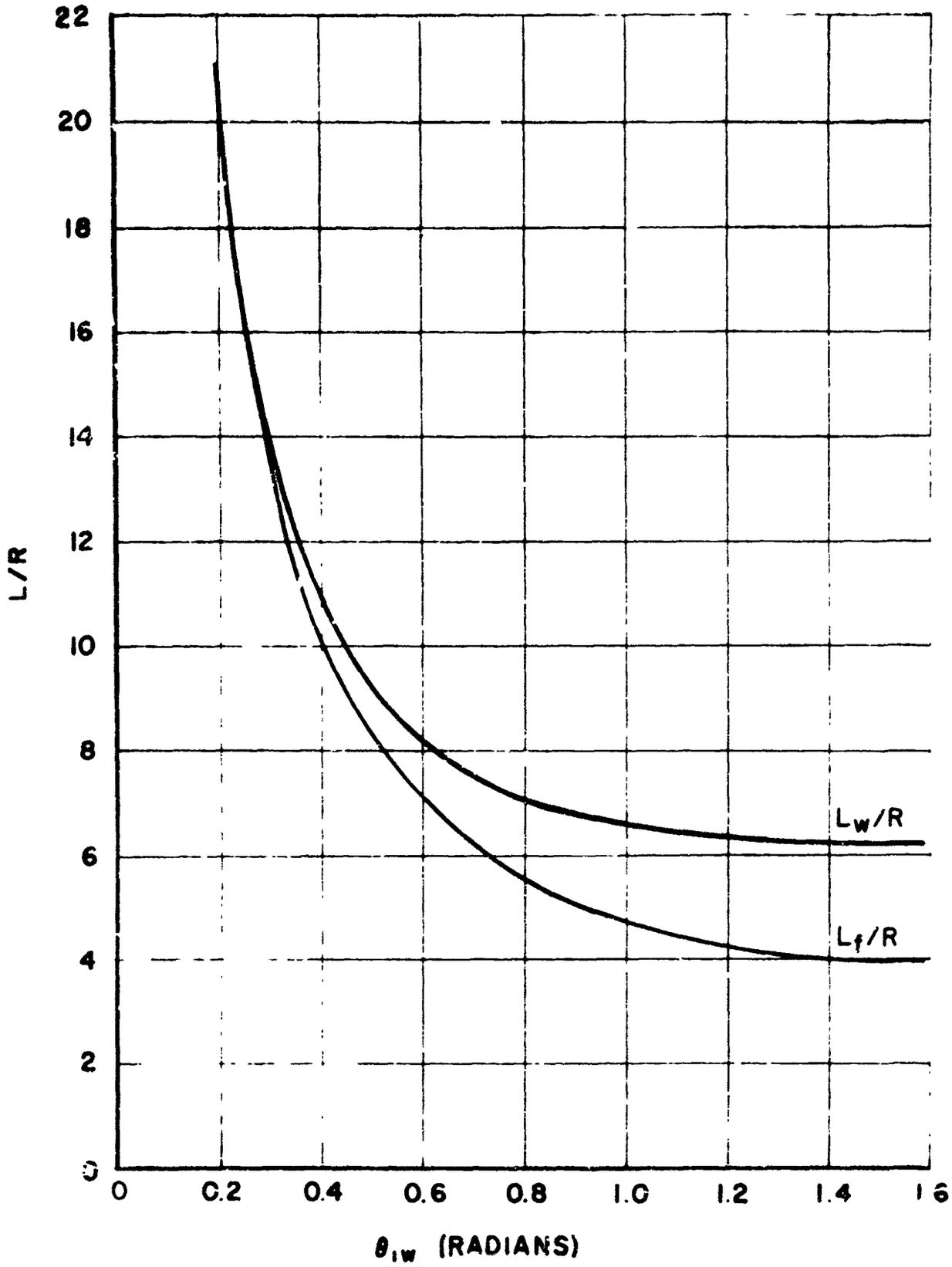

FIGURE II. L/R VS θ_{1w} FOR A FABRIC WITH INEXTENSIBLE YARN AND INITIALLY STRAIGHT FILLING.

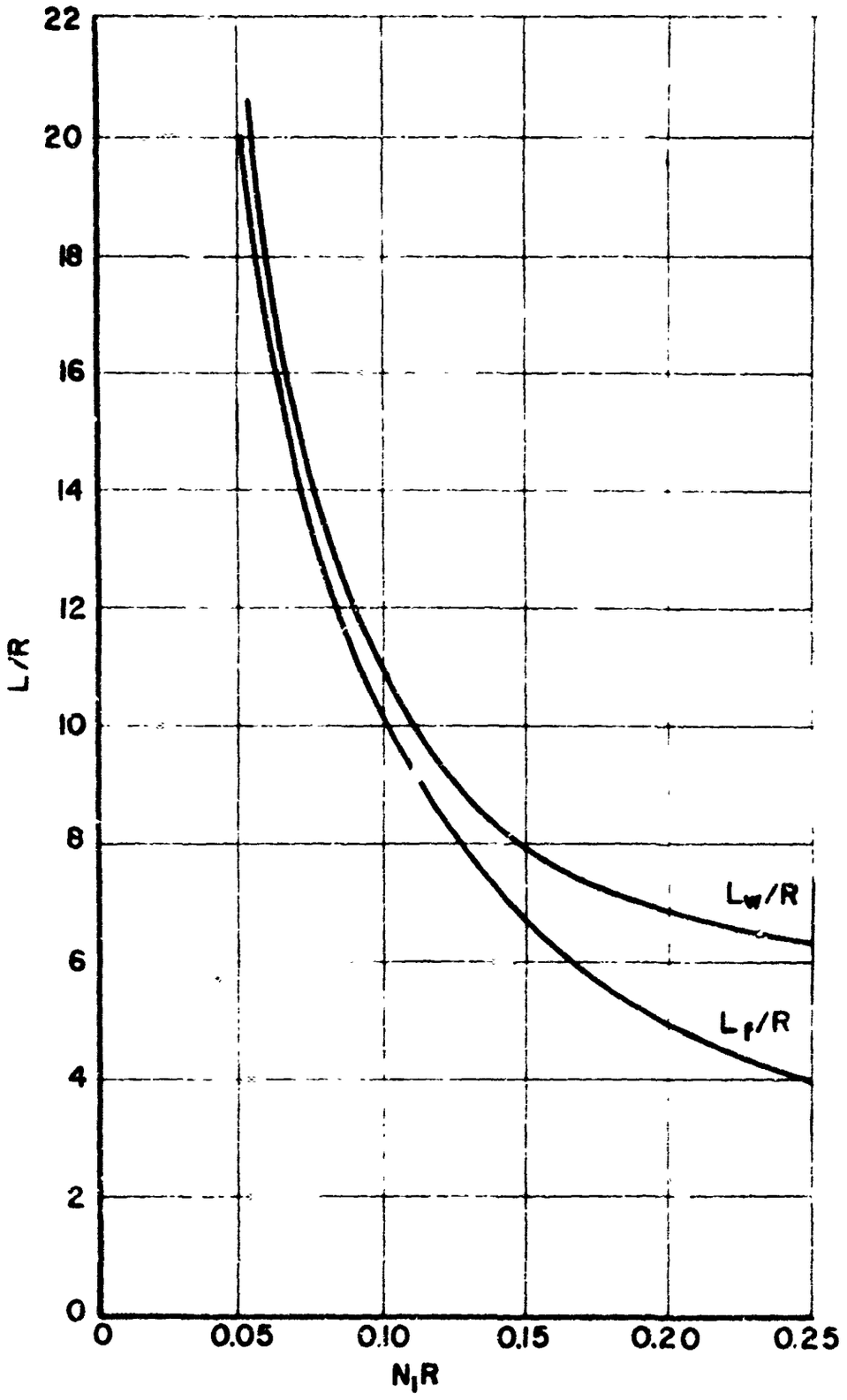

FIGURE 12. L/R VS N_1R FOR A FABRIC WITH INEXTENSIBLE YARN AND INITIALLY STRAIGHT FILLING.

Again, once θ_{2w} and θ_{2f} are determined, $N_{2f}R$ and $N_{2w}R$ are obtained from Equations (6) and (7) and the fractional fabric extensions in the warp and filling directions from Equations (39) and (40).

Equations (41) through (45), (6), [illegible], and (39) (40) were solved for N_1R = 0.240, 0.220, 0.200, 0.150, 0.125, 0.100, 0.050, and σ_w/σ_f = 0.5, 1, 2, 3, 4, 5, 10. The results of these computations are plotted in Figures 13(a), 13(b), 14(a), and 14(b). Fabric extensions for $\sigma_w/\sigma_f = \infty$ are also given. As for the case of the initially square fabric, these extension values represent the maximum fabric extensions possible from crimp interchange. They were determined in the same manner as for the previous case. The warp yarns are pulled straight as $\sigma_w/\sigma_f \to \infty$ when $N_1R < 0.159$; when $N_1R > 0.159$ the fabric extension in the warp direction is limited by the inability of the fabric to contract further in the filling direction.

As shown in Figures 13 and 14, the fabric elongates in the warp direction and contracts in the filling direction. The magnitude of these extensions increases with increasing values of the loading ratio, approaching the $\sigma_w/\sigma_f = \infty$ extensions asymptotically.

The fabric extension in the warp direction increases also with increasing N_1R. The contraction in the filling direction goes through a turning point with increasing N_1R. The value of N_1R for which the greatest fabric filling contraction occurs varies with the loading ratio. However, in the limit as $\sigma_w/\sigma_f \to \infty$, a fabric with an N_1R = 0.159 exhibits the greatest contraction in the filling direction since this fabric construction is the one in which the maximum filling crimp is first developed. As discussed for the case of an initially square fabric, fabrics with $N_1R > 0.159$ are closer to the jammed state initially, and, therefore, reach this limiting geometry with less filling contraction.

In contrast to the initially square fabric case the warp extension for fabric with initially straight filling continues to increase with increasing N_1R, even for $N_1R > 0.159$. This occurs because the initial crimp in the warp yarns increases significantly with increasing N_1R, since the filling is straight, thereby providing greater warp yarn length between yarn crossovers and thus greater opportunity for higher fabric extensions in the warp direction.

Unlike the initially square fabrics, fabrics with initially straight filling extend at a loading ratio of one. Additionally, a comparison of the extension data in Figures 7 and 8 to those plotted in Figures 13 and 14 shows that for any value of N_1R and σ_w/σ_f, the warp extension is considerably greater and the filling contraction moderately greater when the filling yarns are initially straight. The filling contraction is greater because larger changes in filling crimp can occur when the filling is initially straight. Similarly, the fabric extension in the warp direction is larger because (1) the initial crimp in the warp yarns is larger for a given N_1R when the filling yarns are initially straight; (2) there is greater crimp interchange between the warp and filling yarns when the filling yarns are initially straight.

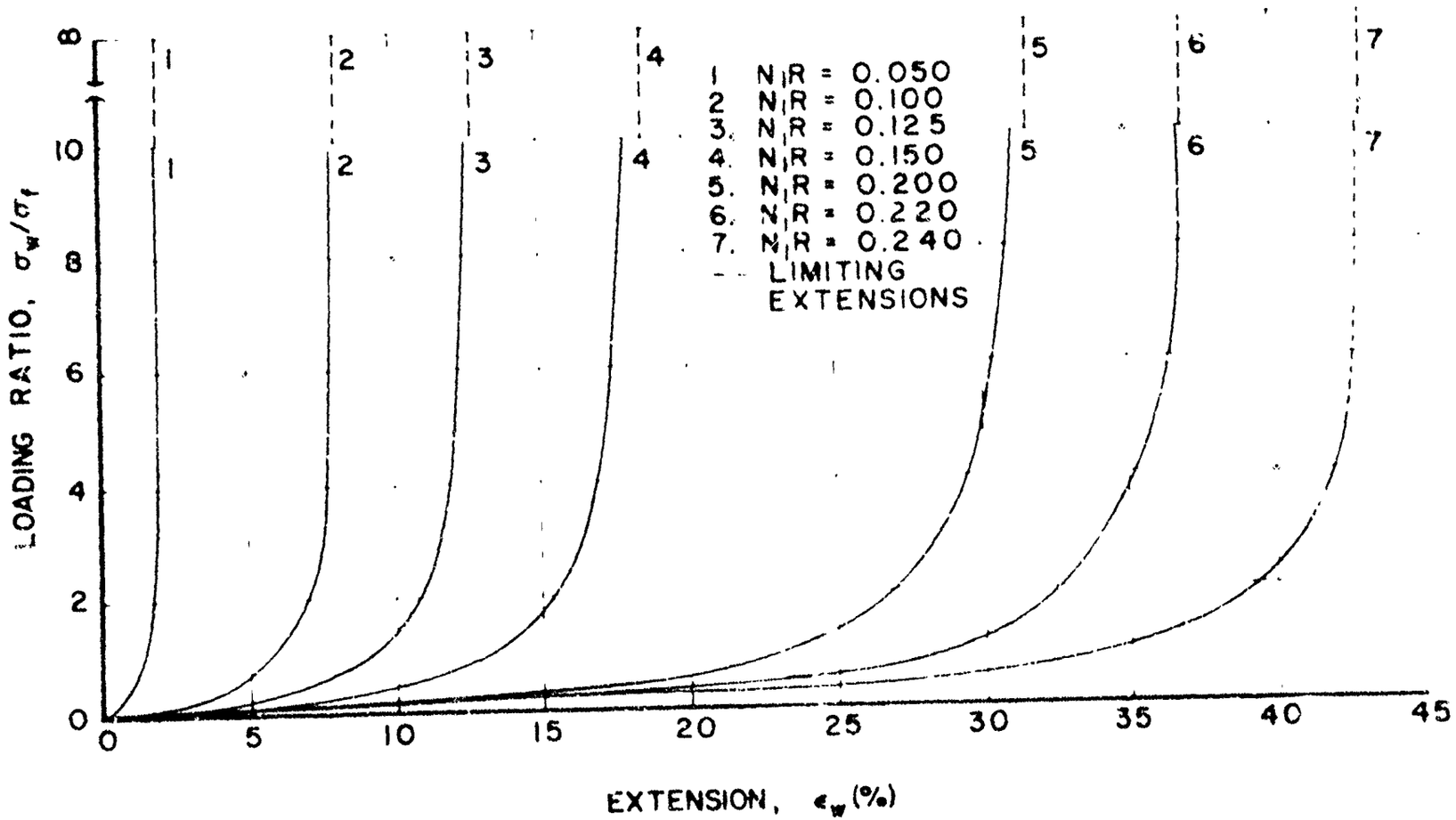

FIGURE 13(a). FABRIC EXTENSION IN THE WARP DIRECTION: INEXTENSIBLE YARN, INITIALLY STRAIGHT FILLING.

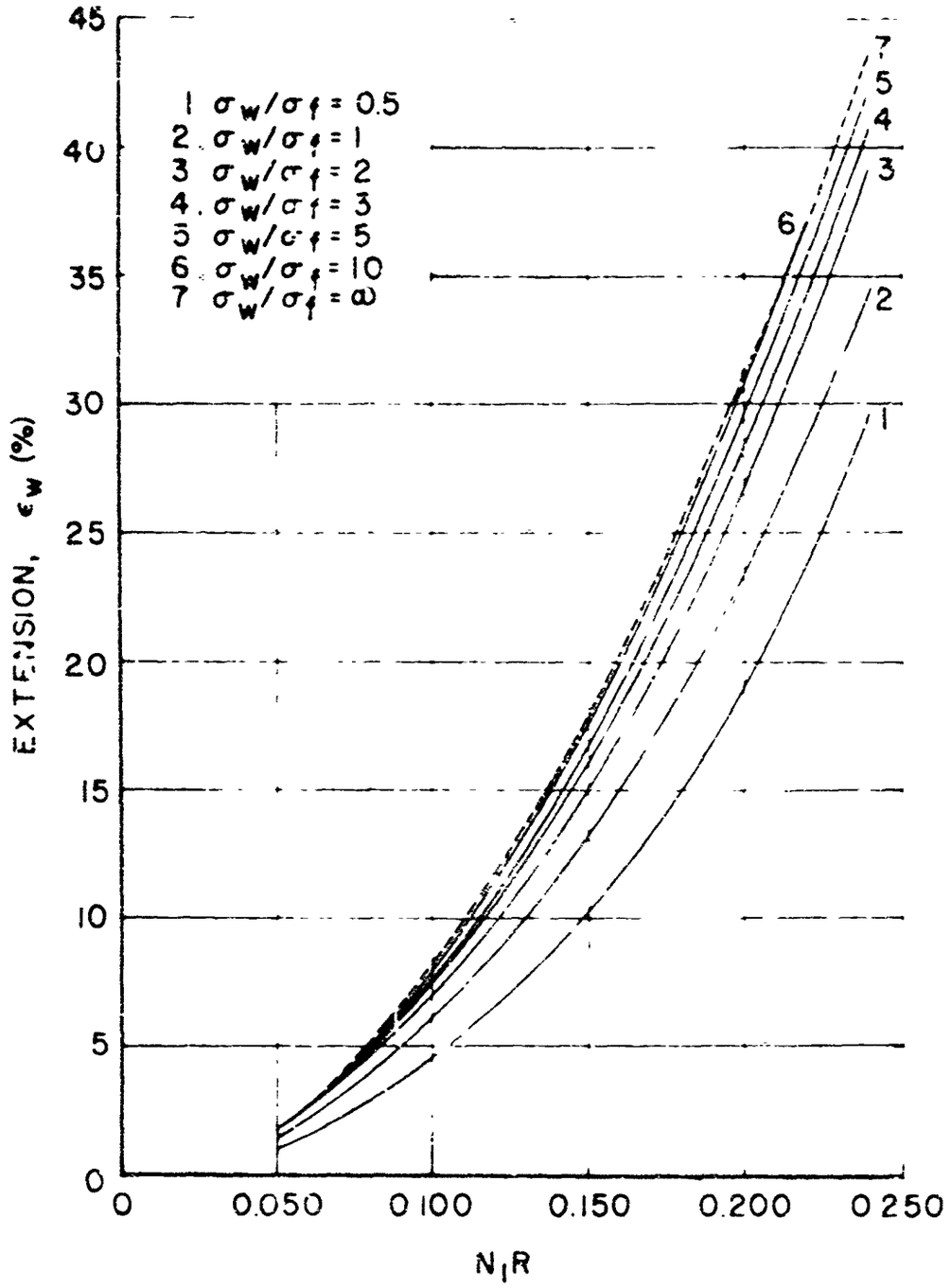

FIGURE 13(b). FABRIC EXTENSION IN THE WARP DIRECTION: INEXTENSIBLE YARN, INITIALLY STRAIGHT FILLING.

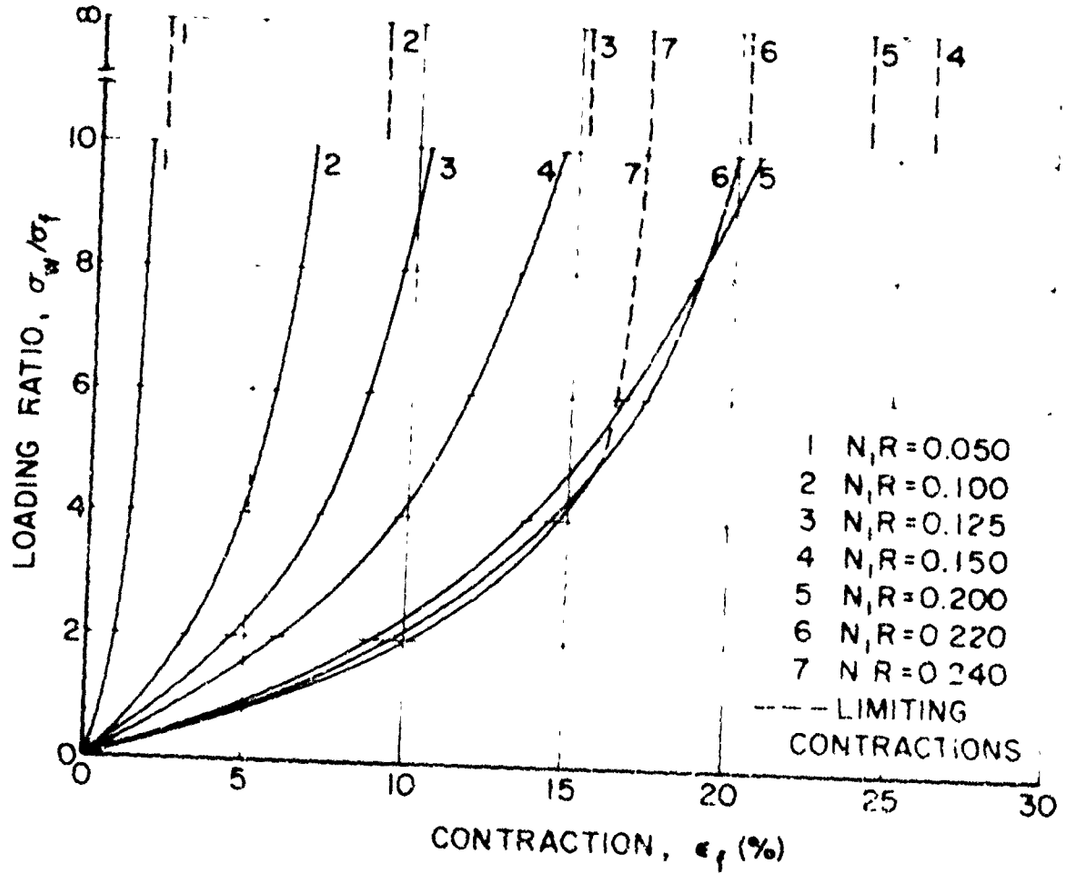

FIGURE 14(a). FABRIC CONTRACTION IN THE FILLING DIRECTION: INEXTENSIBLE YARN, INITIALLY STRAIGHT FILLING.

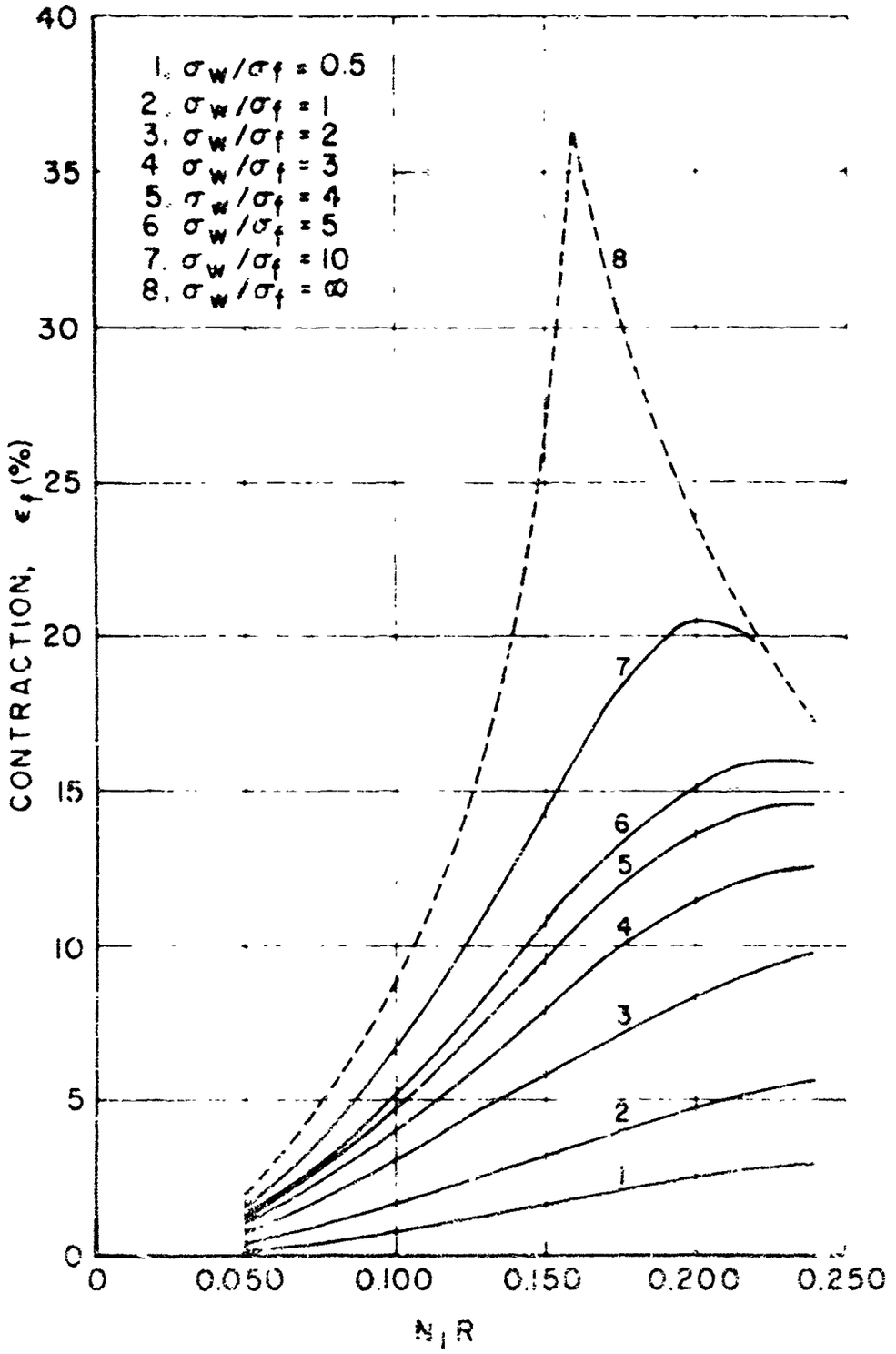

FIGURE 14 (b). FABRIC CONTRACTION IN THE FILLING DIRECTION: INEXTENSIBLE YARN, INITIALLY STRAIGHT FILLING.

The effective Poisson's ratio μ, of the fabric is plotted in Figures 15(a) and 15(b) as a function of loading ratio and N_1R. The values for an infinite loading ratio are also noted. As shown, μ increases with increasing loading ratio and decreasing N_1R when $\sigma_w/\sigma_f \leq 10$. However, at $\sigma_w/\sigma = \infty$ μ increases up to a maximum of $\mu = 1.73$ at $N_1R = 0.159$, at larger N_1R values μ decreases with increasing N_1R. At a loading ratio of one $\mu = 0.16 - 0.32$, the exact value depending on the appropriate N_1R, at a loading ratio of ten, $\mu = 0.39 - 0.83$; and at an infinite loading ratio, $\mu = 0.040 - 1.73$. As a comparison of the data in Figures 9 and 15 shows, when the filling yarn is initially straight the fabric exhibits a lower effective Poisson's ratio.

Square Fabric, Extensible Yarn (Linearly Elastic, $\nu = 0$), $\sigma_w/\sigma_f = 1$

For a square, plain-weave fabric with the same infinitely flexible yarn in both the warp and filling

$$N_{1f} = N_{1w} = N_1$$

$$R_{1f} = R_{1w} = R$$

$$\theta_{1f} = \theta_{1w} = \theta_1$$

$$L_{1f} = L_{1w} = L_1$$

Therefore, the equations describing the geometry of the fabric in the unloaded state, Equations (1) - (5), reduce to the two simplified expressions given in Equations (33) and (34) with $L = L_1$.

If it is further assumed that the radii of the circular yarns in the fabric remain constant during the fabric extension and equal to the yarn radii prior to loading, i.e., that the Poisson's ratio, ν of the yarn is zero and additionally that the load applied to the fabric in the warp direction is equal to the load applied in the filling direction throughout the loading cycle

$$R_{2f} = R_{2w} = R$$

$$L_{2f} = L_{2w} = L_2$$

$$\theta_{2f} = \theta_{2w} = \theta_2$$

$$N_{2f} = N_{2w} = N_2$$

$$\sigma_w = \sigma_f = \sigma$$

With these assumptions, the Equations describing the geometry of the fabric in the deformed state, Equations (6) - (13), reduce to the three expressions given below. Equations (10) and (13) are not independent expressions due to the geometric symmetry of the assumed fabric model. Equations (6) and (7) reduce to identical expressions, Equation (46); similarly Equations (8) and (9) reduce to Equation (47).

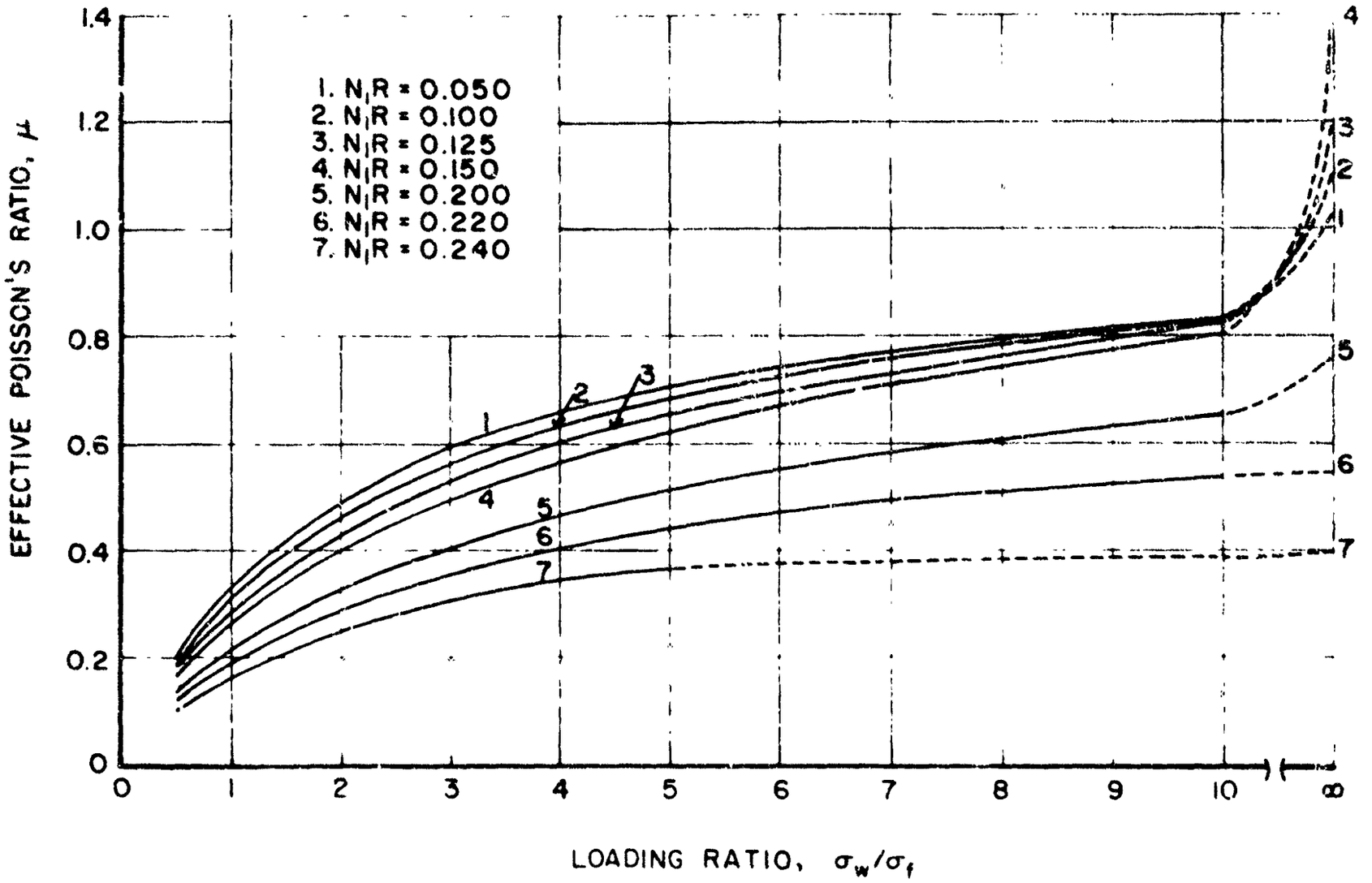

FIGURE 15(a). POISSON'S RATIO FOR FABRIC WITH INEXTENSIBLE YARN AND INITIALLY STRAIGHT FILLING.

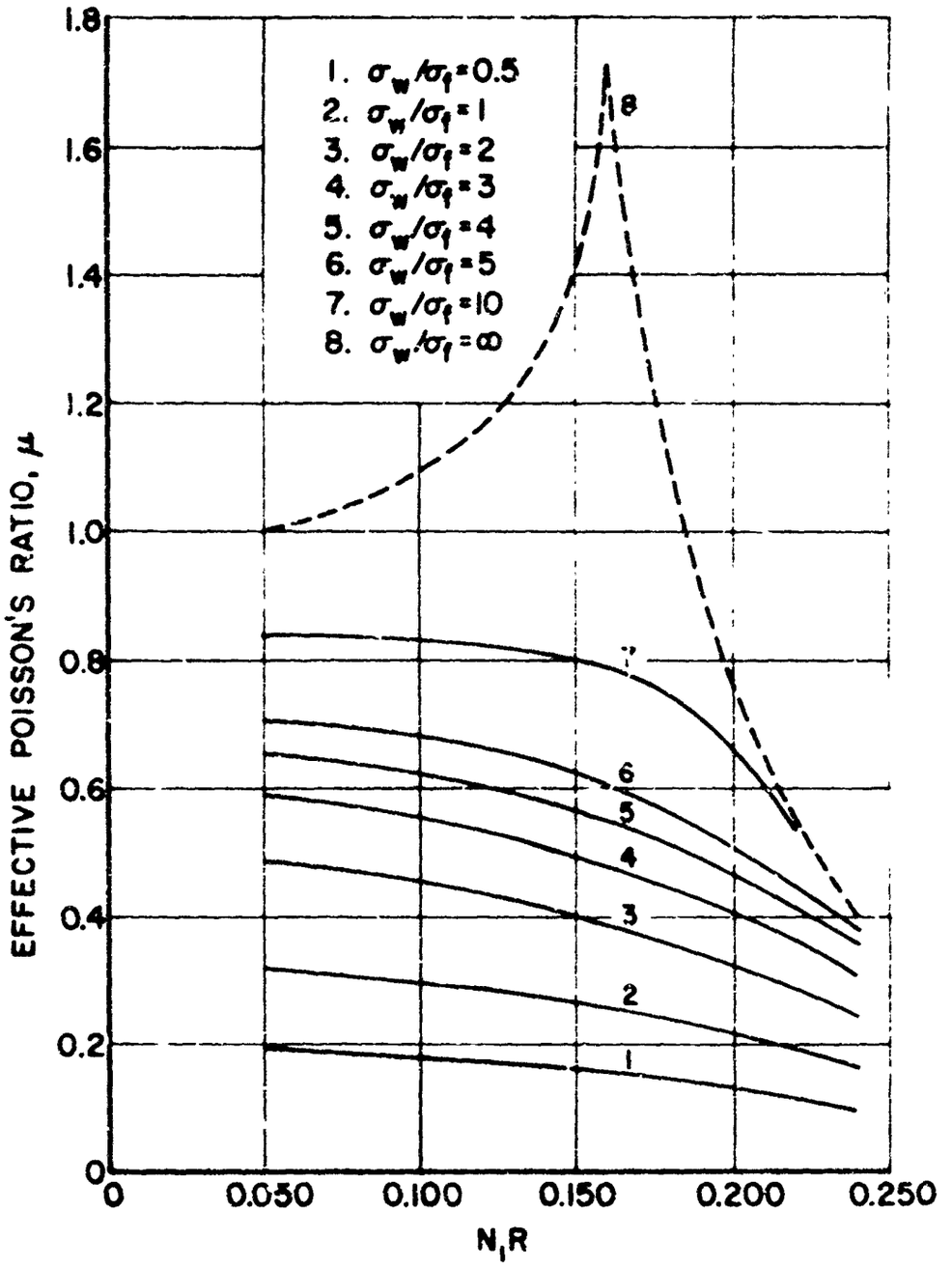

FIGURE 15(b). POISSON'S RATIO FOR FABRIC WITH INEXTENSIBLE YARN AND INITIALLY STRAIGHT FILLING.

Equations (11) and (12), to Equation (48), after substitution of Equation (19). Since the fabric yarns are assumed to be linearly elastic and the yarn extension to be at constant radius, $A = 0$ and $B = pE_f A_y \cos^2 \theta_s$ in Equation (19), the yarn strain $\epsilon_y = \left(\frac{L_2/R}{L_1/R} - 1\right)$.

$$\frac{1}{N_2 R} = [L_2/R - 4\theta_2] \cos \theta_2 - 4 \sin \theta_2 \tag{46}$$

$$2 = [L_2/R - 4\theta_2] \sin \theta_2 + 4(1 - \cos \theta_2) \tag{47}$$

$$\sigma = (N_2 R)\, pE_f \pi R \cos^2 \theta_s \left(\frac{L_2/R}{L_1/R} - 1\right) \cos \theta_2 \tag{48}$$

The fractional fabric extensions in the warp and filling directions are equal, $\epsilon_f = \epsilon_w$, and are given by either Equation (39) and (40).

Equations (33) - (34), (46) - (48) and (39) were solved for. $N_1 R = 0.240$, 0.200, 0.150, 0.100, 0.050; $\sigma = 10$, 50, 100, 300, 500 lbs/inch width, $R = 0.010$, 0.005 inch; $\theta_s = 0°$, 25°, 35°, and $E_f = 2 \times 10^5$, 1×10^6, 10×10^6, 30×10^6 lbs/inch^2. The results of these computations are presented in Figure 16 in terms of the dimensionless parameters ϵ, $N_1 R$ and $\sigma/p(N_1 R)\, E_f \pi R \cos^2 \theta_s$.

The extension at constant radius of a straight, linearly elastic, twisted yarn is also given in Figure 16 as a function of the same parameters. This can be done since σ/N_1 represents the load applied to each yarn in the fabric and, from Equation (19), the extension, ϵ_y, of a linearly elastic yarn is given by

$$\epsilon_y = \frac{P_y}{p \pi R_y^2 E_f \cos^2 \theta_s}$$

where P_y is the load applied to the yarn. As shown in Figure 16, the fabric is more easily extended than a straight yarn identical to those from which the fabric is woven. This is because the yarn axes are not parallel to the plane of the fabric.

It can also be shown that for any specific load, σ, (lbs/inch width of fabric) applied to the fabric, the fabric extension increases with decreasing $N_1 R$ values. The smaller $N_1 R$, the fewer are the number of yarns available for supporting the applied load and thus, the greater each yarn's share of the total load applied to the fabric. The fabric extension also increases with decreasing yarn radius, decreasing yarn modulus and increasing yarn twist (surface helix angle, θ_s).

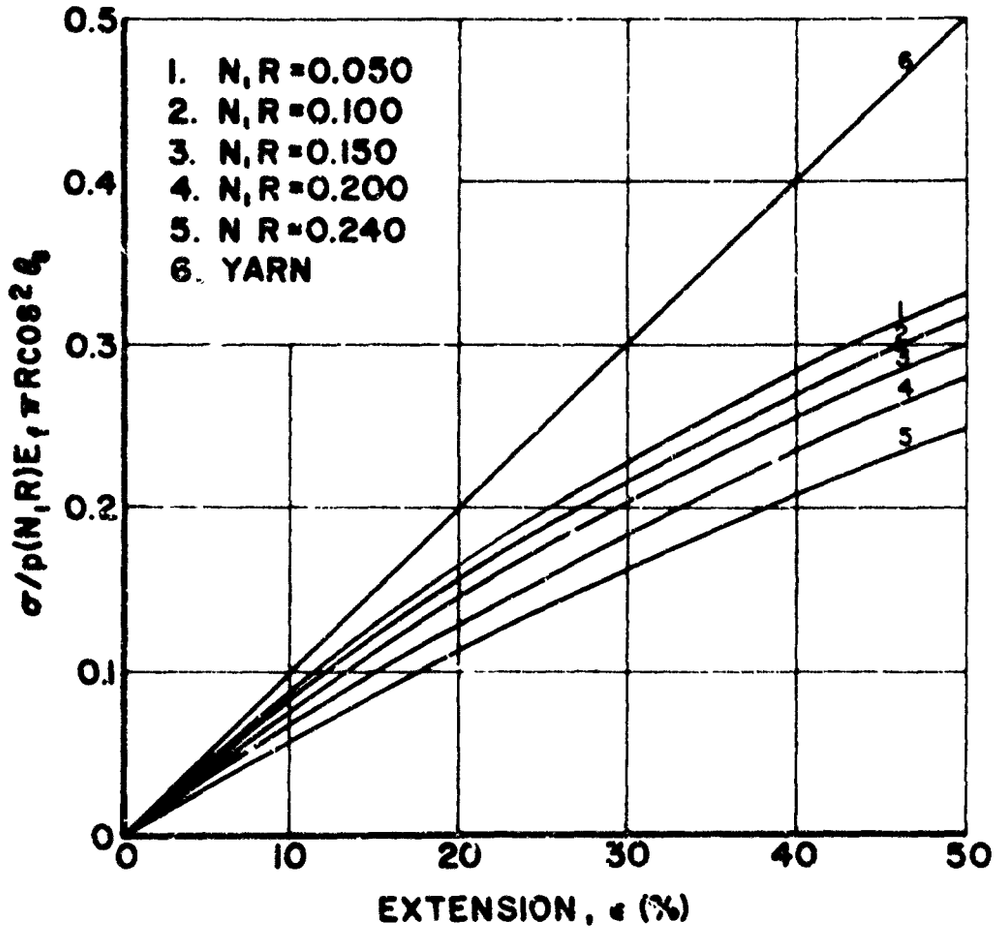

FIGURE 16. FABRIC EXTENSION: LINEARLY ELASTIC YARN ($\nu = 0$), SQUARE FABRIC, $\sigma_w / \sigma_f = 1$.

The effective Poisson's ratio, ν, of a square fabric woven from linearly elastic yarn is -1 when equal loads are applied in both the warp and filling directions.

Square Fabric, Extensible Yarn (Linearly Elastic, $\nu = 1/2$), $\sigma_w/\sigma_f = 1$

The case of an initially square, plain-weave fabric with the same infinitely flexible yarn in both the warp and filling and the ratio of applied loads equal to one, $\sigma_w/\sigma_f = 1$, was also solved assuming constant-volume yarn extension, i.e., with the Poisson's ratio ν of the yarn equal to 1/2. This case shows the effect on the magnitude of the fabric extension of assuming that the radii of the yarns in the fabric remain constant during fabric extension. As for the previous case

$$N_{1f} = N_{1w} = N_1$$

$$R_{1f} = R_{1w} = R$$

$$\theta_{1f} = \theta_{1w} = \theta_1$$

$$L_{1f} = L_{1w} = L_1$$

$$L_{2f} = L_{2w} = L_2$$

$$\theta_{2f} = \theta_{2w} = \theta_2$$

$$N_{2f} = N_{2w} = N_2$$

$$\sigma_w = \sigma_f = \sigma$$

However, for constant-volume yarn extension

$$R_{2f} = R_{2w} = R_2 = R\sqrt{\frac{L_1}{L_2}}$$

With these assumptions the geometry of the fabric in the unloaded state is given by Equations (33) and (34) (with $L = L_1$) and Equations (6) - (13) reduce to the three expressions given below. As in the previous case, Equations (10) and (13) are not independent expressions due to the geometric symmetry of the assumed fabric model; Equations (6) and (7) reduce to identical expressions, Equation (49); Equations (8) and (9), to Equation (50), and Equations (11) and (12), to Equation (51) after substitution of Equation (19). Since the yarn in the fabric is assumed to be linearly elastic and the yarn extension to be at constant volume, $A = 0$ and $B = pE_fA_y[3 \sin^2 \theta_s - \ln \sec^2 \theta_s]/2 \tan^2 \theta_s$ in Equation (19).

$$\frac{1}{N_2 R}\left(\frac{L_2/R}{L_1/R}\right)^{1/2} - \left[\frac{(L_2/R)^{3/2}}{(L_1/R)^{1/2}} - 4\theta_2\right]\cos\theta_2 - 4\sin\theta_2 - 0 \tag{49}$$

$$2 - \left[\frac{(L_2/R)^{3/2}}{(L_2/R)^{1/2}} - 4\theta_2\right]\sin\theta_2 - 4(1 - \cos\theta_2) = 0 \tag{50}$$

$$\frac{\sigma}{pE_f \pi R} - N_2 R \frac{[3\sin^2\theta_s - \ln\sec^2\theta_s]}{2\tan^2\theta_s}\left(\frac{L_2/R}{L_1/R} - 1\right)\cos\theta_2 = 0 \tag{51}$$

The fractional fabric extensions in the warp and filling directions are again equal and given by either Equation (39) or (40).

Equations (33) - (34), (49) - (51) and (39) were solved for the same range of values of the parameters as were used for the case of constant-radius yarn extension. The results are presented in Figure 17 in terms of the dimensionless parameters ϵ, $N_1 R$ and $\sigma/p(N_1 R)E_f \pi R\,\beta$ where

$$\beta = \left[\frac{3\sin^2\theta_s - \ln\sec^2\theta_s}{2\tan^2\theta_s}\right] \tag{52}$$

The extension at constant volume of a straight, linearly elastic, twisted yarn is also given in Figure 17. As for the previous case the fabric is more easily extended than the yarns from which it is woven due to fabric yarn crimp

A comparison of the data in Figures 16 and 17 shows that for identical fabrics loaded to the same level, constant-volume yarn extension results in greater fabric elongation than constant-radius yarn extension. When $N_1 R$ = 0.050, θ_s = 0° and the fabric extension $\epsilon_w = \epsilon_f$ = 20% for constant radius yarn extension, the fabric extension for constant volume yarn extension to the same load $\sigma/pN_1 R\, E_f \pi R$ = 0.168 is 20.8% ($\beta \to 1$ as $\theta_s \to 0°$), i.e., the constant volume fabric extension is 4% greater. Similarly when $N_1 R$ = 0.050, θ_s = 35° and the fabric extension $\epsilon_w = \epsilon_f$ = 20% for constant radius yarn extension, the fabric extension for constant volume yarn extension is 18% greater. When $N_1 R$ = 0.240, θ_s = 0° and the fabric extension $\epsilon_w = \epsilon_f$ = 20% for constant radius yarn extension, the fabric extension for constant volume yarn extension to the same load $\sigma/pN_1 R\, E_f \pi R$ = 0.114 is 10% greater, and similarly when $N_1 R$ = 0.240 and θ_s = 35°, 24% greater.

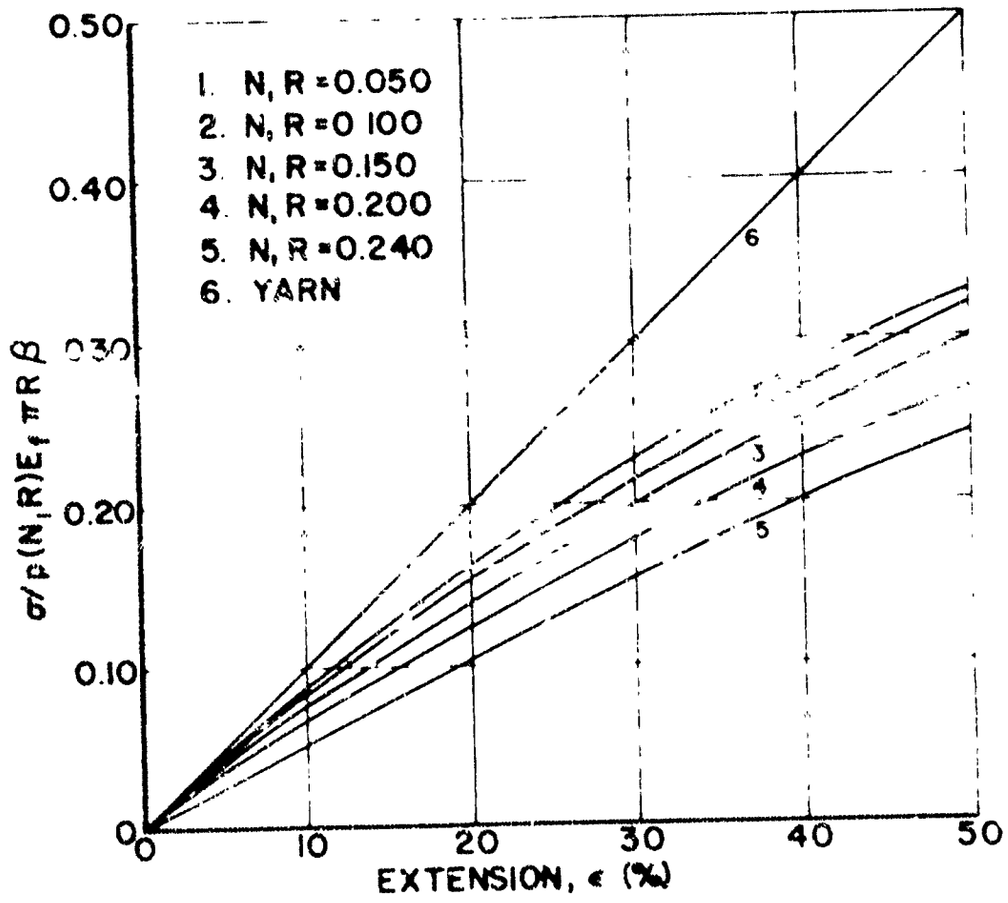

FIGURE 17. FABRIC EXTENSION: LINEARLY ELASTIC YARN ($\nu = 1/2$), SQUARE FABRIC, $\sigma_w / \sigma_f = 1$.

Filling Yarn Initially Straight, Extensible Yarn (Linearly Elastic, $\nu = 0$), $\sigma_w/\sigma_f = 1$

For a plain-weave fabric with the same number of identical, infinitely flexible yarns in both the warp and filling and the filling yarns initially straight

$$N_{1f} = N_{1w} = N_1$$

$$R_{1f} = R_{1w} = R$$

$$\theta_{1f} = 0$$

Therefore, Equations (1) - (5) describing the geometry of the fabric in the unloaded state reduce to three simplified expressions, Equations (41) - (43) (with $L_f = L_{1f}$ and $L_w = L_{1w}$). It is further assumed that the yarn radii remain constant during fabric extension, $R_{2f} = R_{2w} = R$, and that equal loads are applied in the warp and filling directions, $\sigma_w = \sigma_f = \sigma$.

With these assumptions Equations (6) - (12) describing the geometry of the fabric in the deformed state reduce to the six expressions given below. Equation (55) is obtained by substituting Equations (8) and (9) into Equation (10). Equation (56) is obtained by substituting Equation (19) into Equation (11), assuming a linearly elastic material and constant-radius yarn extension. Equation (57) is obtained similarly. Equation (58) is obtained by substituting Equations (11) and (12) into Equation (13)

$$\frac{1}{N_{2f}R} = \left(\frac{L_{2w}}{R} - 4\theta_{2w}\right)\cos\theta_{2w} + 4\sin\theta_{2w} \tag{53}$$

$$\frac{1}{N_{2w}R} = \left(\frac{L_{2f}}{R} - 4\theta_{2f}\right)\cos\theta_{2f} + 4\sin\theta_{2f} \tag{54}$$

$$\left(\frac{L_{2w}}{4R} - \theta_{2w}\right)\sin\theta_{2w} - \cos\theta_{2w} = (\cos\theta_{2f} - 1) - \left(\frac{L_{2f}}{4R} - \theta_{2f}\right)\sin\theta_{2f} \tag{55}$$

$$\frac{\sigma}{pE_f\pi R\cos^2\theta_s} = (N_{2w}R)\left(\frac{L_{2w}/R}{L_{1w}/R} - 1\right)\cos\theta_{2w} \tag{56}$$

$$\frac{\sigma}{pE_f\pi R\cos^2\theta_s} = (N_{2f}R)\left(\frac{L_{2f}/R}{L_{1f}/R} - 1\right)\cos\theta_{2f} \tag{57}$$

$$\frac{\tan\theta_{2w}}{N_{2w}R} - \frac{\tan\theta_{2f}}{N_{2f}R} = 0 \tag{58}$$

The fractional fabric extensions in the warp and filling directions are given by Equations (39) and (40).

Equations (41) - (43), (53) - (58) and Equations (39) and (40) were solved for the same range of values of the parameters as were the previous two cases. The results are given in Figures 18 and 19.

As shown in Figures 18 and 19, the fabric load-extension curves appear to intersect the zero-load axes at finite levels of strain The strain values at these apparent intercepts are the same as the strains given in Figures 13 and 14 at an applied loading ratio of one ($\sigma_w/\sigma_f = 1$). When infinitesimal, but equal, loads are applied to the fabric in the warp and filling directions, the fabric deforms, elongates in the warp direction and contracts in the filling direction, with the amount given by these intercepts. These deformations result solely from crimp interchange. This is in contrast to the case where the fabric is initially square. As shown in Figure 16, for that case all the load-extension curves converge at the zero-load, zero-extension point. An initially square fabric which is assumed to be woven from inextensible yarns does not exhibit any crimp interchange when equal loads are applied in the warp and filling directions.

As the level of applied load is increased, the fabric elongates further in the warp direction and extends from the contracted state in the filling direction. The magnitude of the extension increases with increasing applied load, decreasing yarn radius, decreasing yarn modulus, increasing yarn twist and decreasing number of yarns per unit width of fabric.

A comparison between Figure 16 for the initially square fabric and Figures 18 and 19 shows that when the filling yarns are initially straight the warp extension is considerably greater at any given load level and the filling extension somewhat less.

The effective Poisson's Ratio, μ, of fabric with initially straight filling yarn is given in Figure 20 as a function of the dimensionless load parameter $\sigma/p(N_1R)E_f\pi R\cos^2\delta_z$ for various N_1R values. The curves have been terminated at the point where the fabrics exhibit about 50% extension in the warp direction. As shown, μ is positive, i.e., the fabric contracts in the filling direction, at small values of the loading parameter and μ decreases rapidly with increasing values of the loading parameter; it is negative, i.e., the fabric extends in the filling direction, over most of the loading parameter range. The Poisson's ratios at the points where the various N_1R curves in Figure 20 intersect the zero-load axis, correspond to the Poisson's ratios for fabric with initially straight, inextensible filling yarn at a loading ratio of one (see Figure 15).

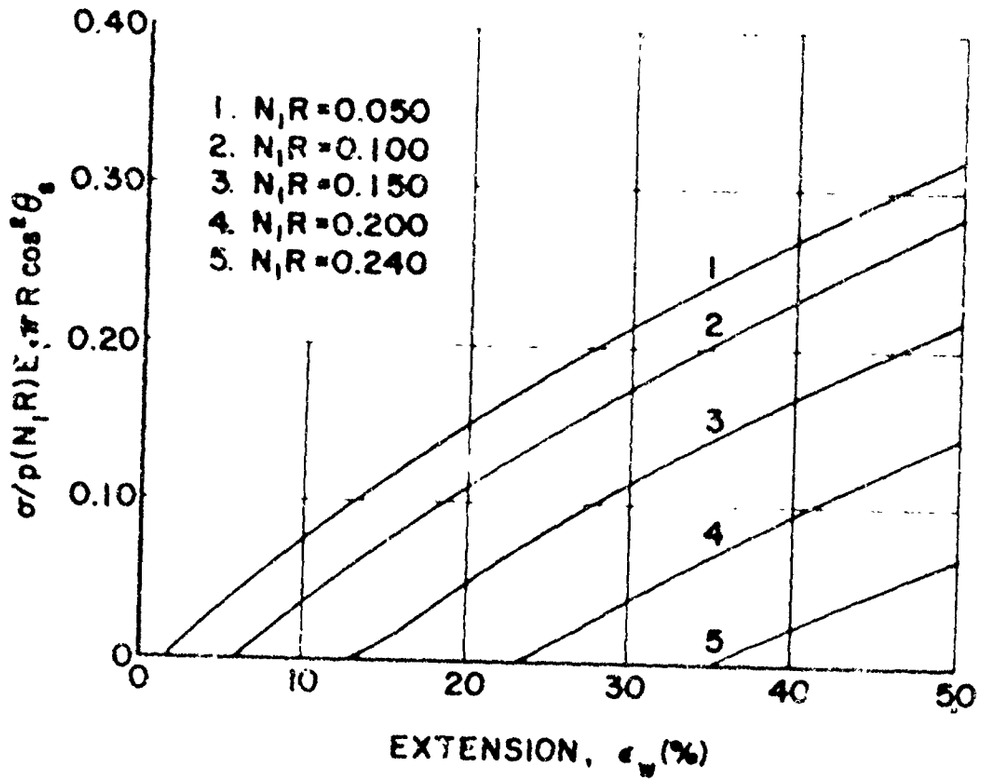

FIGURE 18. FABRIC EXTENSION IN THE WARP DIRECTION · LINEARLY ELASTIC YARN ($\nu = 0$), INITIALLY STRAIGHT FILLING, $\sigma_w / \sigma_f = 1$.

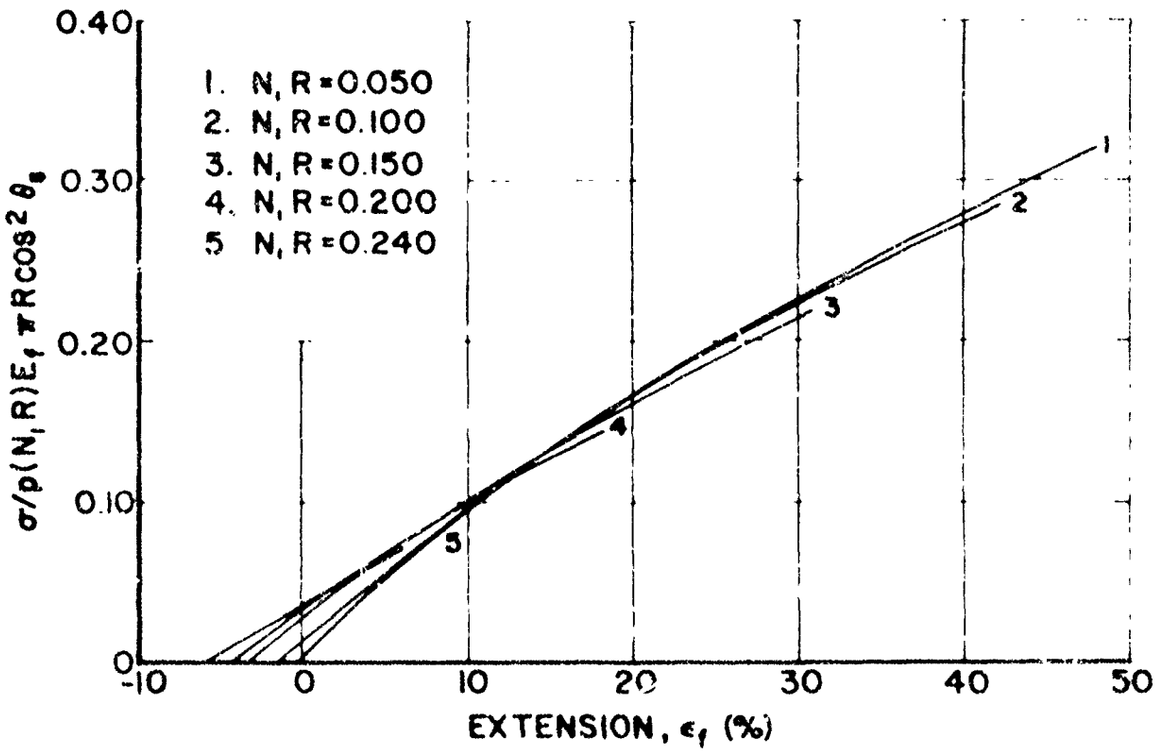

FIGURE 19. FABRIC EXTENSION IN THE FILLING DIRECTION. LINEARLY ELASTIC YARN ($\nu = 0$), INITIALLY STRAIGHT FILLING, $\sigma_w/\sigma_f = 1$.

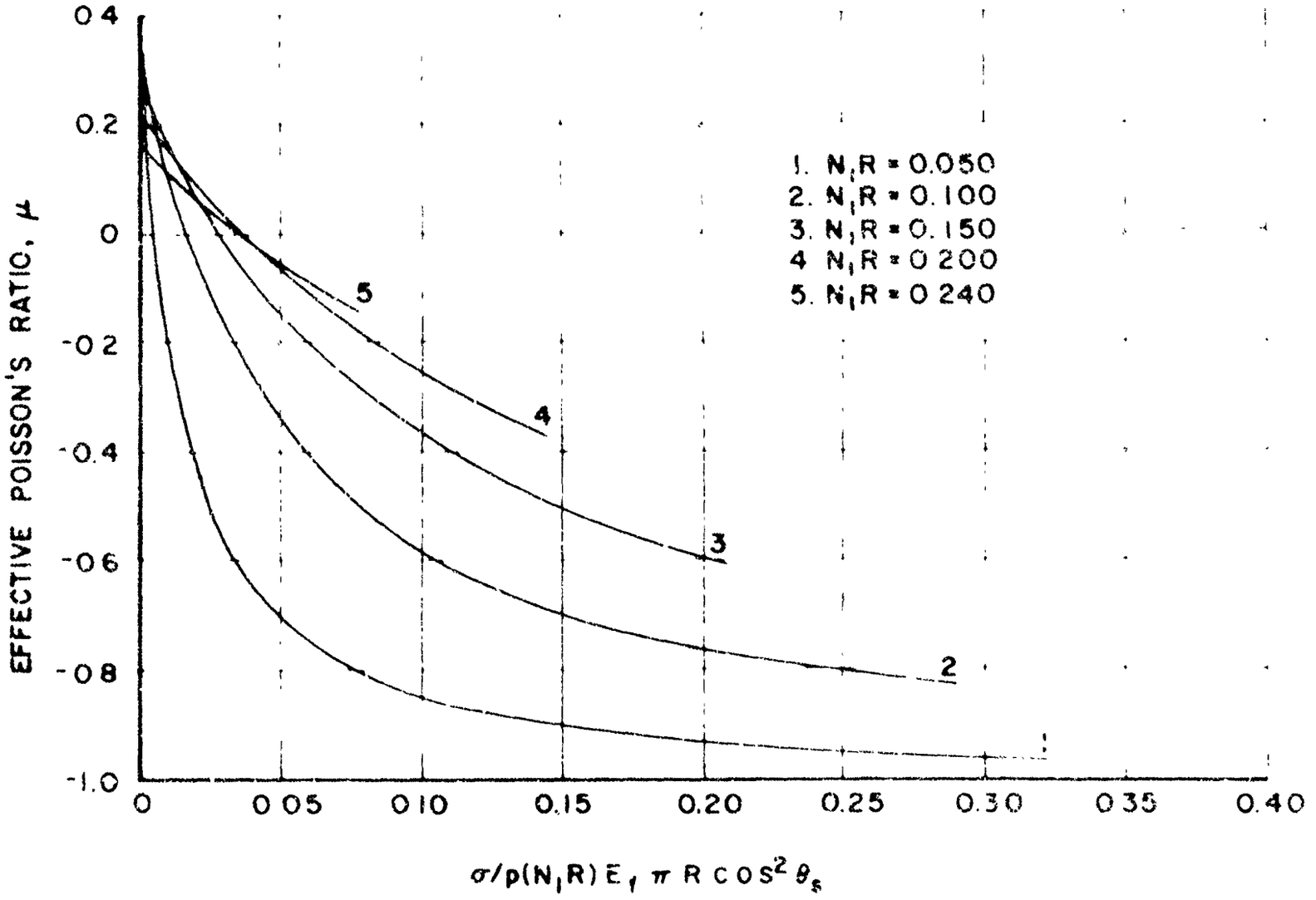

FIGURE 20 FABRIC POISSON'S RATIO, LINEARLY ELASTIC YARN ($\nu = 0$), INITIALLY STRAIGHT FILLING, $\sigma_w / \sigma_f = 1$

Square Fabric, Extensible Yarn (Linearly Elastic, $\nu = 0$), $\sigma_w/\sigma_f > 1$

As previously noted, for an initially square, plain-weave fabric with the same infinitely flexible yarn in both the warp and filling, the equations describing the geometry of the fabric in the unloaded state reduce to the expressions given in Equations (33) and (34) (with $L = L_1$). It is further assumed below that the yarns from which the fabric is woven are linearly elastic and that the yarn radii remain constant during fabric extension, $R_{2f} = R_{2w} = R$.

With these assumptions the equations describing the geometry of the fabric in the deformed state, Equations (6) - (13), reduce to the six expressions given below; Equations (8) and (9) reduce to Equation (61); Equation (11) reduces to Equation (62) after substitution of Equation (19) with $A = 0$ and $B = pE_f A_y \cos^2 \theta_s$ (see Equation (20)); Equation (12) reduces to Equation (63) in a similar manner (see Equation (21))

$$\frac{1}{N_{2f}R} = \left(\frac{L_{2w}}{R} - 4\theta_{2w}\right) \cos \theta_{2w} + 4 \sin \theta_{2w} \tag{59}$$

$$\frac{1}{N_{2w}R} = \left(\frac{L_{2f}}{R} - 4\theta_{2f}\right) \cos \theta_{2f} + 4 \sin \theta_{2f} \tag{60}$$

$$\left(\frac{L_{2w}}{4R} - \theta_{2w}\right) \sin \theta_{2w} - \cos \theta_{2w} = (\cos \theta_{2f} - 1) - \left(\frac{L_{2f}}{4R} - \theta_{2f}\right) \sin \theta_{2f} \tag{61}$$

$$\sigma_f = (N_{2f}R)\, pE_f R \cos^2 \theta_s \left(\frac{L_{2f}/R}{L_1/R} - 1\right) \cos \theta_{2f} \tag{62}$$

$$\sigma_w = (N_{2w}R)\, pE_f R \cos^2 \theta_s \left(\frac{L_{2w}/R}{L_1/R} - 1\right) \cos \theta_{2w} \tag{63}$$

$$\frac{\sigma_w}{\sigma_f} = \frac{\tan \theta_{2f}}{\tan \theta_{2w}} \left(\frac{N_{2w}R}{N_{2f}R}\right) \tag{64}$$

As for the previous cases, the fractional fabric extensions in the warp and filling directions are given by Equations (39) and (40), respectively.

Equations (33) - (34), (59) - (64) and (39) - (40) were solved for $N_1R = 0.240$ 0.200, 0.150, 0.100, 0.050; $R = 0.010$, 0.005 inch; $\theta_s = 10°$, 25°, 35°; $E_f = 3 \times 10^5$, 1×10^6, 10×10^6, 30×10^6 lbs/square inch and various combinations of applied loads σ_w and σ_f from 10 to 3000 lbs/inch width of fabric. The results of these computations are presented in Figures 21 through 27.

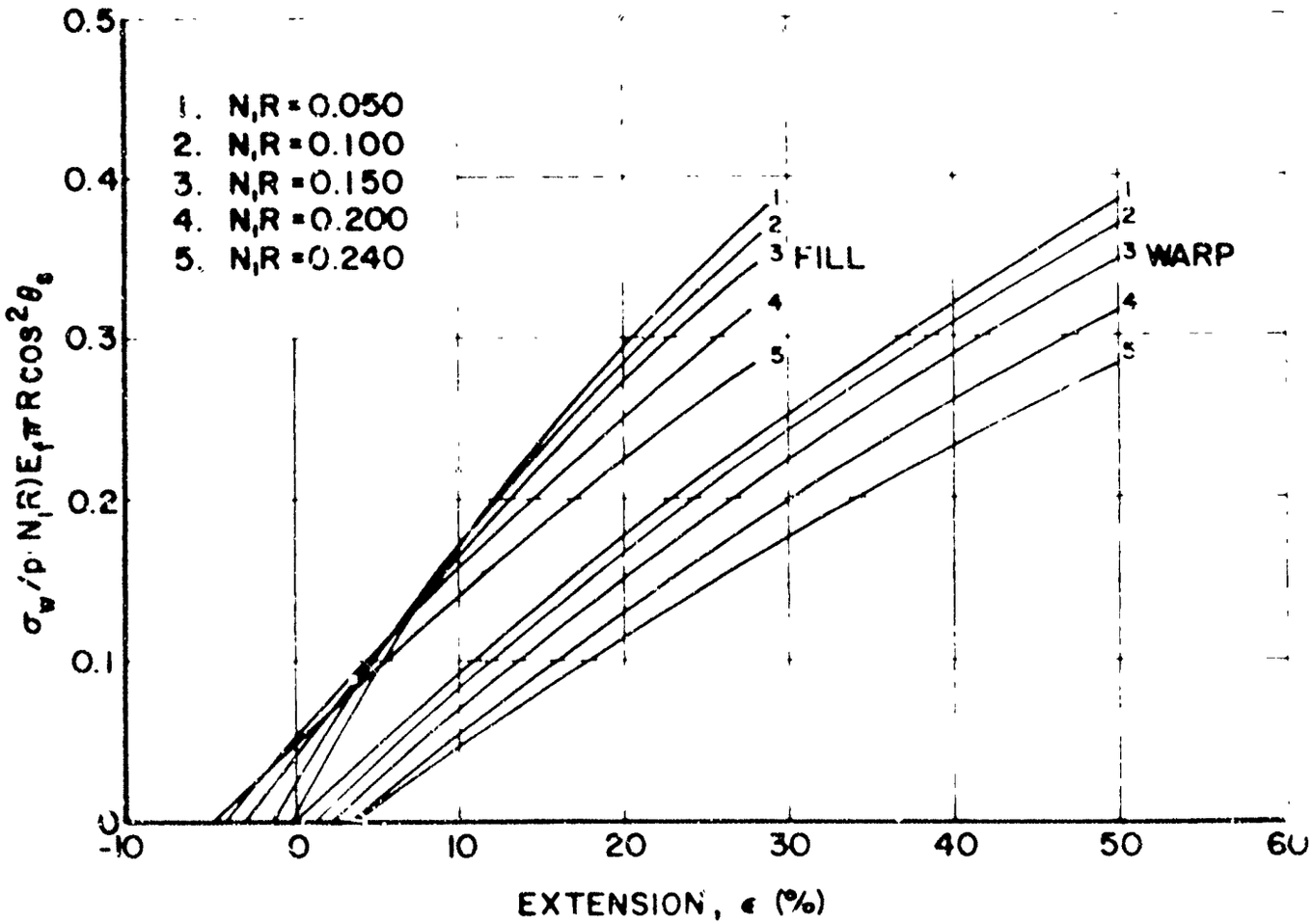

FIGURE 21 FABRIC EXTENSION: LINEARLY ELASTIC YARN (ν = 0), INITIALLY SQUARE FABRIC, σ_w/σ_f = 2.

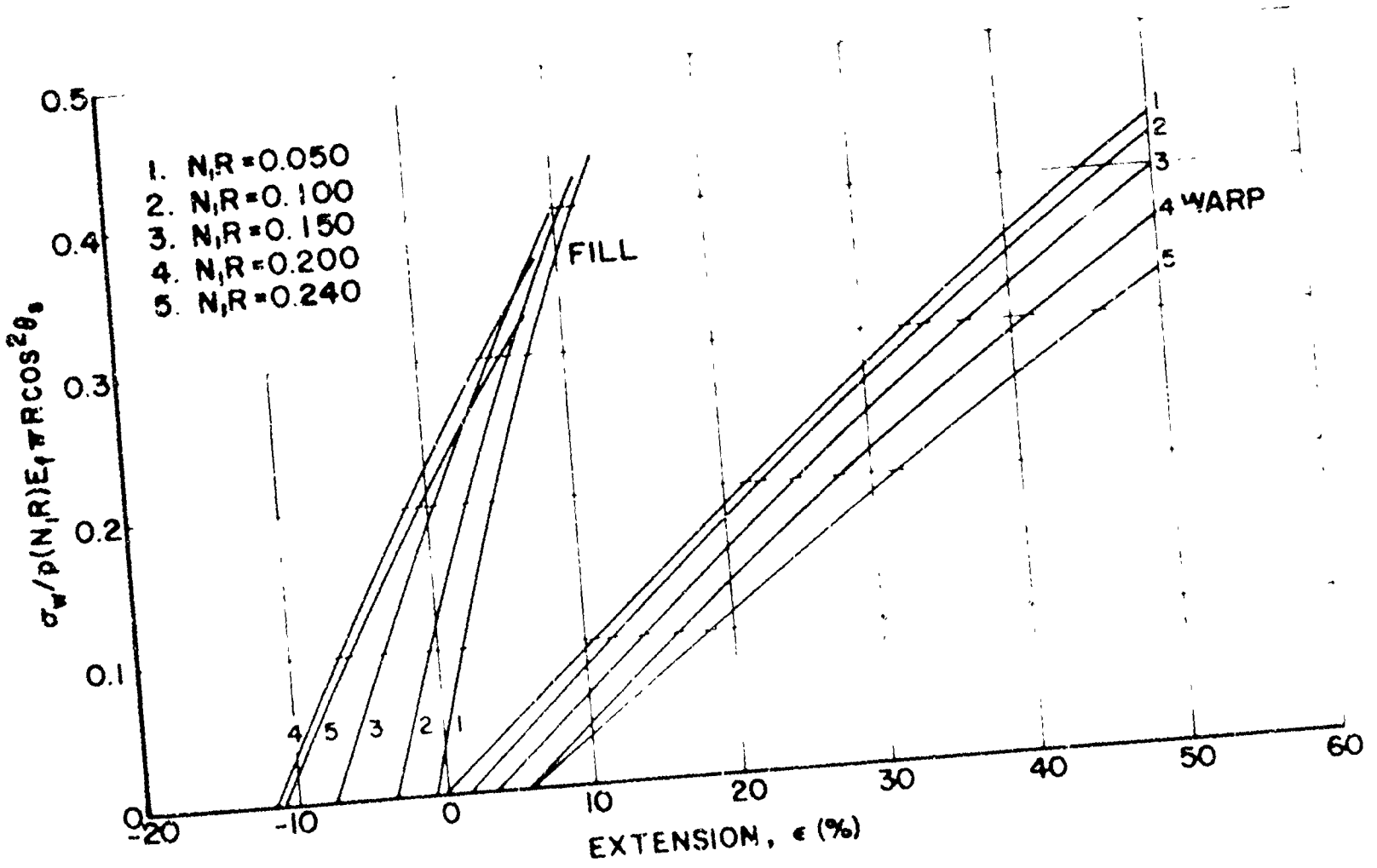

FIGURE 22 FABRIC EXTENSION. LINEARLY ELASTIC YARN ($\nu = 0$), INITIALLY SQUARE FABRIC, $\sigma_w/\sigma_f = 5$

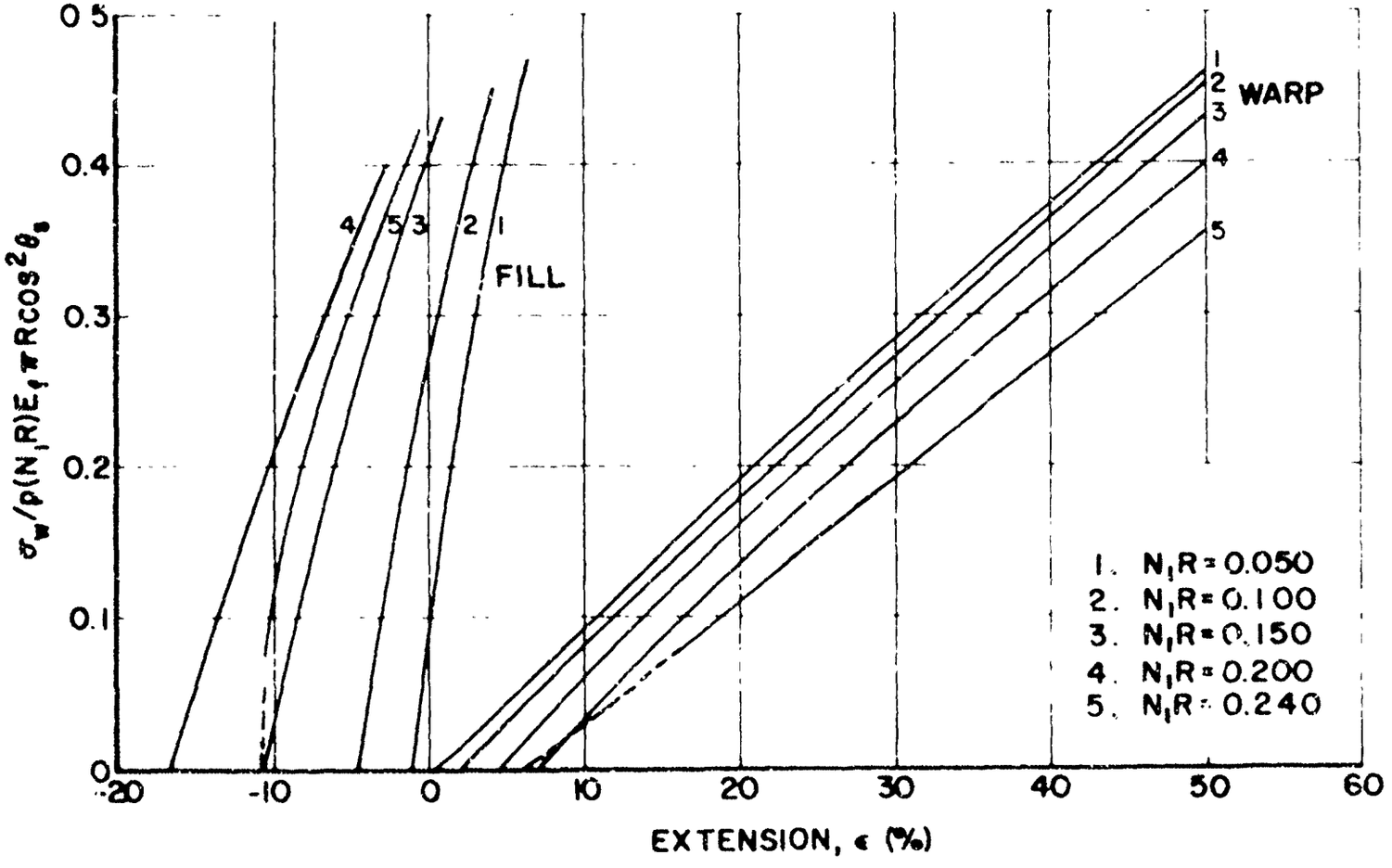

FIGURE 23. FABRIC EXTENSION: LINEARLY ELASTIC YARN ($\nu = 0$), INITIALLY SQUARE FABRIC, $\sigma_w/\sigma_f = 10$

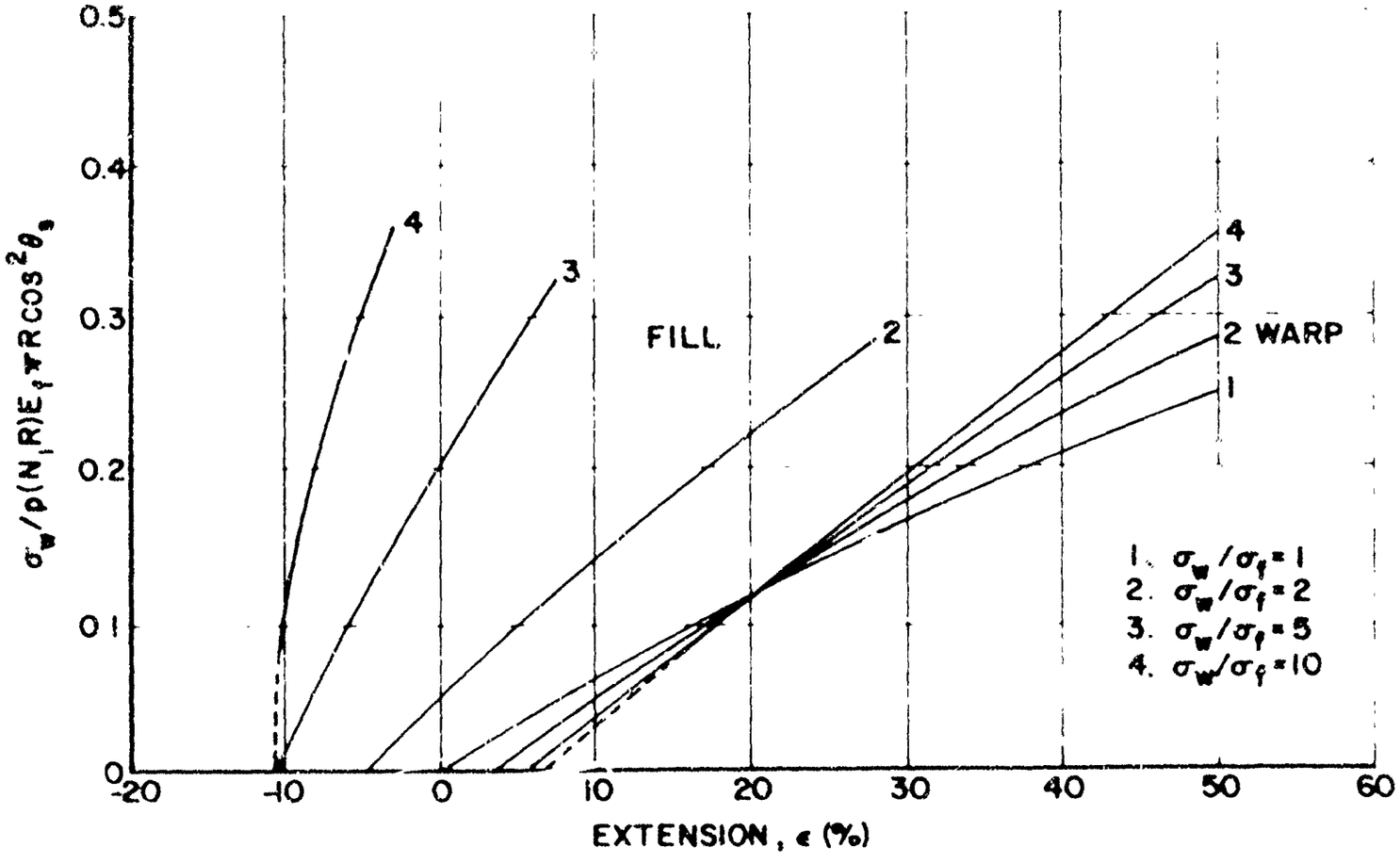

FIGURE 25. FABRIC EXTENSION: LINEARLY ELASTIC YARN ($\nu = 0$), INITIALLY SQUARE FABRIC, $N_1R = 0.240$.

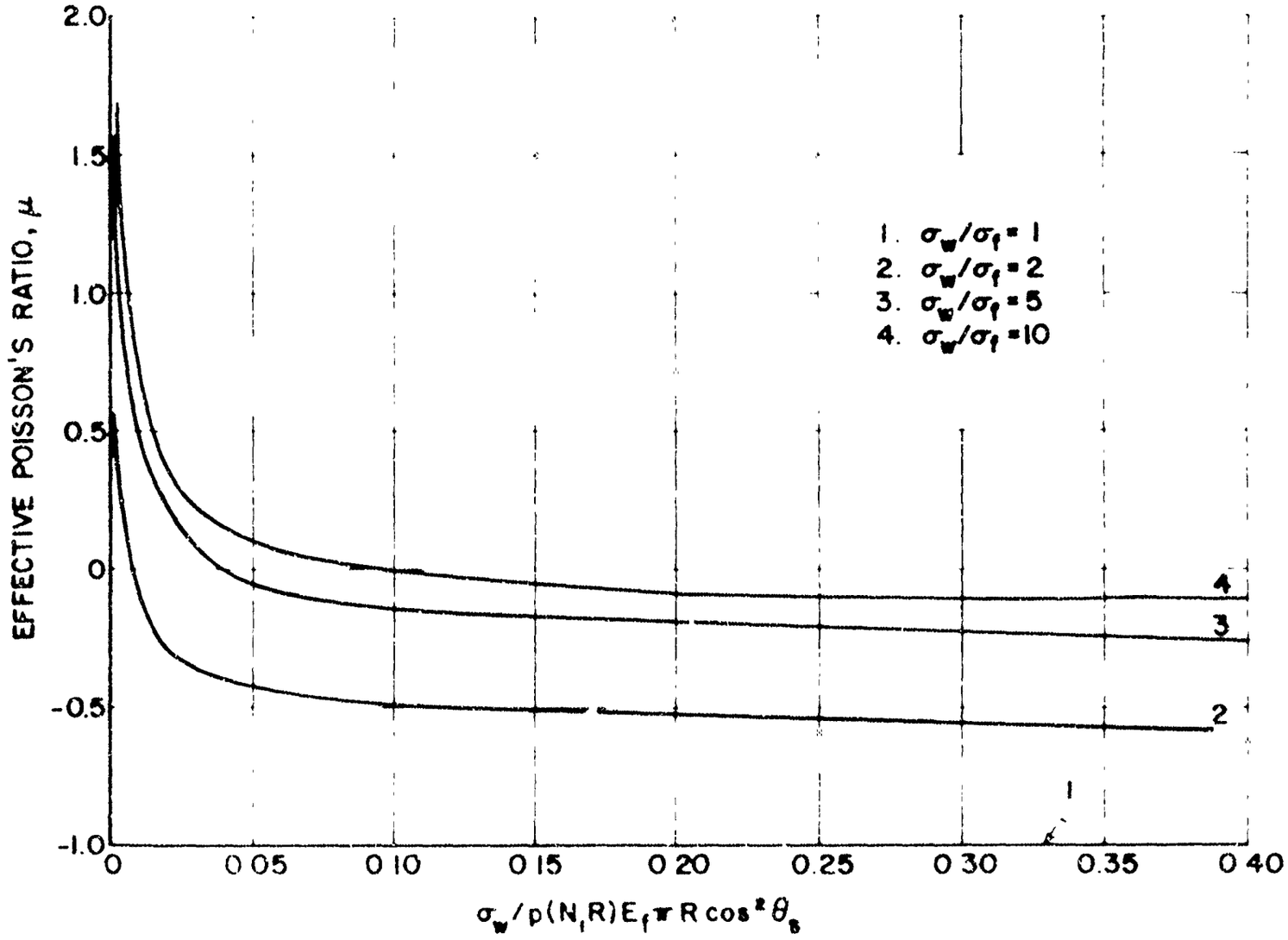

FIGURE 26 FABRIC POISSON'S RATIO LINEARLY ELASTIC YARN ($\nu = 0$), INITIALLY SQUARE FABRIC, $N_1R = 0.050$

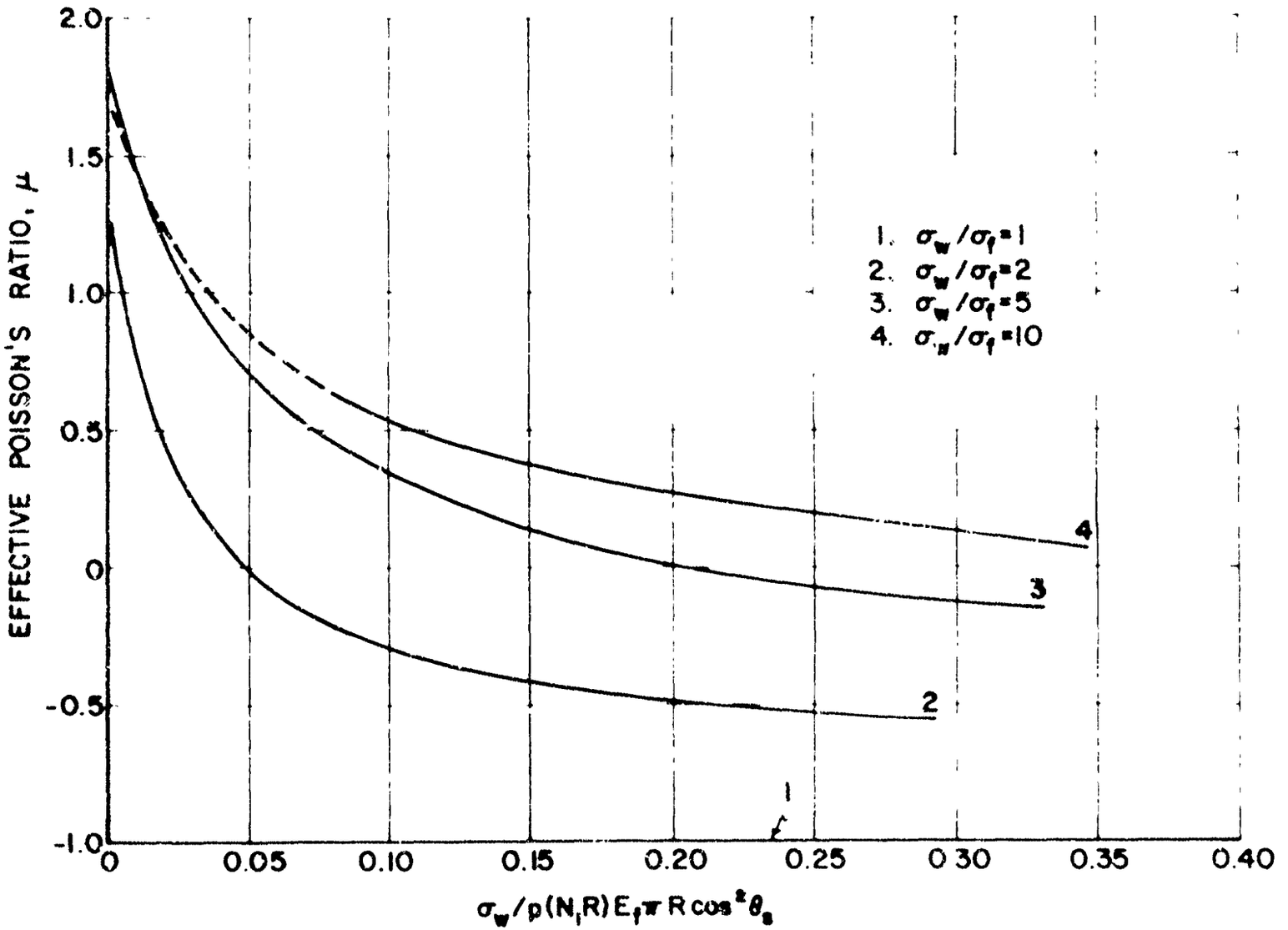

FIGURE 27. FABRIC POISSON'S RATIO: LINEARLY ELASTIC YARN ($\nu = 0$), INITIALLY SQUARE FABRIC, $N_1R = 0.240$.

The fabric load-extension diagrams for the warp and filling directions are given in Figure 21 for the various N_1R values and a loading ratio $\sigma_w/\sigma_f = 2$ Both sets of diagrams are plotted as a function of the load applied in the warp direction. Figure 22 gives similar load-extension diagrams for $\sigma_w/\sigma_f = 5$ and Figure 23, for $\sigma_w/\sigma_f = 10$. All the filling load-extension diagrams are terminated at the point corresponding to 50% extension in the warp direction.

The analytical results were examined to check that none of the solutions gave a physically impossible fabric deformation, i.e., a deformation that violated the second and third types of limiting geometries discussed previously. L_{2f} was found to be less than $2(R_{2f} + R_{2w})\,\theta_{2f}$ only over a narrow range of the loading parameter $\sigma/p(N_1R)E_f\pi R\cos^2\epsilon_s$ when $N_1R = 0.24$ and $\sigma_w/\sigma_f = 10$. The corresponding portions of the $N_1R = 0.240$ curves in Figure 23 and the $\sigma_w/\sigma_f = 10$ curves in Figures 25 and 27 are therefore dotted. Although the actual deformations must be less than that predicted by the dotted curves, the difference is probably small.

No solutions were found where contact between adjacent warp yarns was indicated, i.e., where $1/N_{2w} < 2R_{2w}$.

As shown in Figures 21 through 23, the fabric load-extension curves appear to intersect the zero-load axes at finite strains. The strain values at these apparent intercepts are the same as those given for initially square fabrics woven from inextensible yarn at the corresponding loading ratios (see Figures 7 and 8).

As for the $\sigma_w/\sigma_f = 1$ case, the magnitude of the fabric extension in the warp direction increases with increasing applied load, decreasing yarn radius, decreasing yarn modulus, increasing yarn twist and decreasing number of yarns per unit width of fabric.

The fabric contracts in the filling direction at low levels of applied loads, the contraction is greater at the higher loading ratios. However, the fabric extends from the contracted state as the applied load is increased. The level of load that must be applied in the warp direction to eliminate the filling contraction increases with increasing loading ratio. For a given applied load and loading ratio, the magnitude of the fabric extension in the warp direction is considerably greater than the extension (or contraction) in the filling direction; the difference increases with increasing loading ratio.

The fabric load-extension diagrams are replotted in Figures 24 and 25 as a function of loading ratio for the largest and smallest values of N_1R As shown in Figure 24, for $N_1R = 0.050$ the fabric extension in the warp direction is approximately the same for all loading ratios at low load levels and at any given level of applied load increases with decreasing loading ratio, the loading ratio $\sigma_w/\sigma_f = 1$ gives the greatest fabric extension. The latter evidently is the result of the greater filling extension that occurs when the load applied in the filling direction approaches that applied in the warp direction. Increased filling

yarn extension permits a decrease in filling yarn crimp, and, consequently, through the balance of the vertical components of the forces in the two orthogonal systems of yarns, a decrease in warp yarn crimp, thereby permitting increased fabric extension in the warp direction.

As shown in Figuer 25, for $N_1R = 0.240$ the initial "instantaneous" fabric extension in the warp direction increases with increasing loading ratio. However, the extension at the lower loading ratios increases at a faster rate with increasing applied load. As shown, the load-extension curves intersect - at a warp extension of about 21%. At load levels resulting in extensions greater than 21%, the extension is larger in the warp direction for the lower loading ratios, as found for the $N_1R = 0.050$ case at all extensions (see Figure 24). The fabric behavior in the filling direction for $N_1R = 0.240$ is similar to that for $N_1R = 0.050$.

The effective fabric Poisson's ratio, μ, is given in Figure 26 as a function of the dimensionless loading parameter $\sigma_w/\upsilon(N_1R)E_f \sim R\cos^2\theta_s$ for various loading ratios and $N_1R = 0.050$, and in Figure 27 for $N_1R = 0.240$. The curves have been terminated at a fabric warp extension of about 50%. For a loading ratio of one, $\mu = -1$ at all loads. For $\sigma_w/\sigma_f \geq 2$ the Poisson's ratio is positive and greater than one at small values of the loading parameter, decreases with increasing values of the parameter becoming negative over a large portion of the load-parameter range; μ increases positively with increasing loading ratio. A comparison of the curves in Figures 26 and 27 shows that μ is slightly larger throughout the load-parameter range for $N_1R = 0.240$ than for $N_1R = 0.050$.

Square Fabric, Extensible Yarn (Elasto-Plastic, $\nu = 0$), $\sigma_w/\sigma_f = 1$

As noted in the previous case, for an initially square, plain-weave fabric with the same infinitely flexible yarn in both the warp and filling, the equations describing the geometry of the fabric in the unloaded state reduce to the expressions given in Equations (33) and (34) (with $L = L_1$). In addition, also as in a previous case, if constant-radius yarn extension and a loading ratio of one, $\sigma_w/\sigma_f = 1$, are assumed

$$R_{2f} = R_{2w} = R$$

$$L_{2f} = L_{2w} = L_2$$

$$\theta_{2f} = \theta_{2w} = \theta_2$$

$$N_{2f} = N_{2w} = N_2$$

$$\sigma_w = \sigma_f = \sigma$$

It is further assumed that the yarns in the fabric are twisted from elasto-plastic fibers - fibers which are linearly-elastic before the yield and exhibit linear work-hardening beyond the yield.

The equations describing the geometry of the fabric in the deformed state are, therefore, Equations (65) and (66) which are identical to Equations (46) and (47) and Equation (67) which is derived from Equation (11) or (12) after substitution of Equation (19) with $A = p\epsilon^*(E_f - \alpha) A_y(1 - 1/2 \tan^2 \theta_s)$ and $B = p\alpha A_y \cos^2 \theta_s$.

$$\frac{1}{N_2 R} = [L_2/R - 4\theta_2] \cos \theta_2 + 4 \sin \theta_2 \tag{65}$$

$$2 = [L_2/R - 4\theta_2] \sin \theta_2 + 4(1 - \cos \theta_2) \tag{66}$$

$$\sigma = N_2 R\, p\left[\epsilon_f^* (E_f - \alpha) \pi R(1 - 1/2 \tan^2 \theta_s) + \alpha \pi R \cos^2 \theta_s \left(\frac{L_2/R}{L_1/R} - 1\right)\right] \cos \theta_2 \tag{67}$$

The fabric extensions in the warp and filling directions are equal, $\epsilon_f = \epsilon_w$, and are given by either Equation (38) or (40).

Equations (33), (34), (65) - (67) and (39) were solved for R = 0.010, 0.005 inch; θ_s = 0°, 25°, 35°; $E_f = 1 \times 10^6$ psi with $\epsilon_f^* = 0.015$ and $\alpha = 8 \times 10^4$ psi, $E_f = 30 \times 10^6$ psi with $\epsilon_f^* = 0.005$ and $\alpha = 3 \times 10^5$ psi, and a series of values of σ from 10 to 1200 lbs/inch width of fabric. However, only those solutions obtained which result in yielding of some portion of the yarn cross-section are valid. The fabric extension at loads below which this occurs is the same as for the case of a square fabric woven from linearly elastic yarns ($\alpha = 0$, $\sigma_w/\sigma_f = 1$). The combination of initial modulus $E_f = 1 \times 10^6$ psi, yield strain $\epsilon_f^* = 0.015$, and post-yield mosulus $\alpha = 8 \times 10^4$ psi approximate the properties of some polymeric fibers. Similarly the properties $E_f = 30 \times 10^6$ psi, $\epsilon_f^* = 0.005$ and $\alpha = 3 \times 10^5$ psi approximate the properties of some metallic fibers.[3]

The results of the computations are presented in Figures 28 and 29. (The data given in Figure 16 was used in constructing the initial portions of the load-extension curves.) The fabric extension increases only slightly with increasing values of the loading parameter up to $\sigma/p(N_1 R) E_f \pi R \cos^2 \theta_s = 0.012 - 0.017$ in one case and 0.0041 - 0.0054 in the other, but increases rapidly with increasing values of the loading parameter beyond these points. This latter large increase in fabric extension with increasing load is the result of the yarn having yielded. A comparison of the data given in Figures 28 and 29 to that given in Figure 15 for a fabric woven from yarns composed of linearly elastic fibers that do not yield shows that yielding results in considerably higher fabric extensions after a certain minimum load has been exceeded.

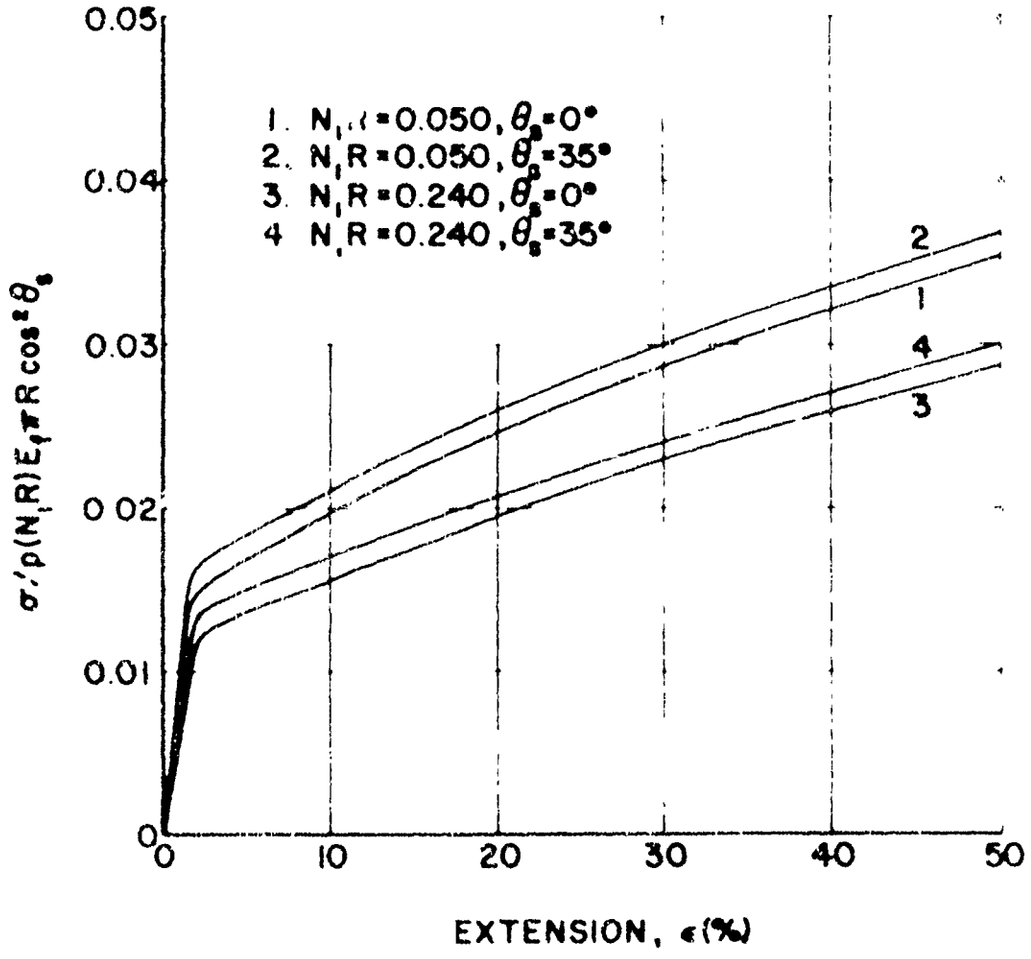

FIGURE 28. FABRIC EXTENSION: ELASTO-PLASTIC YARN ($E_f = 1 \times 10^6$ psi, $\epsilon_f^* = 0.015$, $\alpha = 8 \times 10^4$ psi, $\nu = 0$), SQUARE FABRIC, $\sigma_w / \sigma_f = 1$.

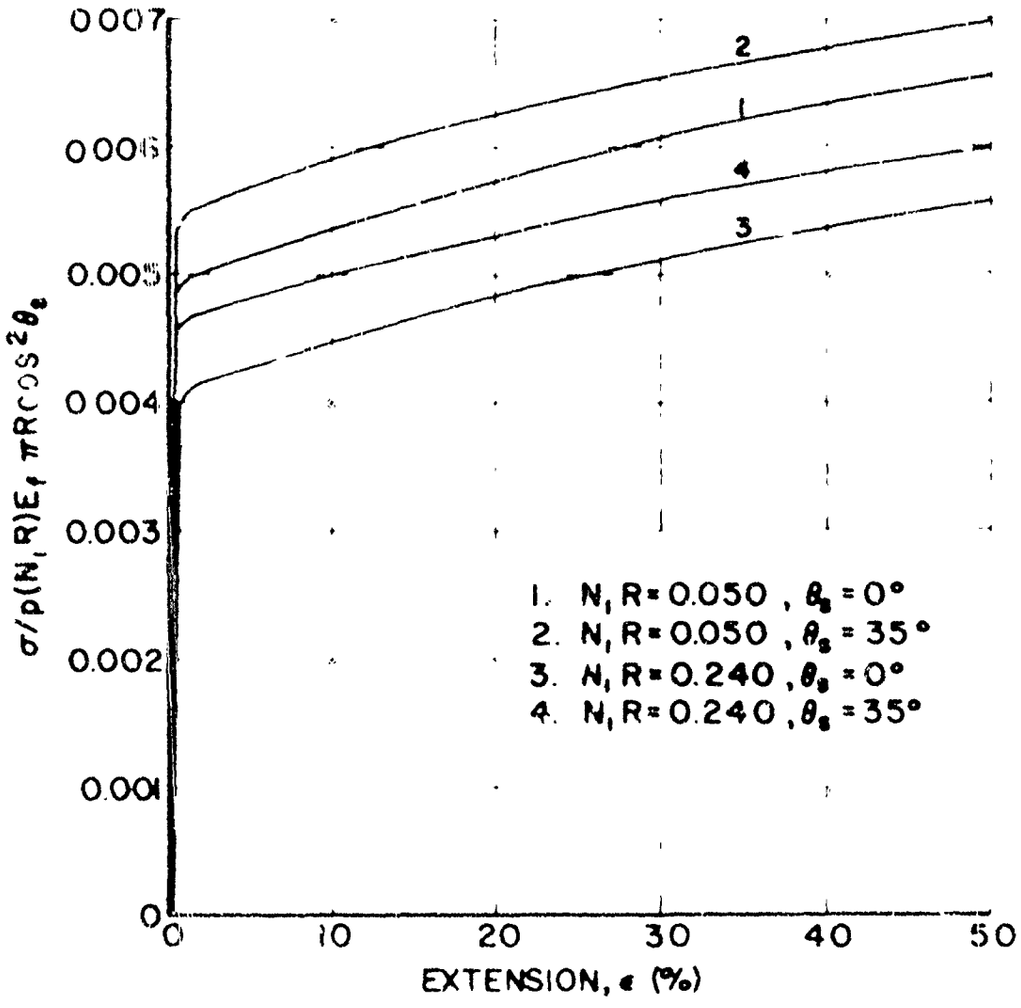

FIGURE 29 FABRIC EXTENSION: ELASTO-PLASTIC YARN ($E_f = 30 \times 10^6$ psi, $\epsilon_f^* = 0.005$, $a = 3 \times 10^5$ psi, $\nu = 0$), SQUARE FABRIC, $\sigma_w/\sigma_f = 1$.

EXPERIMENTAL PROCEDURE

A test instrument for determining the stress-strain response of fabrics under two-dimensional loading is not commercially available. However, several organizations have built suitable testers of this type for their own use. The experimental results reported herein were obtained with a biaxial tensile tester built by the MRD Division of General American Transportation Corp. under contract to the Air Force Materials Laboratory[2, 7] and loaned to FRL®. An overall photograph of the instrument is shown in Figure 30. It uses a cruciform test specimen (see Figure 31). Specimens with tails up to 4 inches wide can be accommodated, giving a 4-inch by 4-inch biaxially loaded region at the center of the specimens, the center 2-inch by 2-inch portion of which is under uniform biaxial stress.

The tails of the test specimens are gripped in capstan-type jaws which are free to rotate about an axis perpendicular to the plane of the test specimen to permit shear deformations. Care was taken in mounting test specimens to insure that the central region was not distorted and that all yarns shared the applied loads equally. The tail length, i.e., the initial distance from the edge of the 4-inch by 4-inch biaxially loaded region to the jaws, is approximately 5-1/2 inches.

The separate loads applied to the jaws are gathered to a single point by a series of variable-length lever arms (see Figure 30); the load is applied at this point by a hydraulic cylinder. The ratio of the loads applied along the two major axes of the cruciform is maintained constant throughout the test; loading ratios of 1:0, 1:1, 2:1, 3:1, 5:1, and 10:1 can be achieved.

The total load level is increased by pumping the hydraulic cylinder manually. For the work reported herein, total load increments of 25 (or 50 lbs) were used. Using test specimens with 4-inch wide tails and a 1:1 loading ratio, this means load increments of about 1-1/2 to 3 lbs per inch of test specimen width. The total applied load is measured with a tensile model, 1000-lb capacity, Dillon mechanical force gauge. The gauge was checked in an Instron and against a dynamometer. The agreement was within the precision with which readings can be made from the gauge.

The response of the fabric is recorded photographically, and the fabric extension determined by measuring the displacement of lines previously inscribed on the fabric (see Figure 32). A 35-mm Leica camera with a 3.5 Elmar lens and extension tube and a very fine-grain film were used. The test specimens were illuminated with a circular fluorescent tube through the center of which the camera lens was focused (see Figure 30).

A 2-inch by 2-inch square was inscribed at the center of each test specimen prior to its being mounted in the tester. The lines were drawn on the fabric with ink using a very fine brush. A color was used which contrasted with the color of the fabric in an effort to insure sharp photographs. Each line followed a single yarn.

FIGURE 30. BIAXIAL TENSILE TESTER.

FIGURE 31. CRUCIFORM TEST SPECIMEN.

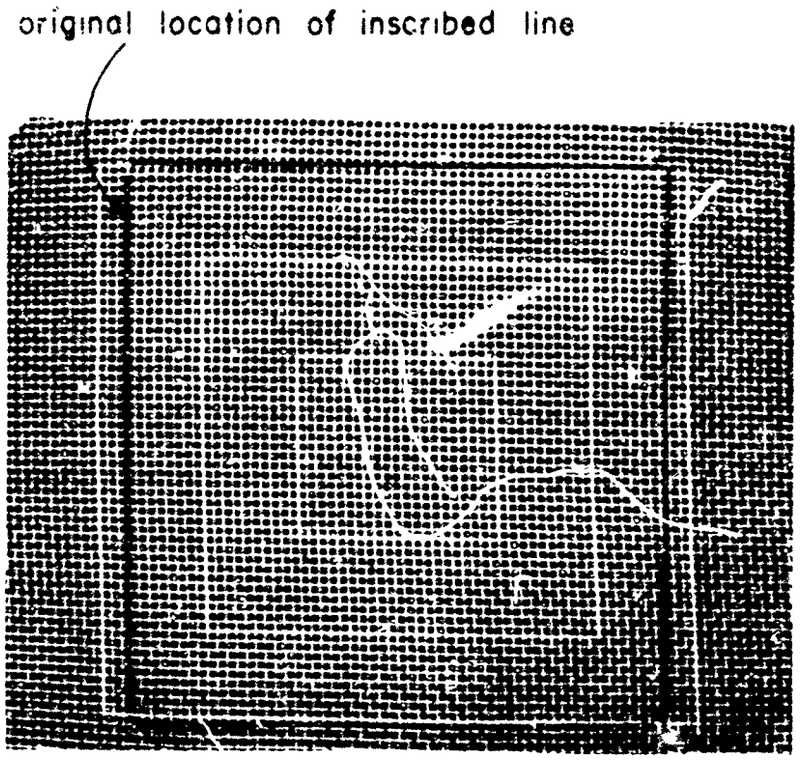

FIGURE 32. BIAXIALLY STRESSED FABRIC.

The change in dimensions of the 2-inch by 2-inch inscribed square was measured with a steel rule after projecting the film in a microfilm reader. (This gives a magnification of about 3.5X.) Two readings were taken from each frame of the film in both of the principal directions. These readings were made about one inch in from the edge of the projected square. The distance between opposite pairs of the projected lines was measured approximately to the nearest 0.01 inch. Each pair of readings taken from each frame of the film were averaged. They usually agreed within 0.02 - 0.03 inch.

EXPERIMENTAL RESULTS ON MODEL FABRICS

The theoretical and experimental biaxial stress-strain response of two monofilament screen fabrics are compared in Figures 33 through 38. The constructions of the fabrics are given in Table 1. Both are plain weave woven from saran monofilaments with the same monofilament in both the warp and filling directions. The filament diameters given in Table 1 are the average of many measurements made with a fiber projection microscope at a magnification of 500X.

The uniaxial tensile properties of the fabrics are given in Table 2. The data was obtained on an Instron using one-inch wide, ravelled-strip test specimens, a 5-inch gauge length and 0.5-inch per minute jaw speed.

The average crimp in the filaments in both fabrics was also measured using the fiber projection microscope. Both the warp and filling in the gray saran fabric exhibit the same amount of crimp, about 2-1/2%. However, the warp filaments in the undyed saran fabric exhibit about 5-1/2% crimp and the filling 2-3/4% crimp. Additionally, as shown in Table 1, both fabrics have roughly the same number of monofilaments per unit width in the warp and filling directions – the difference is less than $\pm$1/2% of the average of the two values. Therefore, both fabrics are approximately square, although the gray saran fabric is closer to being perfectly square.

The theoretical curves in Figures 33 through 38 are for the N_1R values which are the averages of the warp and filling N_1R values calculated for the particular fabric being considered; $N_1R = 0.127$ for the gray saran fabric and 0.165 for the undyed saran fabric. The theoretical $N_1R = 0.125$ curves given in Figures 16, 21 and 22 were assumed insignificantly different from the theoretical curves for $N_1R = 0.127$ and are, therefore, reproduced in Figures 33, 34, and 35, repsectively. The $N_1R = 0.165$ curves in Figures 36, 37, and 38 were obtained by interpolating between the 0.150 and 0.200 curves of Figures 16, 21, and 22, respectively.

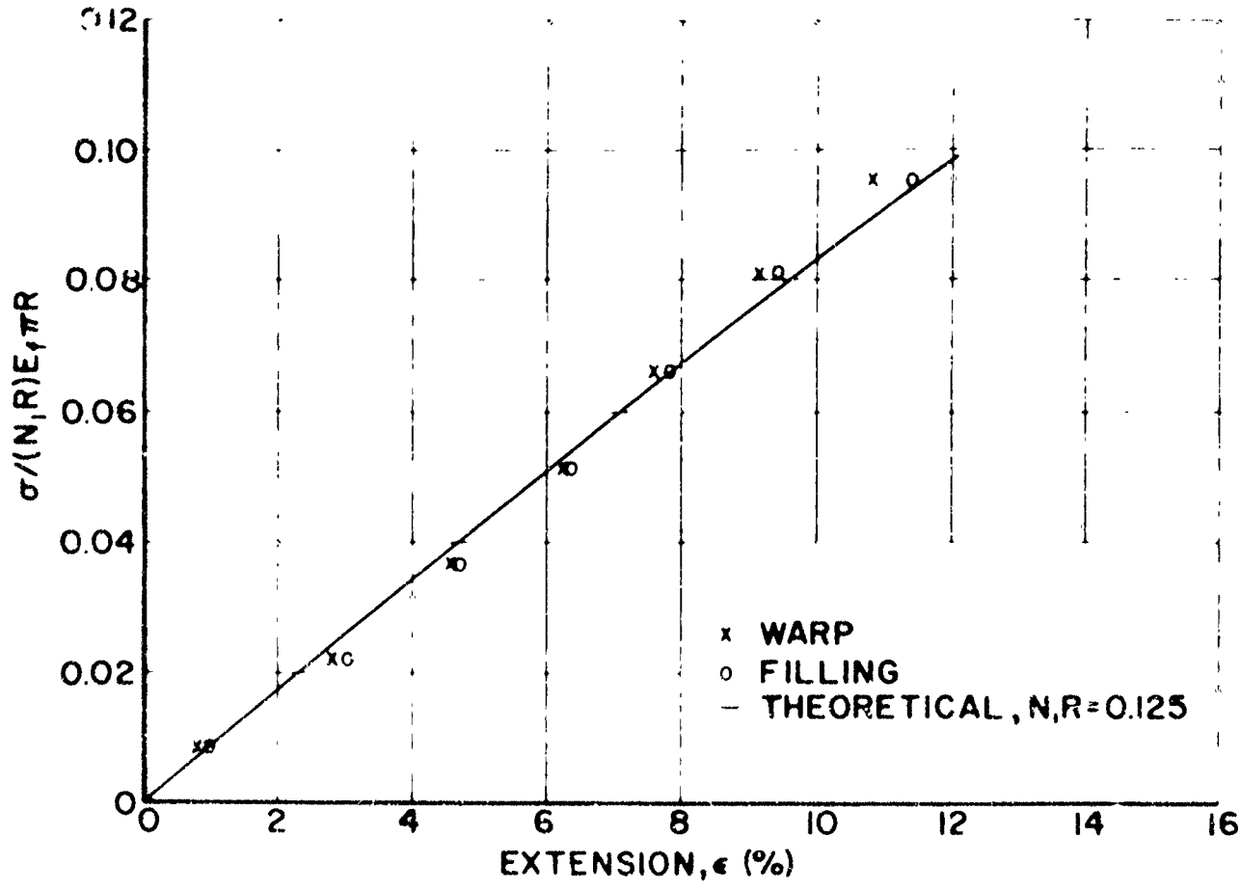

FIGURE 33. BIAXIAL LOAD-EXTENSION RESPONSE OF GRAY SARAN FABRIC AT $\sigma_w / \sigma_f = 1$

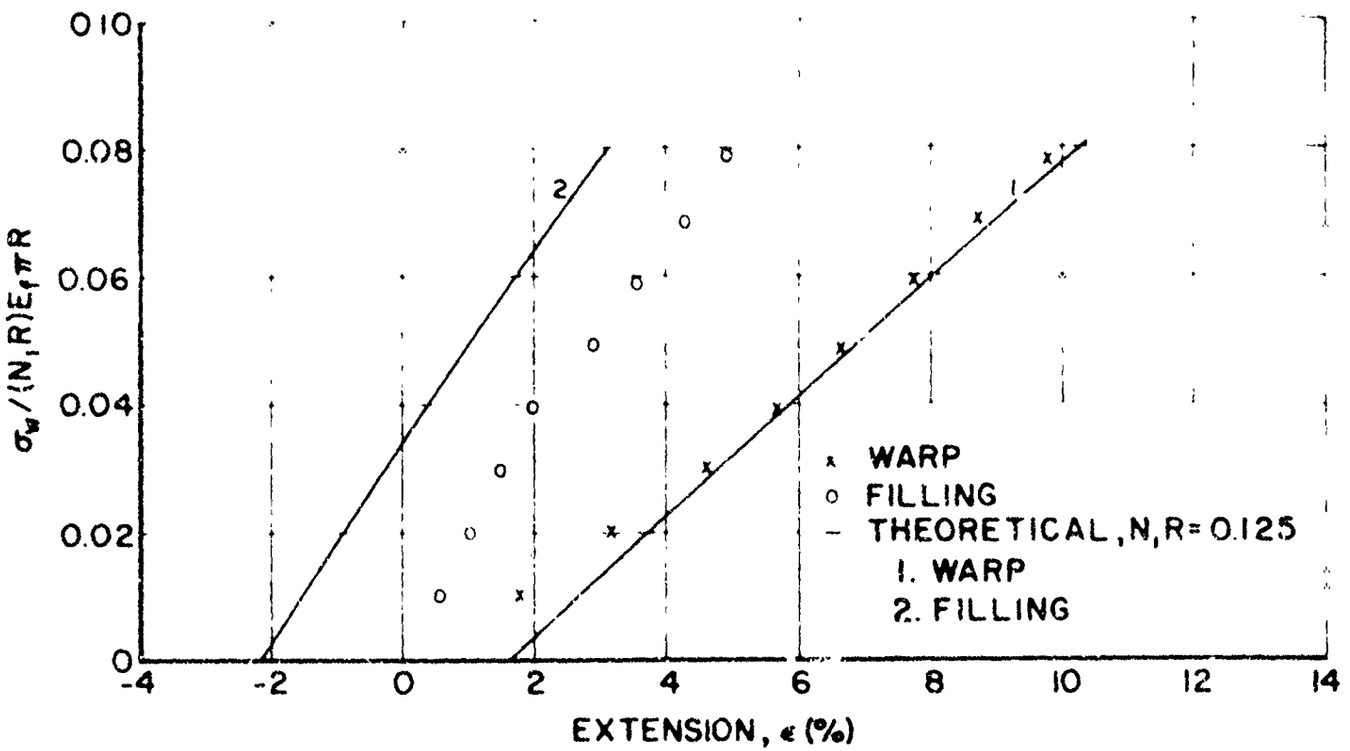

FIGURE 34 BIAXIAL LOAD-EXTENSION RESPONSE OF GRAY SARAN FABRIC AT $\sigma_w/\sigma_f = 2$

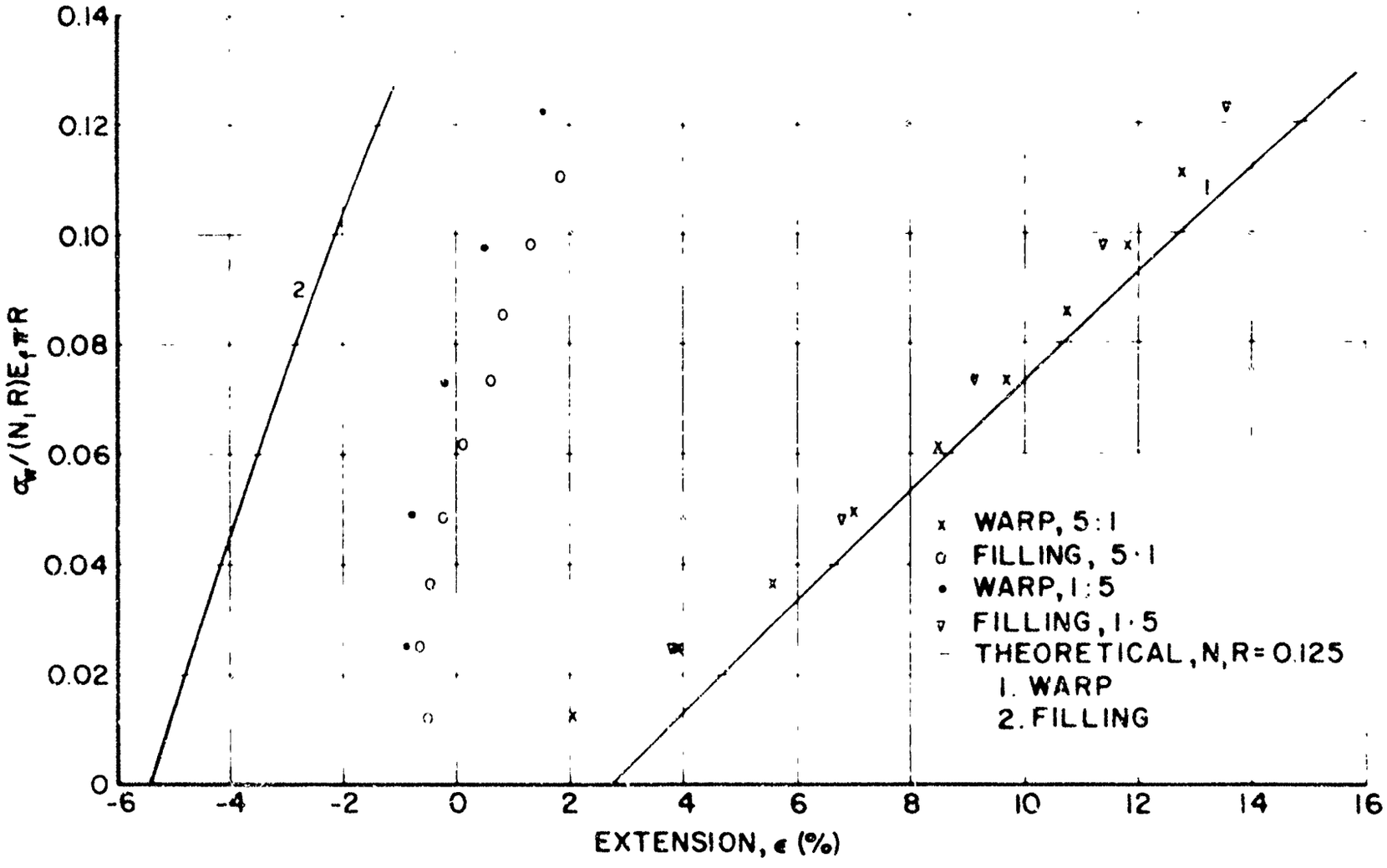

FIGURE 35 BIAXIAL LOAD-EXTENSION RESPONSE OF GRAY SARAN FABRIC AT σ_w/σ_f = 5:1 & 1:5

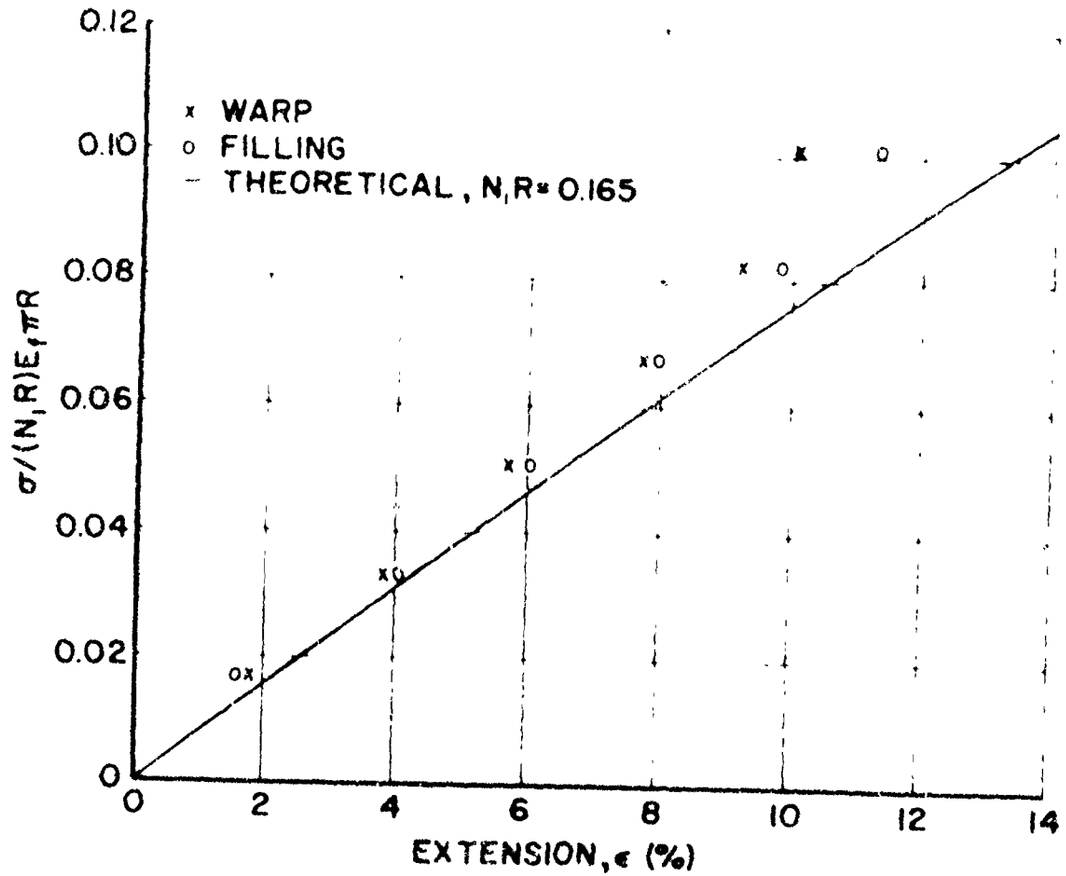

FIGURE 36. BIAXIAL LOAD-EXTENSION RESPONSE OF UNDYED SARAN FABRIC AT $\sigma_w/\sigma_f=1$.

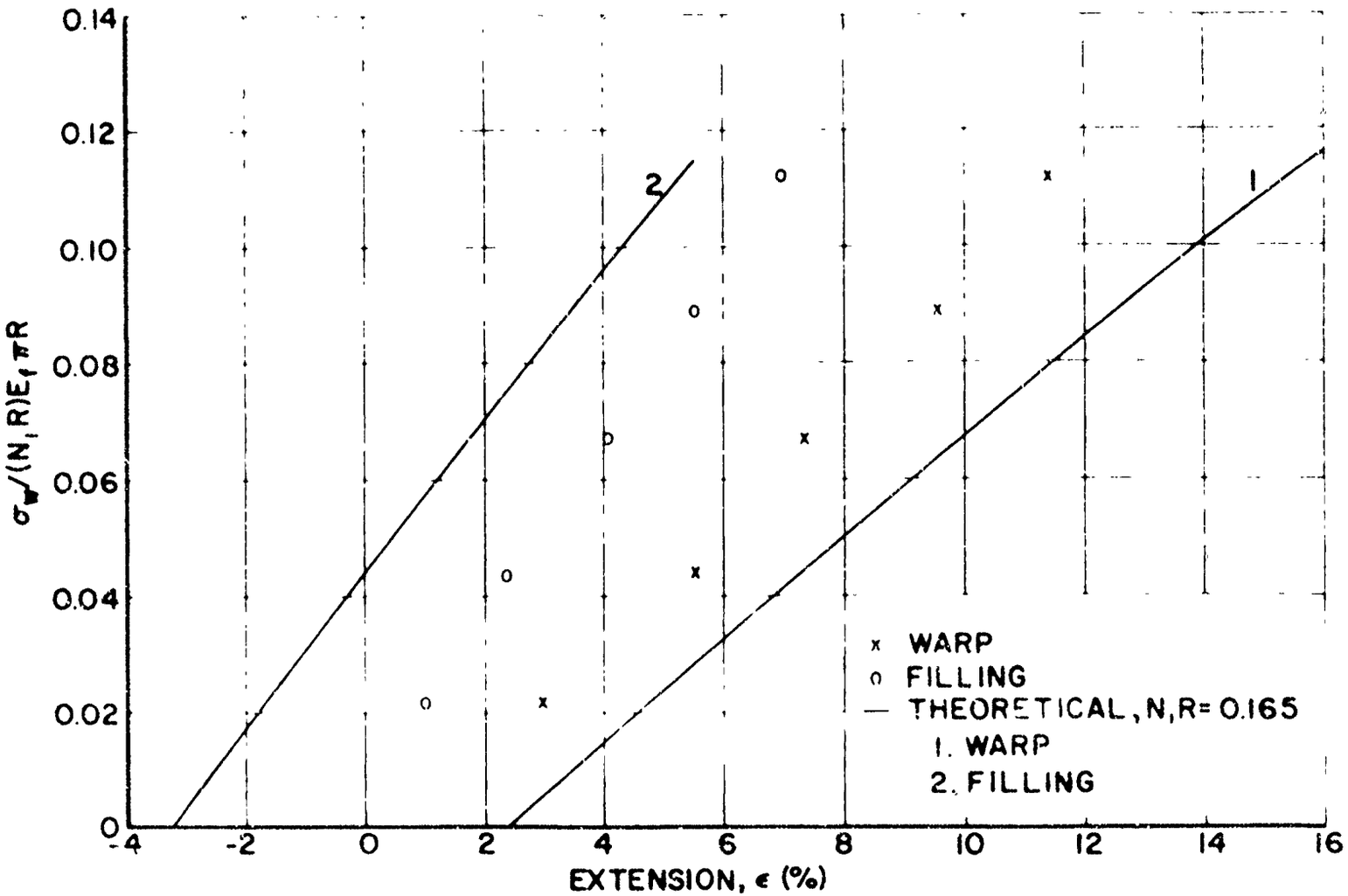

FIGURE 37. BIAXIAL LOAD-EXTENSION RESPONSE OF UNDYED SARAN FABRIC AT $\sigma_w/\sigma_f = 2$.

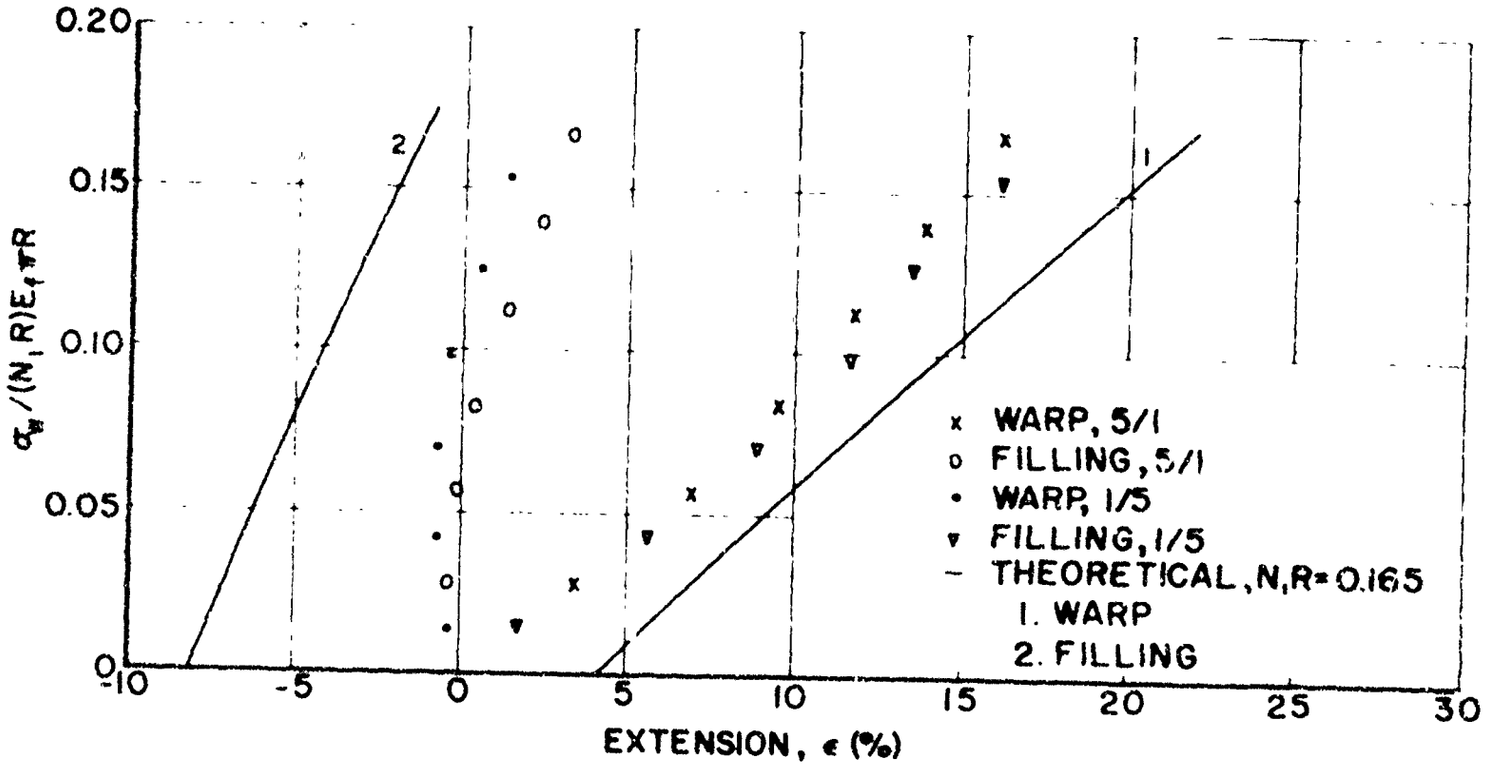

FIGURE 38. BIAXIAL LOAD-EXTENSION RESPONSE OF UNDYED SARAN FABRIC AT σ_w/σ_f = 5:1 & 1:5.

TABLE 1

FABRIC CONSTRUCTION

Fabric	Yarn Diameter (mils)	Weave	Picks per Inch	Ends per Inch	Weight (oz/sq yd)	Yarn Crimp (%) Warp	Yarn Crimp (%) Filling
Gray Saran	12.4	plain	21	20	6.2	2-1/2	2-1/2
Undyed Saran	10.2	plain	33-1/4	31-1/2	7.0	5-1/2	2-3/4

TABLE 2

FABRIC UNIAXIAL TENSILE PROPERTIES

Fabric	Rupture Elongation (%) Warp	Rupture Elongation (%) Filling	Rupture Load (lbs/inch width) Warp	Rupture Load (lbs/inch width) Filling
Gray Saran	18.7	19.9	58.7	61.0
Undyed Saran	24.0	25.9	68.2	71.0

For $N_1 R = 0.125$, $\theta_1 \approx 15°$, i.e., the warp and filling yarns in the gray saran fabric are at an angle of about 15° to the plane of the fabric at the mid-point between yarn crossovers prior to loading. Similarly, for $N_1 R = 0.165$, i.e., the undyed saran fabric, $\theta_1 \approx 20°$. The characteristic tensile moduli of the monofilaments from which the fabrics were woven were determined by tensile testing filaments ravelled from the fabrics. A 5-inch gauge length and a 5-inch per minute jaw speed were used. In determining the moduli from the slope of the linear portion of the load-elongation diagrams, (the load-extension diagrams of the monofilaments were approximately linear from initiation of load to failure) the test-specimen gauge length was taken as one plus the fractional crimp times the sum of the initial distance between jaws plus the jaw displacement to the point where a load buildup was first indicated. This procedure gave a modulus of 175,000 psi for the 12.4-mil diameter monofilaments in the gray saran fabric and 145,000 psi for the 10.2-mil diameter monofilaments in the undyed saran fabric. These moduli values were used in determining the appropriate value for the dimensionless loading parameter for each experimental point plotted.

The test instrument and experimental procedure described in the previous section were used in determining the stress-strain response of the two fabrics under biaxial loading. Cruciform test specimens with nominal 4-inch wide tails were used. Instead of ravelling the tails exactly to a 4-inch width, they were ravelled to a specific number of ends. Each tail of the gray saran fabric test specimens contained 80 ends and each tail of the undyed saran fabric test specimens, 126 ends.

Considerable care was taken in mounting every test specimen in the jaws to ensure that distortion during loading in the central, biaxially stressed section of the specimen would be minimized. This was particularly difficult with the undyed saran fabric because the filling was bowed. The monofilaments in the filling of the gray saran fabric were parallel to each other and also perpendicular to the warp yarns, throughout the fabric.

The fabrics were tested at ratios of the load applied in the warp direction to the load applied in the filling direction of 1:1, 2:1, 5:1, and 1:5. Three tests were made on both fabrics at the 1:1 ratio; two on both at the 2:1 ratio; two on the gray saran and four on the undyed saran at 5:1; two on the gray saran and one on the undyed saran at 1:5. The measured fabric strains are given in Figures 33 through 38 as a function of the dimensionless loading parameter, $\sigma/(N_1 R) E_f \sim R$. Each point plotted is the average of the several tests made at that value of the loading ratio and loading parameter. The individual test results agreed within ±5% of their average.

The last experimental points in Figures 33 through 38, the points at the highest strain, were recorded in most instances at the last load increment before the test specimen failed. However, this load level cannot be considered the true breaking strength of the fabric under biaxial loading. Stress concentrations occur where the tails join the biaxially stressed central portion of the cruciform test specimens and cause premature failure.

As shown in Figures 33 through 38, the experimental points are in reasonable agreement with the theoretical curves. The difference between the predicted and measured values of warp and filling strains for the gray saran fabric at the 1:1 loading ratio is small at all levels of strain - about 5% (one hundred times the predicted strain minus the measured strain at the same load divided by the measured strain) in the warp direction and < 1% in the filling direction at 10% measured strain (see Figure 33).

At the 2:1 loading ratio the difference between the predicted and measured strains in the warp direction is about 2% at 9% strain. However, as shown in Figure 34, the percent difference becomes large at low loads. At the load level where the measured strain in the warp direction is 1.75%, the predicted strain is 2.7%. As also shown in Figure 34, the difference between the predicted and measured strains in the filling direction is considerable at all loads; when the measured filling strain is +0.55%, that predicted is -1.5%, when the measured strain is 4.9%, that predicted is 3%.

At the 5:1 loading ratio the difference between the predicted and measured strains in the warp direction is about 6% at 12% strain. However, as at the 2:1 loading ratio, the difference becomes large at low load levels, the difference between the measured and predicted strains in the filling direction is also large throughout the test load range.

As indicated in Figure 35, the gray saran fabric was tested at both 5:1 and 1:5 loading ratios. Approximately the same results were obtained at both loading ratios, further indicating that the fabric is square.

The difference between the predicted and measured values of strain for the undyed saran fabric at the 1:1 loading ratio is 17% in the warp direction and 9% in the filling direction at 9% measured strain. As shown in Figure 36, the difference becomes less at lower loads.

Similarly, the difference between the predicted and measured strains in the warp direction at the 2:1 loading ratio is about 22% at 10% strain. However, the percent difference becomes larger at lower load levels (see Figure 37). When the measured strain is 3%, that predicted is 4.8%. Additionally, as for the gray saran fabric, the difference between the predicted and measured strains in the filling direction is quite large at all load levels, when the measured strain is +1%, that predicted is -1.6%, when the measured strain is 1% that predicted is 5.4%.

At the 5:1 loading ratio the difference between theory and experiment is large; a difference of 32% at a warp strain of 14%. Also, as at the 2:1 loading ratio, the difference becomes larger at lower loads and the difference in the filling direction is large throughout the load range.

Results are also given in Figure 38 for a single test run at a 1:5 loading ratio. As shown, these results agree reasonably well with those at 5:1.

The differences between the predicted and experimentally measured results may be attributed to the deviation of the fabric geometries, monofilament properties and fabric deformations from those assumed in the analysis. Discussion of some of these deviations follows. However, the quantitative effect of various possible causes of the differences is difficult to estimate.

The theoretical analysis on which the predicted fabric response is based assumes perfectly square fabrics. As noted above, the fabrics do not have exactly the same number of picks per inch as ends per inch. However, the differences are small and this probably does not contribute significantly to the variance between theory and experiment. The assumption of an initially square fabric not only assumes the same number of yarns in both directions but also the same degree of crimp in both sets of yarns. Although the warp and filling monofilaments of the gray saran fabric have roughly the same crimp, the crimp in the warp filaments of the undyed saran fabric is twice that in the filling yarns. This is probably one of the reasons that agreement between theory and experiment is not as good with the undyed saran fabric as with the gray saran fabric.

Another possible reason that the experimental results obtained using the undyed saran fabric do not better agree with the theoretically predicted results is that the filling yarn in the fabric is moderately bowed. This undoubtedly affects the response of the fabric under biaxial loading.

Examination of filaments removed from both fabrics under the microscope reveals some permanent flattening of the filaments at yarn cross-overs. This flattening is considerably more severe in the undyed saran fabric and, undoubtedly, also affects the response of the fabric.

The procedure used to arrive at a value for the tensile modulus of the monofilaments from which the fabrics are woven has several shortcomings. The monofilaments are permanently deformed – crimped – during weaving; when removed from the fabrics they maintain this crimped configuration. Furthermore, careful observation of the filament response during tensile testing indicates that some filament axial extension probably takes place before all the crimp is removed. As noted previously, the axial length of the test specimen was taken as the test gauge-length, not the shorter distance between jaws. This results in a larger measured modulus. However, if some of the filament crimp is removed as the filament extends, the measured modulus will be smaller than the true value; additionally, the magnitude of the effect of the latter on the measured modulus is considerably larger than the former. Therefore, the true tensile moduli of the monofilaments might be somewhat greater than the values used in plotting the experimental data in Figures 33 through 38. A larger value of filament modulus would decrease the difference between theory and experiment in the warp direction and increase the difference in the filling direction.

CONCLUSION

The foregoing investigation shows that the stress-strain response of monofilament screens under two-dimensional loading can be predicted with reasonable accuracy when the effects of yarn extension are included. However, as noted, the divergence between theory and experiment becomes quite large at low levels of applied load when the loading ratio is greater than one. This is because the load-deformation behavior of monofilament screen fabrics at low to moderate loads – in the crimp-interchange region — is strongly dependent on yarn bending rigidity, which was not considered in the analysis. It is anticipated that the agreement between theory and experiment for fabrics woven from multifilament yarns would be better because of the inherently lower bending rigidity of multifilament yarns.

As a first step in incorporating yarn rigidity into an analysis of fabrics, a theoretical analysis of the load-deformation behavior of a twisted multifilament crimped yarn should be developed. Such an analysis would be an extension of the work done by Chicurel[1] on monofilaments and Platt[14] on twisted multifilament yarns. The effects of yarn twist and filament plastic flow could be included Although perfect translation of yarn proper s into fabric properties is not to be expected, past experience has shown that a thorough understanding of fabric properties requires a knowledge of the influence of yarn structure and filament properties on yarn properties.

The load-deformation behavior of a fabric woven from multifilament yarn is also influenced by yarn flattening. Low-twist multifilament yarns will flatten more easily than high-twist yarns. The occurrence yarn flattening during fabric extension will result in a decrease in the slope of the fabric load-elongation diagram.

Since the extension of a fabric is mainly dependent on the thickness, perpendicular to the fabric plane, of the yarns from which it is woven, the effects of yarn flattening might be included in the load-deformation analysis of a fabric by utilizing a yarn radius that is a function of the normal force on the yarns at yarn crossovers, i.e., $R = R(P_y \sin \xi_2)$. The explicit expression for the dependence of yarn radius on normal pressure would probably have to be determined experimentally.

Fabric deformation is further affected by yarn twist magnitude and direction because of the bedding (nesting) tendency at yarn intersections of the surface filaments of the yarns. Such bedding serves both to increase the surface of contact between the two yarn systems, warp and filling, and also to partially lock the yarn intersections at their points of contact. Therefore, nesting restricts yarn movement and may increase the slope of the fabric load-elongation diagram.

For parallel nesting of the contact filaments at yarn crossovers the local helix angle must be approximately 45°. Although straight yarn helix angles do not usually approach 45°, the local helix angle of the yarn at yarn crossovers can approach the required 45° due to the geometry of a bent yarn, even for conventional yarn twists.

For sophisticated fabric applications, the design engineer must be able to predict not only the load-deformation behavior of a fabric but also the ultimate strength of the fabric. That is, a rupture criteria for biaxially stressed fabrics must be formulated. A rough approximation of the ultimate strength, σ, of a fabric stressed uniaxially is given by $\sigma = N_1 \cos \xi_1 P_y$ where N_1 is the number of yarns per unit width; ξ_1 is the angle between the yarn and the fabric plane at the midpoint between yarn crossovers, and P_y is the strength of the yarn. However, a rupture criteria for a biaxially stressed fabric will undoubtedly be more complex than this.

The response of biaxially stressed coated fabrics should also be investigated. However, it is anticipated that it would be difficult to obtain quantitative relationships. The response of coated fabrics is dependent on the coating modulus. The presence of the coating material in the interstices between yarns increases the fabric modulus in the low-load region and decreases the fabric elongation and strength at rupture compared to the response of the same fabric when coated. [7]

LITERATURE CITED

1. Chicural, R. and Suppiger, E., Textile Research Journal 30, 568, (1960).

2. Davidson, D. A., ML-TDR-64-239, 1964.

3. Freeston, W. D., Jr., and Platt, M. M., Textile Research Journal 34, 308 (1964).

4. Haas, R. and Dietzius, A., NACA Report No. 16, 1917.

5. Hamburger, W. J., Platt, M. M., and Morgan, H. M., Textile Research Journal 22, 695 (1952).

6. Hearle, J. W. S., Journal of the Textile Institute 49, T389 (1958).

7. Milenkovic, V., AFML-TR-65-241, 1965.

8. Painter, E. V., Textile Research Journal 22, 153 (1952).

9. Peirce, F. T., Journal of the Textile Institute 28, T45 (1937).

10. Peirce, F. T., Textile Research Journal 17, 123 (1947).

11. Platt, M. M., Textile Research Journal 20, 1 (1950).

12. Platt, M. M., Textile Research Journal 20, 519 (1950).

13. Platt, M. M., Klein, W. G., and Hamburger, W. J., Textile Research Journal 24, 132 (1954).

14. Platt, M. M., Klein, W. G., and Hamburger, W. J., Textile Research Journal 29, 592 (1959).

15. Popper, P., WADD-TR-60-897, 1961.

16. Popper, P., ASD-TDR-62-457, 1962.

17. Topping, A. D., Aeronautical Engineering Review 16, 56 (1957).

18. Womersley, J. R., Journal of the Textile Institute 28, T97 (1937).

APPENDIX 2

EVALUATION OF GOVERNMENT-FURNISHED COATED FABRICS

A preliminary evaluation of two typical coated fabrics used for air-supported tents was carried out. The fabrics supplied by the U. S. Army Natick Laboratories were a vinyl-coated nylon (MIL-C-43086) fabric and a polyurethane-coated nylon fabric. The vinyl-coated fabric weighs about 20-1/4 oz/sq yd and the polyurethane-coated fabric 2-9/10 oz/sq yd. It is our understanding that these two fabrics represent approximately the extremes in fabric weight and strength currently of interest for air-supported tent applications.

The uniaxial tensile properties of the fabrics in both the warp and filling directions are given in Table 1. Test specimens dinked one inch by six inches were used. The specimens were tested in an Instron using three-inch wide flat jaws lined with masking tape, a 3-inch gauge length and 2-inch/min jaw speed. As the data in Table 1 shows, the 20-1/4 oz/sq yd fabric is considerably stronger than the 2-9/10 oz/sq yd fabric and exhibits about 25% less elongation to rupture in both the warp and filling directions.

Efforts were made to determine the biaxial load-extension response of both fabrics using the biaxial tester and procedures described in Appendix 1. . However, since the filling yarn in both fabrics is bowed, this was an impossible task. The extent of the yarn bow in the 20-1/4 oz/sq yd fabric is so severe that when cruciform test specimens are cut, there are no through-going yarns, i.e., none of the same yarns can be gripped in opposite jaws.

Cruciform test specimens were also prepared from the 20-1/4 oz/sq yd fabric by cutting the tails parallel to the yarns in the fabric. However, when these samples were mounted in the tester, the central section became so distorted, it was decided that any test results that might be obtained would be meaningless. All efforts to eliminate fabric distortion in the center section were unsuccessful.

Although the filling yarn in the 2-9/10 oz/sq yd fabric is also bowed, the bowing is not as severe as in the 20-1/4 oz/sq yd fabric and biaxial tensile-test results were obtained. The fabric was tested under ratios of loading in the two orthogonal directions of 1:1, 2:1, (i.e., the load applied in the warp direction was twice that applied in the filling direction throughout the test), 5:1 and 1:5. Three tests were made at the 1:1 loading; two at 2:1; two at 5:1; and one at 1:5. The results of these tests are presented graphically in Figures 1 through 3. The results from the uniaxial tests are also presented graphically for comparison in Figure 4. The load-elongation diagrams given in these Figures are the average of the test results obtained at each loading ratio.

Best Available Copy

TABLE 1

COATED FABRIC UNIAXIAL TENSILE PROPERTIES

Material	Rupture Elongation (%)		Rupture Load (lbs/inch width)	
	Warp	Filling	Warp	Filling
Vinyl-Coated Nylon	28.8	29.6	430	38[illegible]
	24.9	27.7	392	36[illegible]
	25.7	29.9*	395	37[illegible]
	26.9	31.9*	410	42[illegible]
	29.6	29.8	435	4[illegible]
		30.9		41[illegible]
		28.3		41[illegible]
Average	27.1	29.7	412	401
Polyurethane-Coated Nylon	34.3	44.1	59.5	32.[illegible]
	36.8	47.6	59.5	34.7
	41.4	45.9	62.0	33.0
	39.1	40.9	60.8	30.6
	37.1	41.3*	60.4	33.0*
		43.4		32.7
Average	37.7	43.8	60.4	32.8

*Jaw break.

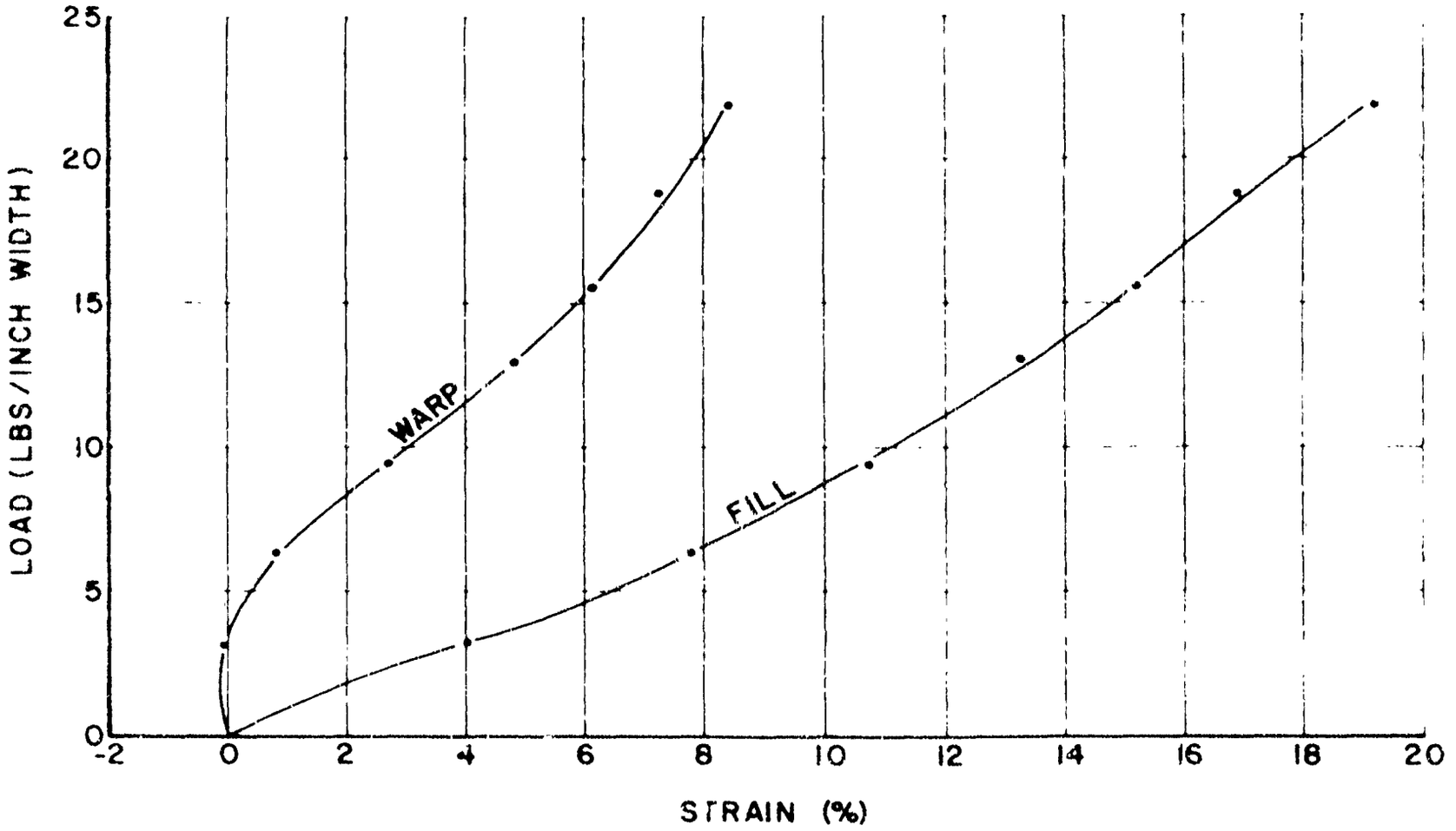

FIGURE 1. BIAXIAL LOAD-EXTENSION RESPONSE OF 2.9-OZ/SQ YD VINYL-COATED NYLON FABRIC AT $\sigma_w / \sigma_f = 1$.

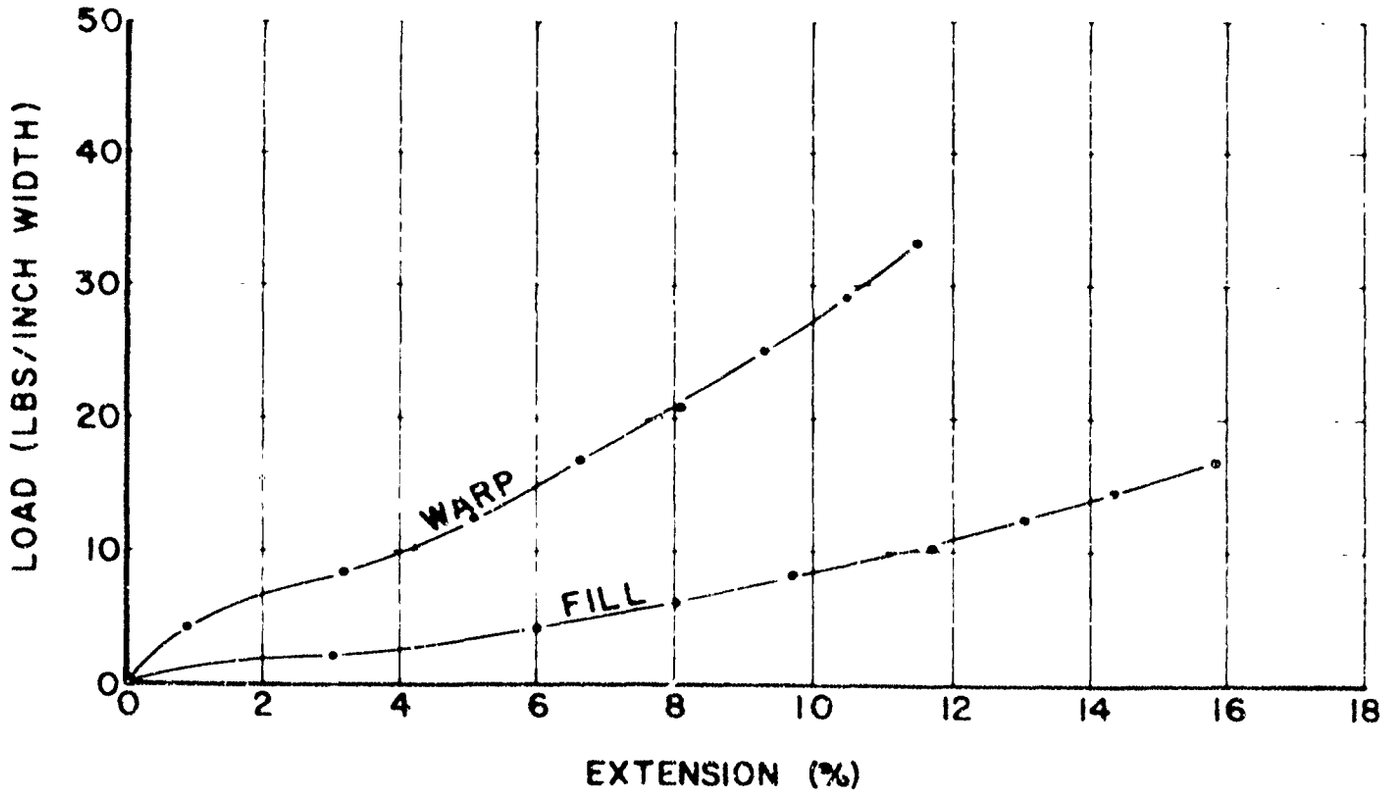

FIGURE 2. BIAXIAL LOAD-EXTENSION RESPONSE OF 2.9-OZ/SQ YD VINYL-COATED NYLON FABRIC AT $\sigma_w / \sigma_f = 2$.

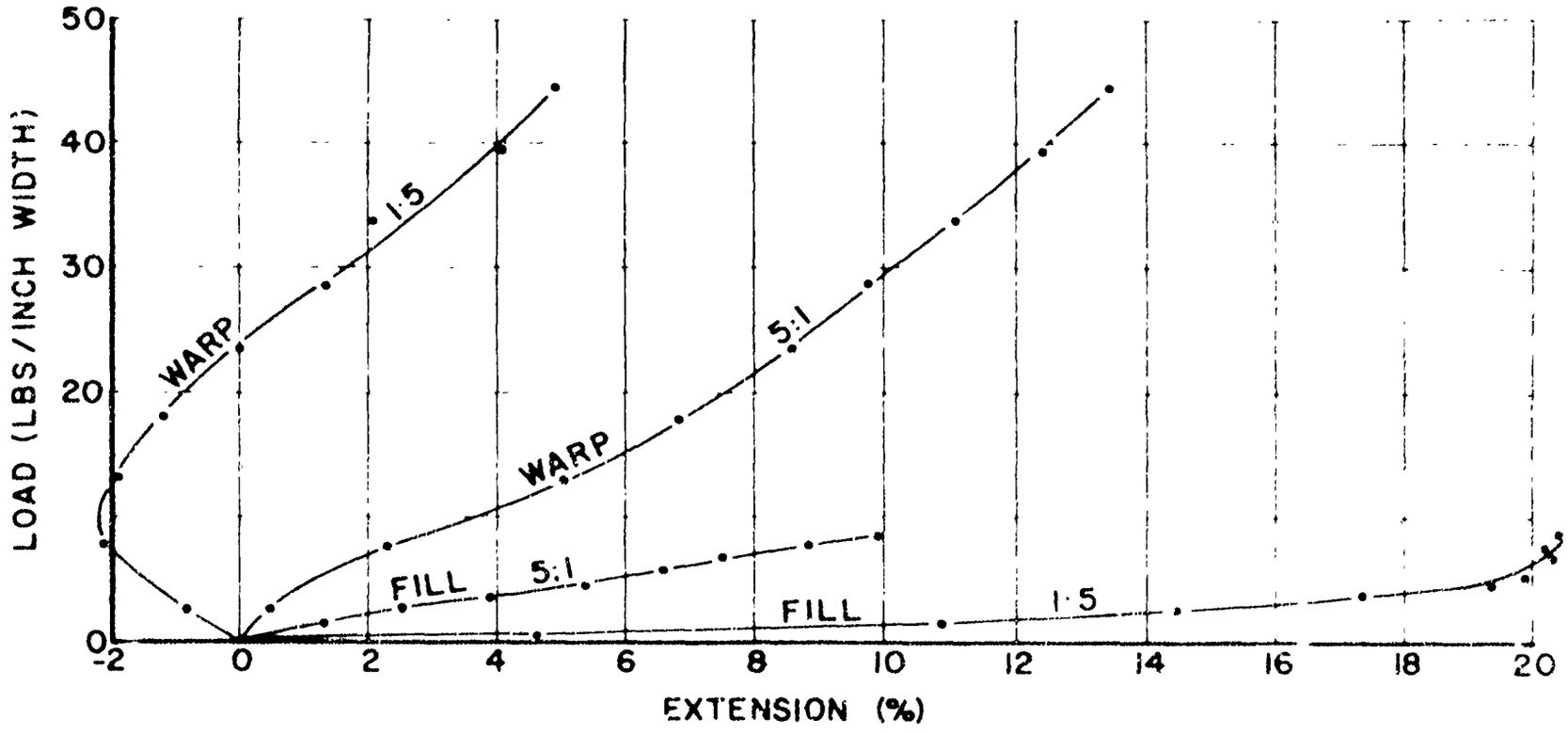

FIGURE 3. BIAXIAL LOAD-EXTENSION RESPONSE OF 2.9-OZ/SQ YD VINYL-COATED NYLON FABRIC AT $\sigma_w / \sigma_f = 5:1$ & $1:5$.

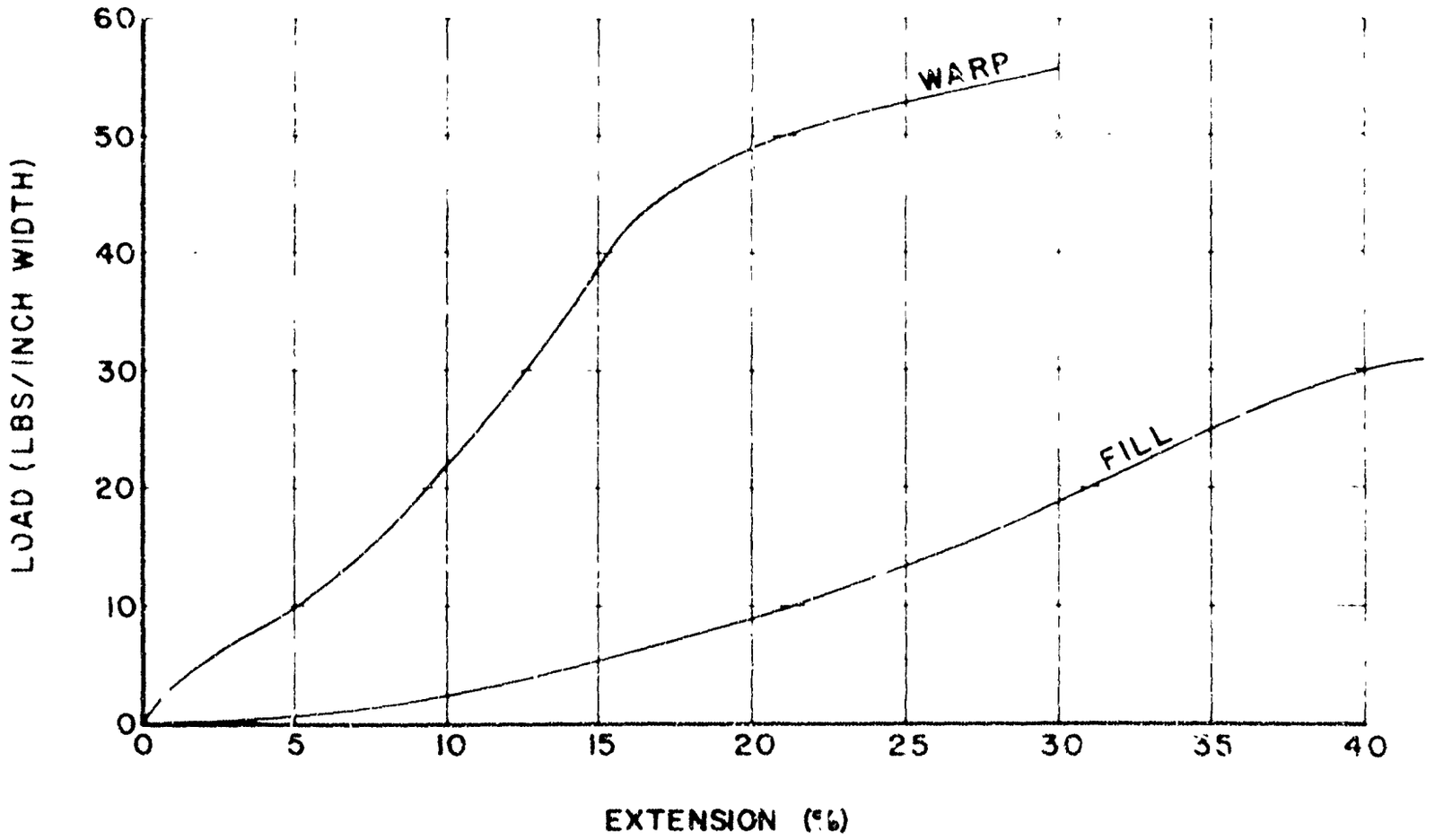

FIGURE 4. UNIAXIAL LOAD-EXTENSION DIAGRAMS FOR 2.9-OZ/SQ YD VINYL-COATED NYLON FABRIC.

An effort was made to take the test specimens to rupture. However, due to the high extensibility of the fabric in the filling direction, in two of the three tests run at the 1:1 loading ratio and the one test run at 1.5, the tails reached their maximum extension before the test specimens failed. In all the other tests the specimens failed, one tail breaking off suddenly and completely, with the exception of the one specimen that failed at the 1:1 loading ratio where two tails broke at the same time.

In a biaxial tensile test using cruciform-shaped test specimens rupture usually occurs in the tails immediately adjacent to the biaxially stressed central section of the test specimen. As pointed out in the previous section such tests therefore do not necessarily give a good indication of the true fabric strength under biaxial loading. The stress concentrations that occur at the corners where the tails join the biaxially stressed portion of the test specimen can result in premature failure of the specimen.

However, when testing the polyurethane-coated nylon fabric it is interesting to compare the maximum loads observed before failure at the various loading ratios to each other and to the strength of the fabric under uniaxial loading. As shown in Figures 1-3, the maximum measured load in the warp direction under 1:1 biaxial loading is roughly 50% of the uniaxial breaking strength of the fabric in the warp direction. However, this maximum load increases with increasing biaxial loading ratio. At 5:1 the maximum load is about 80% of the uniaxial fabric strength. The maximum measured load in the filling direction under 1:1 biaxial loading is about 70% of the uniaxial breaking strength of the fabric in the filling direction and this maximum load decreases with increasing biaxial loading ratio. At 5:1 the maximum load is about 50% of the fabric strength uniaxially.

As shown in Figure 3, the response of the 2-9/10 oz/sq yd coated fabric at a loading ratio of 5:1 is considerably different from that measured at 1.5. This indicates that the construction of the fabric is far from square.

The various test results reported above further demonstrate that the performance specifications of the new biaxial tester to be designed and built under this program are more than adequate. They also indicate that the coated fabrics currently used in air-supported tents would probably exhibit improved performance if the filling yarns in the fabric were straight and perpendicular to the warp yarns rather than bowed. Since such fabrics could be more meaningfully tested, structures fabricated from them would be more ameanable to accurate design procedures.

DISTRIBUTION LIST

Copies	
1	Commanding General, U.S. Army Materiel Command, Washington D.C. 20315
1	Commanding General, U.S. Army Missile Command, Redstone Arsenal, Alabama 35809
1	Commanding General, U.S. Army Mobility Command, Warren, Michigan 48089
1	Commanding General, U.S. Army Munitions Command, Picatinny Arsenal Dover New Jersey 07801
1	Commanding General, U.S. Army Supply and Maintenance Command, Washington, D.C. 20315
1	Commanding General, U.S. Army Test and Evaluation Command, Aberdeen Proving Ground, Md. 21005
1	Commanding General, U.S. Army Weapons Command, Rock Island Arsenal, Rock Island, Illinois 61201
1	Commandant, U.S. Army War College, Attn: Dir., Doctrine and Studies Division, Carlisle Barracks, Pa. 17013
1	Commanding Officer, U.S. Army Combat Service Support Group, Ft. Lee, Virginia 23801
1	Commandant, U.S. Army Command and General Staff College, Attn: Archives, Ft. Leavenworth, Kansas 66027
1	Chief, AMC Liaison Office, ASDL-8 Aeronautical Systems Division, Wright-Patterson Air Force Base, Ohio 45433
1	Chief, Bureau of Supplies and Accounts, Dept. of the Navy, Washington D.C. 20390
1	Commander, Defense General Supply Center, Richmond, Virginia 23212
1	U. S. Army Natick Laboratories Representative, Defense General Supply Center, Richmond, Virginia 23212
1	National Research Council, 2101 Constitution Avenue, Washington D.C. 20418
1	Commandant, Industrial College of the Armed Forces, Ft. McNair, Washington, D.C. 20315
1	Commandant, The QM School, Attn: Library, Ft. Lee, Virginia 23801
1	The Army Library, Pentagon Bldg., Washington, D.C. 20301
1	Commander, Letterkenny Army Depot, Chambersburg, Pa. 17201
1	Commander, New Cumberland Army Depot, New Cumberland, Pa. 17070
1	Commandant, U.S. Army Logistics Management Center, Ft. Lee, Va. 23801
1	Commander, U.S. Army Major Items Supply Management Agency, Chambersburg, Pa. 17201
1	Commanding General, U.S. Army Mobility Equipment Command, St. Louis, Mo. 63166
1	Commanding General, Defense Personnel Support Center, 2800 South 20th St Phil, Pa. 19145
1	Commanding Officer, U.S. Army General Equipment and Test Activity, Ft. Lee, Virginia 23801
1	Senior Standardization Representative, U.S. Army Standardization Group, Ottawa, Canada

UNCLASSIFIED

Security Classification

DOCUMENT CONTROL DATA - R&D

(Security classification of title, body of abstract and indexing annotation must be entered when the overall report is classified)

1. ORIGINATING ACTIVITY (Corporate author)
Fabric Research Laboratories, Inc.
Dedham, Massachusetts

2a. REPORT SECURITY CLASSIFICATION
Unclassified

2b. GROUP

3. REPORT TITLE
Biaxial Tensile Tester for Fabrics

4. DESCRIPTIVE NOTES (Type of report and inclusive dates)

5. AUTHOR(S) (Last name, first name, initial)
Sebring, Robert E.
Freeston, Denney W. Jr.

6. REPORT DATE
May 1967

7a. TOTAL NO. OF PAGES
104

7b. NO. OF REFS
2[illegible]

8a. CONTRACT OR GRANT NO.
DA19-129-AMC-1042(N)

b. PROJECT NO.

c.

d.

9a. ORIGINATOR'S REPORT NUMBER(S)

9b. OTHER REPORT NO(S) (Any other numbers that may be assigned this report)
67-71-GP

10. AVAILABILITY/LIMITATION NOTICES
Distribution of the document is unlimited.
Release to CFSTI is authorized.

11. SUPPLEMENTARY NOTES

12. SPONSORING MILITARY ACTIVITY
U. S. Army Natick Laboratories
Natick, Mass.

13. ABSTRACT

The overall goal of the program is the development of an instrument for determining the stress-strain response of coated fabrics used in the construction of air-supported tents.

During Phase I of the program a survey of the scientific literature on biaxial tensile testers was carried out. The purpose of the survey was to examine the design features and operating techniques of previously constructed testers and to note design innovations and shortcomings.

A theoretical analysis of the load-extension behavior of idealized plain-weave fabrics subjected to biaxial stresses is presented. Fabric strains resulting from both crimp interchange and yarn extension are considered. The analytical expressions derived have been solved with the aid of a digital computer for both linearly elastic and elasto-plastic materials. Time effects, although not explicitly included, are discussed.

Generalized plots of the results are given for the two extremes of initial fabric structure: (1) equal crimp distribution in both sets of yarns; (2) one set of yarns straight (noncrimped). The predicted and measured response of two model fabrics are compared.

Two typical coated fabrics representing approximately the extremes in fabric weight and strength currently of interest for air-supported tent applications were evaluated.

The design of an improved biaxial tensile tester is outlined. The proposed design concept utilizes the results of the literature survey, model fabric study and coated fabric evaluation.

DD FORM 1473

UNCLASSIFIED

Security Classification

14 KEY WORDS	LINK A ROLE	LINK A WT	LINK B ROLE	LINK B WT	LINK C ROLE	LINK C WT
Evaluation	8					
Tensile testers	8,9		10			
Biaxial	0		0			
Measurement	4		8			
Strains	4					
Fabrics	4		9			
Coated	0		0			
Tensile properties			9			
Tents			4			
Armed Forces equipment			4			

INSTRUCTIONS

1. ORIGINATING ACTIVITY: Enter the name and address of the contractor, subcontractor, grantee, Department of Defense activity or other organization *(corporate author)* issuing the report.

2a. REPORT SECURITY CLASSIFICATION: Enter the overall security classification of the report. Indicate whether "Restricted Data" is included. Marking is to be in accordance with appropriate security regulations.

2b. GROUP: Automatic downgrading is specified in DoD Directive 5200.10 and Armed Forces Industrial Manual. Enter the group number. Also, when applicable, show that optional markings have been used for Group 3 and Group 4 as authorized.

3. REPORT TITLE: Enter the complete report title in all capital letters. Titles in all cases should be unclassified. If a meaningful title cannot be selected without classification, show title classification in all capitals in parenthesis immediately following the title.

4. DESCRIPTIVE NOTES: If appropriate, enter the type of report, e.g., interim, progress, summary, annual, or final. Give the inclusive dates when a specific reporting period is covered.

5. AUTHOR(S): Enter the name(s) of author(s) as shown on or in the report. Enter last name, first name, middle initial. If military, show rank and branch of service. The name of the principal author is an absolute minimum requirement.

6. REPORT DATE: Enter the date of the report as day, month, year; or month, year. If more than one date appears on the report, use date of publication.

7a. TOTAL NUMBER OF PAGES: The total page count should follow normal pagination procedures, i.e., enter the number of pages containing information.

7b. NUMBER OF REFERENCES: Enter the total number of references cited in the report.

8a. CONTRACT OR GRANT NUMBER: If appropriate, enter the applicable number of the contract or grant under which the report was written.

8b, 8c, & 8d. PROJECT NUMBER: Enter the appropriate military department identification, such as project number, subproject number, system numbers, task number, etc.

9a. ORIGINATOR'S REPORT NUMBER(S): Enter the official report number by which the document will be identified and controlled by the originating activity. This number must be unique to this report.

9b. OTHER REPORT NUMBER(S): If the report has been assigned any other report numbers *(either by the originator or by the sponsor)*, also enter this number(s).

10. AVAILABILITY/LIMITATION NOTICES: Enter any limitations on further dissemination of the report, other than those imposed by security classification, using standard statements such as:

(1) "Qualified requesters may obtain copies of this report from DDC."

(2) "Foreign announcement and dissemination of this report by DDC is not authorized."

(3) "U. S. Government agencies may obtain copies of this report directly from DDC. Other qualified DDC users shall request through _____."

(4) "U. S. military agencies may obtain copies of this report directly from DDC. Other qualified users shall request through _____."

(5) "All distribution of this report is controlled. Qualified DDC users shall request through _____."

If the report has been furnished to the Office of Technical Services, Department of Commerce, for sale to the public, indicate this fact and enter the price, if known.

11. SUPPLEMENTARY NOTES: Use for additional explanatory notes.

12. SPONSORING MILITARY ACTIVITY: Enter the name of the departmental project office or laboratory sponsoring *(paying for)* the research and development. Include address.

13. ABSTRACT: Enter an abstract giving a brief and factual summary of the document indicative of the report, even though it may also appear elsewhere in the body of the technical report. If additional space is required, a continuation sheet shall be attached.

It is highly desirable that the abstract of classified reports be unclassified. Each paragraph of the abstract shall end with an indication of the military security classification of the information in the paragraph, represented as *(TS)*, *(S)*, *(C)*, or *(U)*.

There is no limitation on the length of the abstract. However, the suggested length is from 150 to 225 words.

14. KEY WORDS: Key words are technically meaningful terms or short phrases that characterize a report and may be used as index entries for cataloging the report. Key words must be selected so that no security classification is required. Identifiers, such as equipment model designation, trade name, military project code name, geographic location, may be used as key words but will be followed by an indication of technical context. The assignment of links, rules, and weights is optional.